2011-12-15

Mechanism of G Protein Beta-Gamma Assembly Mediated by Phosducin-Like Protein 1

Chun Wan Jeffrey Lai
Brigham Young University - Provo

Mechanism of G protein Beta-Gamma Assembly Mediated by Phosducin-Like Protein 1

Chun Wan Jeffrey Lai

A dissertation submitted to the faculty of
Brigham Young University
in partial fulfillment of the requirements for the degree of

Doctor of Philosophy

Barry M. Willardson, Chair
Gregory F. Burton
Allen R. Buskirk
David M. Belnap
Jeffrey Barrow

Department of Chemistry and Biochemistry

Brigham Young University

April 2012

ABSTRACT

Mechanism of G protein Beta-Gamma Assembly Mediated by Phosducin-Like Protein 1

Chun Wan Jeffrey Lai
Department of Chemistry and Biochemistry, BYU
Doctor of Philosophy

G-protein coupled receptor signaling (GPCR) is essential for regulating a large variety of hormonal, sensory and neuronal processes in eukaryotic cells. Because the regulation of these physiological responses is critical, GPCR signaling pathways are carefully controlled at different levels within the cascade. Phosducin-like protein 1 (PhLP1) can bind the G protein βγ dimer and participate in GPCR signaling. Recent evidence has supported the concept that PhLP1 can serve as a co-chaperone of the eukaryotic cytosolic chaperonin complex CCT/TRiC to mediate Gβγ assembly. Although a general mechanism of PhLP1-mediated Gβγ assembly has been postulated, many of the details about this process are still missing. Structural analysis of key complexes that are important intermediates in the Gβγ assembly process can generate snapshots that provide molecular details of the mechanism beyond current understanding. We have isolated two important intermediates in the assembly process, the $G\beta_1$-CCT and PhLP1-$G\beta_1$-CCT complexes assembled *in vivo* in insect cells, and have determined their structures by cryo-electron microscopy (cryo-EM). Structural analysis reveals that $G\beta_1$, representing the WD40 repeat proteins which are a major class of CCT substrates, interacts specifically with the apical domain of CCTβ. $G\beta_1$ binding experiments with several chimeric CCT subunits confirm a strong interaction of $G\beta_1$ with CCTβ and map $G\beta_1$ binding to α-Helix 9 and the loop between β-strands 6 and 7. These regions are part of a hydrophobic surface of the CCTβ apical domain facing the chaperonin cavity. Docking the Gβ molecule into the two 3D reconstructions ($G\beta_1$-CCT and PhLP1-$G\beta_1$-CCT) reveals that upon PhLP1 binding to $G\beta_1$-CCT, the quasi-folded Gβ molecule is constricted to a more native state and shifted to an angle that can lead to the release of folded $G\beta_1$ from CCT. Moreover, mutagenesis of the CCTβ subunit suggests that PhLP1 can interact with the tip of the apical domain of CCTβ subunit at residue S260, which is a downstream phosphorylation target site of RSK and S6K kinases from the Ras-MAPK and mTOR pathways. These results reveal a novel mechanism of PhLP1-mediated Gβ folding and its release from CCT.

The next important step in testing the PhLP1-mediated Gβγ assembly hypothesis is to investigate the function of PhLP1 *in vivo*. We have prepared a rod-specific PhLP1 conditional knockout mouse in which the physiological consequences of the loss of PhLP1 functions have been characterized. The loss of PhLP1 has led to profound consequences on the ability of these rods to detect light as a result of a significant reduction in the expression of transducin (G_t) subunits. Expression of other G protein subunits as well as $G\beta_5$-RGS9-1 complexes was also greatly decreased, yet all of this occurs without resulting in rapid degeneration of the photoreceptor cells. These results show for the first time the essential nature of PhLP1 for Gβγ and $G\beta_5$-RGS dimer assembly *in vivo,* confirming results from cell culture and structural studies.

Keywords: GPCR, Heterotrimeric G proteins, G protein βγ assembly, Phosducin-like protein 1

ACKNOWLEDGEMENTS

I wish to acknowledge everyone who has contributed to this work and thank them for their support throughout these years of study. I am deeply grateful for my mentor, Dr. Barry Willardson, and his enthusiasm in helping me to succeed in every possible way. I am also thankful for working with my colleagues in the department, especially the people in the Willardson lab. I am indebted to Rebecca L. Plimpton, Bradley Turner, Alicia Farmer, and Paul Ludtke, who have contributed directly to this work. I would like to show my heartfelt gratitude to my family, my wife Chui Ying Irene Lai, my oldest son Jit Ching Jonah Lai, my daughter Cordelia Yuet-Yee Lai, my youngest son Helaman Lok-Yin Lai, for their love and support. I would like to thank the Department of Chemistry and Biochemistry and Brigham Young University for maintaining such an excellent environment for me and my fellow graduate students to perform life science research. I am thankful for our Heavenly Father and our Savior Jesus Christ for giving us the gospel and so many blessings in our life.

TABLE OF CONTENTS

LIST OF FIGURES AND TABLES

ABBREVIATIONS

C-	Carboxyl-terminus
CCT	Chaperonin containing tailless complex polypeptide 1
DEP	Disheveled, Egl-10, pleckstrin
DRiP78	Dopamine receptor-interacting protein 78
G	Heterotrimeric GTP binding protein
GAP	GTPase accelerating protein
GDP	Guanosine diphosphate
GGL	Gγ-like
GPCR	G-protein coupled receptor
GTP	Guanosine triphosphate
Gα	G-protein alpha subunit
Gβ	G-protein beta subunit
$G\beta_5$-L	G-protein beta 5 subunit long isoform
$G\beta_5$-S	G-protein beta 5 subunit short isoform
Gβγ	G-protein beta and gamma subunit dimer
GC	Guanylyl-cyclase
GCAP	Guanylyl-cyclase activating protein
Gγ	G-protein gamma subunit
GRK1	Rhodopsine Kinase
HA	Hemagglutinin
HEK-293T cells	Human embryonic kidney 293 cells
LCMSMS	Liquid chromatography coupled to tandem mass spectrometry

MS	Mass spectrometry
MSMS	Tandem mass spectrometry
N-	Amino-terminus
PCR	Polymerase chain reaction
Pdc	Phosducin
PDE	Phosphodiesterase
PhLP1	Phosducin-like protein 1
R9AP	R9 anchoring protein
RGS	Regulator of G protein signaling
siRNA	Short interfering RNA

CHAPTER 1 INTRODUCTION:
FUNCTIONAL PROPERTIES OF PHOSDUCIN-LIKE PROTEINS IN REGULATING G PROTEIN SIGNALING AND CHAPERONE-ASSISTED PROTEIN FOLDING

Summary

G-protein coupled receptor signaling is essential for the regulation of a large variety of physiological responses such as vision, heartbeat, taste, growth, and neuronal signals. The malfunctioning of these signaling processes can lead to devastating diseases such as cancer, heart disease, vision impairment, neural diseases, and hypertension [16-20]. GPCR signaling is particularly important for vision. Therefore, much of the GPCR signaling pathway has been elucidated from the phototransduction processes of the retina. Since the regulation of GPCR-mediated responses is vitally important, GPCR signaling pathways are carefully controlled at multi-levels within the cascade. Recent evidence has suggested that GPCR signaling can be controlled by phosducin (Pdc) and phosducin-like protein 1 (PhLP1), which can bind the G protein βγ dimer (Gβγ) tightly. Pdc is expressed mostly in the retina, whereas PhLP1 is expressed widely among different tissues, suggesting a general role in regulating Gβγ signaling.

Genetic, biochemical and structural analyses have shown that PhLP1 serves as a co-chaperone to assist protein folding activities of the cytosolic chaperonin complex (CCT). CCT is a large protein folding complex that assists in folding β-strand rich, hydrophobic, aggregation-prone proteins such as Gβ, which belongs to a class of WD repeat proteins that form β-propeller structures. Biochemical studies have shown that that PhLP1 is required for Gβγ dimer assembly by forming a ternary complex with Gβ and CCT and releasing Gβ from CCT to interact with Gγ and form the dimer. Phosphorylation of S18-20 in the N-terminal domain of PhLP1 is critical for the release of Gβ from the CCT complex. From these data, an outline of the mechanism of

PhLP1-mediated Gβγ assembly has been put forward. Further analysis has shown that the mechanism of PhLP1-mediated Gβγ assembly is shared among all isoforms of Gβ and Gγ. Furthermore, biochemical experiments have shown that PhLP1 can mediate $G\beta_5$-regulator of G protein signaling protein (RGS) assembly through a different mechanism than the Gβγ assembly. PhLP1 has been proposed to stabilize the binding of $G\beta_5$ to CCT, and then release from CCT to allow RGS7 to associate with $G\beta_5$ while still bound to the CCT complex. These studies have contributed significantly to our understanding of G protein signaling because proper protein folding, post-translational modification, assembly and membrane targeting of heterotrimeric G proteins are crucially important for the proper function of GPCR signaling pathways.

Introduction

GPCR signaling pathways regulate a large variety of physiological responses such as vision, cardiac rhythm, taste, growth, and neuronal signals [15, 21, 22]; and the malfunctioning of these signaling processes can lead to devastating diseases such as cancer, heart disease, vision impairment, neural diseases, and hypertension [16-20]. Owing to the fact that GPCR signaling can mediate a large array of different physiological processes, a significant number of genes encode for the GPCRs (~900 in humans [23]). Many different ligands such as small molecule neurotransmitters, peptide hormones, chemokines, lipids, odorants and even photons of light can trigger the activation of GPCR signaling and in turn initiate the signaling processes through intracellular G proteins. Indeed, a large number of pharmaceutical therapeutics target GPCR signaling pathway components [24]. Therefore, the mechanism of GPCR signaling has been thoroughly elucidated in atomic detail [25] (Figure 1-1).

Upon binding of a ligand to the extracellular domain of a GPCR, conformational changes take place in the packing of the seven transmembrane α-helices of the activated GPCR. This

conformational change propagates to the intracellular surface of the GPCR and activates heterotrimeric G proteins that associate with the receptor. This activation process promotes the exchange of GDP for GTP on the G protein α subunit (Gα) and leads to the dissociation of Gα-GTP from the G protein βγ subunits (Gβγ). Gα-GTP and Gβγ subunits can both mediate activities of downstream effectors such as adenylyl cyclase, cGMP phosphodiesterase, phospholipase Cβ, phosphatidylinositol-3-kinase, Rho guanine nucleotide exchange factors, and ion channels. These effectors can subsequently control activities of second messengers such as cyclic nucleotides, inositol phosphates, Ca^{2+} and the actin cytoskeleton leading to the cellular responses that mediate the physiological response to the ligand. Upon the hydrolysis of GTP to GDP, the G protein cycle terminates and the Gαβγ complex is reformed by the association between Gα-GDP and Gβγ subunits [16].

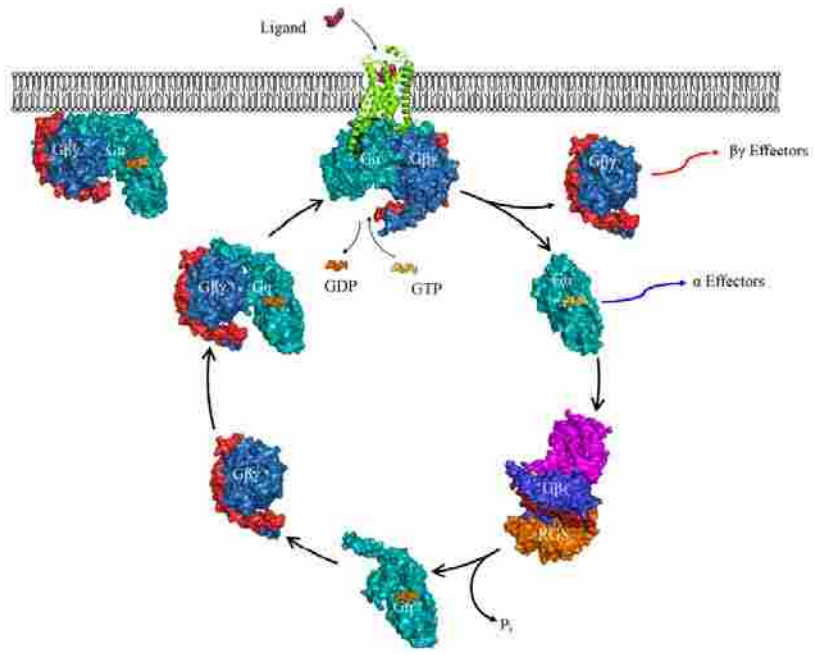

Figure 1-1. G protein-coupled receptor signaling cycle.
The G protein activation/inactivation cycle is shown here using atomic structures of individual molecules. The detailed signaling cycle is described in the text. Color code of individual molecules: GPCR – green, Gα – teal, Gβ1 – blue, Gγ –red, RGS DEP/DHEX domain – pink, $G\beta_5$ – dark blue, RGS Gγ-like domain – dark red, RGS domain – orange. Reference PDB numbers: GPCR-G protein complex (3SN6) [2], G protein heterotrimer (1GOT) [9], Gα-GTP (1TND) [12], $G\beta_5$-RGS (1PB1) [7].

GPCR signaling in phototransduction

GPCR signaling is particularly important in the phototransduction cascade. Much of the GPCR signaling pathway has been elucidated from the study of visual processing in the rod and cone photoreceptor cells of the retina (Figure 1-2A). Therefore, the detailed signaling pathways of GPCRs can be illustrated in the phototransduction processes (Figure 1-2B). Both rods and cones have four primary structural regions, namely an outer segment, an inner segment, a cell body and a synaptic terminus (Figure 1-2A) [26]. The visual pigment rhodopsin and other phototransduction signaling components can be found in the dense membrane disks of the outer segments. Besides serving as the main molecule of phototransduction, rhodopsin is also the major structural component of the outer segment discs [27, 28]. The inner segment contains mitochondria, endoplasmic reticulum and the Golgi apparatus and the cell body contains the nucleus. The synaptic terminus can transmit neuronal signals from rods and cones to bipolar and horizontal cells. In the absence of light, a steady inward cation conductance can be found on the outer segment membrane, keeping the rods and cones in a depolarized state and maintaining a steady synaptic release of glutamate. The inward dark current is controlled by the light-sensitive cGMP-gated channels, whereas the outward current is regulated through the Na^+/K^+ ATPase [29, 30]. When light is absorbed, the cation conductance is blocked, producing a membrane hyper-polarization that terminates the release of glutamate, and this decrease in synaptic glutamate is detected and processed by downstream retinal neurons for visual perception in the brain.

The chromophore, 11-cis-retinal, is covalently bound to rhodopsin through a Schiff-base linkage to a conserved lysine residue (K296 in human rhodopsin) in the seventh transmembrane helix [26]. In the absence of light, the 11-cis-retinal serves as a strong antagonist to lock the rhodopsin in an inactive state [31, 32]. Upon photon absorption, the 11-cis-retinal is isomerized

to all-trans-retinal. This isomerization transforms the retinal to a strong agonist of rhodopsin [33].

Activated rhodopsin associates with the heterotrimeric G protein transducin αβγ subunits (G_t) and catalyzes the exchange of GDP to GTP on the transducin α subunit ($G\alpha_t$). As $G\alpha_t$-GTP dissociates from the activated receptor and $G_t\beta\gamma$ dimers, it interacts with the cGMP phosphodiesterase (PDE) and activates the powerful cGMP hydrolysis activity of PDE. PDE consists of two catalytic α and β subunits and two inhibitory γ subunits to form a tetrameric protein complex [34, 35]. In the dark, the two PDEγ subunits inhibit the activity of the PDEαβ subunits, but in the presence of light, $G\alpha_t$-GTP associates with PDEγ and releases it from the PDEαβ subunits to allow the hydrolysis of cGMP to take place. The rapidly decreased cytoplasmic cGMP concentration results in the closure of cGMP-gated cation channels in the plasma membrane of the photoreceptor outer segment within milliseconds [36] and hyperpolarizes the membrane potential. This channel closure also reduces the cytoplasmic Ca^{2+}

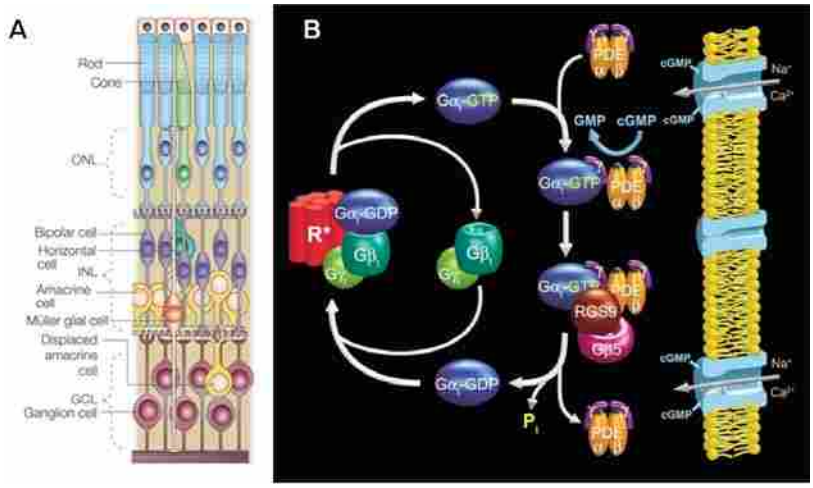

Figure 1-2. Organization of vertebrate retina and scheme of phototransduction signaling.
A) The retina consists of rod and cone photoreceptors, bipolar cells, ganglion cells, amacrine cells, horizontal cells and Müller glia as its seven main classes of cell types, which form three distinct cell layers [5]. The outer nuclear layer (ONL) of the retina refers to the photoreceptor cell bodies. Upon stimulation, photoreceptor cells relay their signals via bipolar cells, located in the inner nuclear layer (INL), to the ganglion cells. These neuronal signals are transmitted from the ganglion cell layer (GCL) along the optic nerve to the brain for visual processing. The amacrine cells and horizontal cells in the inner nuclear layer form lateral connections and regulate signaling pathways from rod and cone cells to the ganglion cells [11]. A significant portion of amacrine cells can also be found in the ganglion cell layer [13]. Müller glial cell bodies are formed in the center of the inner nuclear layer and may also be engaged in the repair and protection functions of retinal neurons. Reprinted from [14]. B) The G protein signaling cycle in phototransduction is shown. Details of are cascade is described in the text. Reprinted from [15].

concentration because of decreased influx of Ca^{2+} through the channels. The reduction in intracellular Ca^{2+} initiates a negative feedback to produce light adaptation.

Rapid recovery of the photoreceptor is critical for image processing. Activated rhodopsin is shut down by phosphorylation events at its C-terminus mediated by rhodopsin kinase (GRK1) and by the binding of visual arrestin to the phosphorylated rhodopsin to block further interaction with G_t [37, 38]. GRK1 activity is mediated by recoverin [39-42], which is a calcium-binding protein. In the presence of light, Ca^{2+} concentration decreases, and recoverin dissociates from GRK1 to allow the phosphorylation of rhodopsin to take place. Moreover, all-trans retinal is released from rhodopsin, forming the weakly active opsin form of the visual pigment. Rhodopsin is regenerated through the binding of a new 11-cis retinal that is made through a series of enzymatic reactions of the visual cycle that converts all-trans retinol back to 11-cis-retinal in the retinal pigment epithelial cells and is subsequently transported to the photoreceptor cells [43].

The rate limiting step of recovery of the light responses is the hydrolysis of GTP on $G\alpha_t$ by a GTPase accelerating (GAP) complex. This GAP complex in the visual system consists of a regulator of G protein signaling protein (RGS9-1), the $G\beta_5$ subunit long isoform ($G\beta_5$-L) and the membrane-anchor protein (R9AP) [44-46]. The RGS9-1 protein has three domains, an RGS GAP domain, a G protein γ-like (GGL) domain that associates with the $G\beta_5$-L subunit and a DEP (Dishevelled/Eg110/Pleckstrin) domain that binds to the plasma membrane anchoring R9AP protein. The RGS9-1/$G\beta_5$-L/R9AP GAP complex accelerates the hydrolysis of GTP in $G\alpha_t$ to GDP resulting in the dissociation of Gα-GDP from PDEγ. PDEγ then reassociates with PDEαβ subunits to inhibit the cGMP hydrolysis [47]. Since the concentration of the GAP complex is higher in cones than in rods, it allows faster visual response in cone vision at high light intensity

[48, 49]. The reduction in PDE-mediated hydrolysis, coupled with light-induced activation of guanylyl-cyclase (GC) restores cGMP levels. In the presence of light, the reduction in Ca^{2+} concentration causes dissociation of Ca^{2+} from the calcium-binding guanylyl-cyclase activating protein (GCAP). The Ca^{2+}-free GCAP can then activate GC. The activated GC rapidly restores the cGMP concentration back to the basal level. Therefore, efficient recovery of the dark state after a light response requires the inactivation of rhodopsin, $G\alpha_t$ and PDE, and the restoration of cGMP concentration.

The role of phosducins in GPCR signaling

The visual system shows just how exquisitely GPCR signaling is controlled at different levels within the cascade. This is the case for all GPCR signaling pathways. They can be inactivated at the receptor level by phosphorylation, arrestin binding and internalization [22]. GPCR signaling can also be regulated at the heterotrimeric G proteins level. $G\alpha$-GTP can be deactivated by accelerating the hydrolysis of GTP through the action of RGS proteins [50, 51]. G protein $\beta\gamma$ subunits can be regulated by associating with Pdc [52-55] and PhLP1 [56, 57] to control the amount of available $G\beta\gamma$ to interact with $G\alpha$-GTP or with other effectors. Pdc is expressed mostly in the photoreceptor cells of the retina and in the pineal gland [52, 58], whereas PhLP1 is expressed widely in most types of cells and tissues [59, 60] implying that PhLP1 has a more general physiological function. However, the precise role of phosducins in $G\beta\gamma$ signaling has been a long-standing challenge in GPCR signaling research.

Genetic components and expression of Pdc and PhLP1

A closer examination of the genetic structures of Pdc and PhLP1 have provided insight into their physiological roles. The rat and human PhLP1 genes have been cloned and characterized to

determine the genetic composition and tissue expressions of PhLP1 [61]. Several splice variants of PhLP1 have been discovered from PhLP1 mRNAs [59]. Isolated cDNAs of PhLP1 revealed a long form (301 amino acids) and a short form (218 amino acids) of PhLP1. The PhLP1 gene contains 4 exons and 3 introns in a similar order to the Pdc gene [62]. All introns contain consensus sequences of donor and acceptor splice junctions that follows the 5'GT-AG-3' rule [61]. The start codon of PhLP1 is located at exon 2, but additional alternative transcription initiation sites have been found in other exons. There is 41% sequence identity and 65% homology between PhLP1 and Pdc, yet the N-terminal domain of PhLP1 is shorter in Pdc [59]. A functionally important phosphorylation site is located in the N-terminus of PhLP1, which is transcribed from the exon 2 and 3, and the thioredoxin-like structural domain is transcribed mostly from exon 4 of the PhLP1 gene. The physical location of the PhLP1 gene has been mapped to the human chromosome 9 and is linked to the genetic markes D9S1876 and D9S1674 (66-71cM), whereas the Pdc gene has been mapped to the human chromosome 1 [63]. Since promoter regions of both PhLP1 and Pdc gene share little homology, it is believed that these two genes have different gene expression regulatory mechanisms, which is consistent with the differences in their tissue distribution. Full length PhLP1 is ubiquitously expressed in all tissues, whereas Pdc is mainly expressed in retina and pineal gland [61]. Low level expression of Pdc has also been described in other tissues [64]. Splice variants of PhLP1 have been detected in brain and retina tissues, but they are expressed at a significantly lower level than the full length PhLP1 transcript [65]. PhLP1 is usually expressed at moderate levels in most tissues in the body, but a high level expression of PhLP1 can be found in the adrenal gland [60, 66].

Functional domains of Pdc and PhLP1

Phosducin and PhLP1 shares homologies on two independent domains [65]. X-ray crystallographic analysis of Pdc has shown two domains that interact with Gβγ [3]. The N-terminal domains from both Pdc and PhLP1 form a helical structure and associate with the loops on top of the WD repeat β-propeller of the Gβ subunit. This binding site is the same region of Gβγ that interacts with Gα and other Gβγ-dependent effectors [67]. The C-terminal domain forms a thioredoxin fold and binds outer strands of the β-propeller blades 1 and 7 of Gβ [3, 68]. The Pdc-Gβγ crystal structure also reveals that the Helix 1,3 and C-terminal domain of Pdc interact with three loops (287-295, 308-318, 329-338) of Gβγ and cause changes in the conformation of these loops when compared to the Gαβγ structure [3]. These Gβγ binding regions of Pdc are also conserved in PhLP1. Although both the N- and C-terminus of PhLP1 can bind Gβγ, the N-terminus of Pdc/PhLP1 is responsible for most contact sites to the Gβγ subunits [69-71]. The conformational changes of Gβγ upon binding to the N-terminal domain of Pdc /PhLP1 creates a groove in Gβ and may facilitate the dissociation of Gβγ from the membrane [52, 55], caused by burying the hydrophobic farnesyl moiety of the Gγ in that groove. The C-terminal domain of Pdc/PhLP1 can also prevent Gβγ from binding to the membrane by binding to the β-propeller blades 1, 7 of Gβ where the farnesylated Gγ C-terminus is located for membrane association [3, 72].

Assembly of the Gβγ dimer

Despite its ability to bind Gβγ, the physiological role of PhLP1 in G protein signaling was a mystery for many years after its discovery in 1993 [59] until a vital function of PhLP1 in the assembly of the Gβγ dimer was reported in 2005 [73]. The mechanism of folding and assembly

of the Gβγ dimer had remained an enigma in the field for some time because the Gβ and Gγ subunits are not stable in their monomeric form. Since Gβ cannot fold into a stable structure on its own, Higgins and Casey suggested in 1994 that Gβ might need accessory proteins for its assembly with Gγ [74]. Interestingly, while Gβ cannot be expressed and folded properly in the bacterial expression system, the Gβγ dimer can be formed and formed in conditions where heterotrimeric G proteins can be normally expressed such as in rabbit reticulocyte lysates [75] and in insect cells [74], suggesting that additional accessory proteins may have co-evolved with G proteins for the folding and assembly process of the Gβγ dimer. Subsequent studies set the stage for the elucidation of the mechanism of Gβγ assembly. Genetic analysis of G protein signaling in the chestnut blight fungus *C. parasitica* revealed that deletion of a gene named *bdm1* phenocopied Gβ gene deletion [75]. This observation was critical because *bdm1* gene is a homolog of Pdc. However, the phenotype of *bdm1* deletion in *C. parasitica* was contradictory to the proposed role of Pdc, which at the time was believed to inhibit the G protein signaling by associating with Gβγ and blocking its interaction with Gα [76]. A more detailed analysis revealed that bdm1 is a closer homolog of PhLP1, which can also associate with a Gβγ dimer like Pdc [77]. A major breakthrough toward resolving this dilemma occurred when our lab discovered that PhLP1 was a binding partner for the cytosolic chaperonin containing tailless polypeptide-1 complex (CCT) [73]. This breakthrough was first to link the Gβγ assembly process to the protein chaperone system.

CCT-mediated protein folding

CCT is a large (~ 1 MDa) protein folding complex and belongs to a class of molecular chaperones called class II chaperonins, which can form a holo-ring structure composed of many

subunits. Chaperonins are classified into group I or group II chaperonins based on their sequences and structures. Group I includes the eubacterial chaperone GroEL and mitochondrial and chloroplast Hsp60 chaperonins. Group II includes archael chaperonins and CCT, which is found in the cytoplasm of all eukaryotes [78]. GroEL chaperonin is formed by homodimerization of one single subunit, whereas archaebacterial chaperonins are formed by oligomerization of two homologous subunits. Both Group I and II chaperonins are necessary for sustaining homeostasis of cellular proteins in the organisms in which they are expressed.

CCT is the most complicated of all chaperonins and consists of eight distinct homologous subunits with each translated from individual genes. These eight CCT subunits α, β, γ, ε, ζ, η, θ (CCT1-8 in yeast) can arrange in two octameric rings. These two rings stack back-to-back to form a central folding cavity in each ring. The arrangement of each subunit in the chaperonin ring seems to be fixed in a specific orientation [79]. It is estimated that approximately 5-10% of newly synthesized cytoplasmic proteins, including many essential genes such as actin and tubulin, require CCT for proper protein folding [80-82].

Group I and II chaperonin subunits share three common domains, namely an equatorial ATP-binding domain, an apical domain that allows substrate binding, and a central intermediate domain that relays structural changes between the equatorial domain and the apical domain. The apical domain sequence is the most divergent of the three domains, providing specificity for substrate recognition and binding, whereas the equatorial and intermediate domains are more conserved among different subunits of CCT [83]. Each equatorial domain contains an ATP-binding site and contact sites for interactions between neighboring subunits.

Each CCT subunit can bind ATP and uses the ATP hydrolysis energy to drive the protein folding process [84, 85]. Although GroEL requires a lid-forming co-chaperone GroES for its

folding, the crystal structure of a group II chaperonin from *Thermoplasma acidophilum*, termed the thermosome, showed that the chaperonin complex contains an iris-like 'built-in' lid structure formed by helical protrusions of the apical domain [86]. This lid structure can open and close during the ATPase cycle of CCT and encapsulate substrates within the central folding cavity [87]. Recent evidence has shown that initial ATP hydrolysis of one subunit in a ring can trigger a ripple effect of ring closing in all other subunits. The folding cavity can provide an optimal environment to minimize entropy and maximize folding potential of the nascent polypeptide to allow protein folding into their native states [88].

In nucleotide-free conditions, apical domains of CCT are in an open conformation that exposes substrate-binding sites [89-91]. ADP-AlF_x [92, 93] mimics the trigonal-bypyramidal transition state of the ATPase reaction and induces formation of lid closure [87], whereas ADP-bound CCT is in an open state [94]. The ATP-binding action within the subunits of the ring seems to be positively cooperative [95, 96], resulted in a concerted mode of action during lid closure. In contrast, the inter-ring cooperativity seems to be negative, resulting in decreased affinity for nucleotide binding in one ring while the other ring is occupied. Although most studies have focused on analyzing CCT as a whole molecular complex, evidence has shown that the CCT oligomer is dynamic and is capable of disassembling and reassembling under physiological conditions and changes of ATP and potassium ions [97, 98]. Moreover, CCT monomers may have activities themselves as monomeric subunits [99].

The complexity of CCT and its divergence in the apical domain allow CCT to recognize a variety of substrates based on their sequence, structural geometry, and physical properties in the context of protein biogenesis [100]. These interactions seem to be highly sequence-specific such as the binding of actin and tubulin [10, 88]. Although most GroEL substrate recognition

sequences are hydrophobic, CCT can bind to its substrates through hydrophobic or electrostatic interactions with different motifs including polar and hydrophobic residues. Most CCT substrates are large, hydrophobic, aggregation-prone proteins with regions of β-strand propensity [81, 101, 102]. Furthermore, many CCT substrates cannot be folded by other prokaryotic and eukaryotic chaperones [103], and many CCT substrates are not found in bacterial genomes [104].

PhLP1 is not a substrate of CCT, but it interacts with CCT in its native form and regulates the activity of CCT [57]. The cryo-EM structure of the dephosphorylated PhLP1-CCT complex [105] revealed that PhLP1 is bound on top of the central cavity, making contacts with the tips of the apical domains of CCT subunits. PhLP1 also spans the entire central cavity and constricts the helical extensions of the apical domains, occluding the folding cavity. This structure is analogous to the prefoldin-CCT structure in which prefoldin sits above the folding cavity to perform its co-chaperone role in delivering actin and tubulin to CCT for folding [106]. It is also similar to the GroES protein that forms a lid for GroEL to entrap its folding substrates. Interestingly, Pdc does not share this CCT-binding ability with PhLP1 [57]. Therefore, this structural evidence suggested that PhLP1 is a co-chaperone of CCT like prefoldin and GroES.

PhLP1 is an important co-chaperone in Gβγ assembly

While efforts in our lab were determining the interaction between PhLP1 and CCT, several studies reported that WD40 repeat proteins such as Gβ were important CCT clients. A proteomic analysis showed that yeast CCT interacts with proteins containing WD40 repeats; these show weak sequence homology within an approximate 40 amino acid sequence ending in WD, and folds into the blades of β-propeller structures. These β-propeller blades consist mostly of anti-parallel β-strands [107, 108]; the folding process is believed to be difficult and to often require chaperones for their folding due to the need for long-range contacts between β-strands that are

hydrophobic and aggregation-prone [109]. Several WD40 repeat proteins have been found to require CCT for their folding.

A genetic study in *Dictyoselium* showed that Gβ requires CCT and PhLP1 for folding - deletion of PhLP1 mimics the phenotype of Gβ deletion [110]. Furthermore, Gβ and Gγ were not able to associate with the plasma membrane in the absence of PhLP1 even though they could be expressed individually, suggesting that the formation of Gβγ dimers was disrupted [110]. All of these data pointed to the possibility that PhLP1 participates in Gβ folding and assembly of the Gβγ dimer. Several experiments have provided evidence to support this hypothesis. First, in a pulse-chase experiment, siRNA-mediated PhLP1 knockdown in HEK-293 cells resulted in a 5-fold reduction in the rate of Gβγ assembly [73]. Second, an ectopically expressed PhLP1 N-terminal truncation (PhLP1 Δ1-75) variant lacking an essential Gβ-binding site in Helix 1 completely inhibited Gβγ assembly [3, 73]. Although this variant still binds CCT, its ability to bind Gβ was greatly diminished. This variant competed strongly with endogenous PhLP1 to bind CCT, but it was not able to bind Gβ and assist in Gβγ assembly. Thus, this variant was acting as a strong dominant negative inhibitor of PhLP1 function by disrupting the assembly process. Intriguingly, this PhLP1 Δ1-75 variant is similar to a splice variant of PhLP1 that occurs naturally. This naturally occurring splice variant lacks the N-terminal 83 amino acids [59, 66], but it is only expressed in low levels and in certain tissues, indicating that it may also be involved in controlling Gβγ signaling. These experiments along with several other reports [111, 112] provided strong support for the hypothesis that PhLP1 can mediate Gβγ assembly.

PhLP1 phosphorylation is important for mediating Gβγ assembly

Several studies have provided clues to the mechanism of PhLP1-mediated Gβγ assembly. One study showed that ATP triggers the release of Gβ from CCT to form Gβγ dimers. No association between Gγ and CCT was detected, suggesting that Gβ was released from CCT upon binding to Gγ [113]. Another study has also shown that PhLP1 can form a ternary complex with Gβ-CCT [114], and the CK2-mediated phosphorylation of PhLP1 at a triple serine sequence near the N-terminal domain affects the stability the PhLP1-$G\beta_1$-CCT complex [114].

PhLP1 phosphorylation at S18-20 by CK2 is a key event in the process of Gβγ assembly [66, 73, 114]. Based on mutagenesis data measuring the effect of S18-20 alanine substitutions on the rate of Gβγ assembly, at least 2 of these 3 serines must be phosphorylated for PhLP1 to facilitate the assembly of Gβγ effectively, and the S20 phosphorylation site is the most important residue [114]. As a result, a PhLP1 S18-20A variant is an effective dominant negative inhibitor of Gβγ assembly. Since PhLP1 Δ1-75 is also missing the S18-20 phosphorylation site and the Gβ binding site, it is an even more potent inhibitor of Gβγ assembly than the S18-20A variant. Both PhLP1 S18-20A and PhLP1 Δ1-75 variants can dramatically increase the binding of Gβ to CCT due to the inability of these PhLP1 variants to [114] release Gβ from the CCT complex.

From this data, a model has been described for the folding of Gβ and its assembly with Gγ (Figure 1-3). First, nascent Gβ polypetides bind CCT soon after synthesis on the ribosome to prevent aggregation of Gβ [102]. PhLP1 then associates with Gβ-CCT to form a PhLP1-Gβ-CCT ternary complex. If PhLP1 is phosphorylated at S18-20 by the protein kinase CK2, it releases Gβ from CCT as a PhLP1-Gβ complex. It is possible that electrostatic repulsion between the phosphates in S18-20 of PhLP1 and negatively charged residues on the apical

domains of CCT is the driving force for the release of PhLP1-Gβ. Once released, Gβ can associate with Gγ and form a PhLP1-Gβγ complex. The dimerized form of Gβγ is very stable and can only be dissociated through denaturation [115]. Proper plasma membrane targeting of heterotrimeric G proteins requires association between Gα and Gβγ subunits [116], so the Gα subunit eventually binds to the Gβγ subunits to form a heterotrimer. In this process, PhLP1 must be displaced since PhLP1 and Gα share a common binding site on the Gβγ subunits [65, 114]. The displacement of PhLP1 allows it to participate in subsequent rounds of Gβγ dimerization. This model explains why G protein signaling is disrupted in cells depleted of PhLP1 because of the inability to form Gβγ dimers [73].

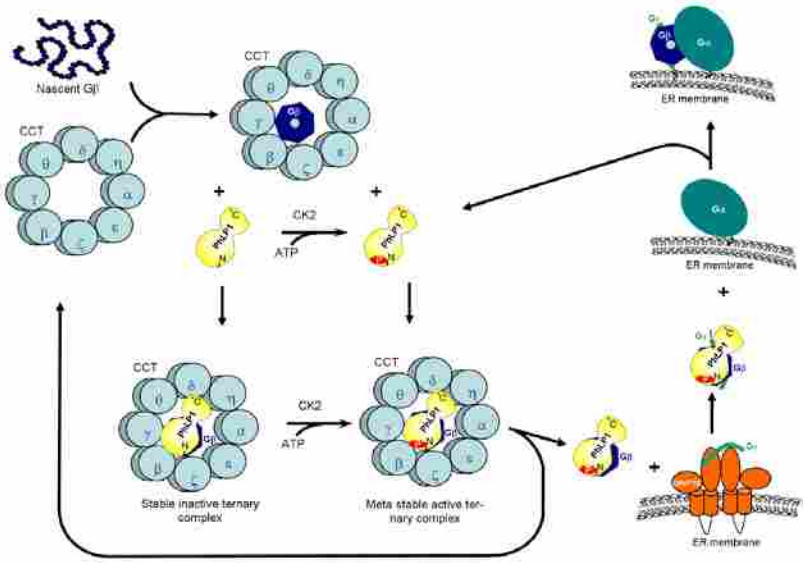

Figure 1-3. A model of PhLP1-mediated Gβγ dimer assembly. PhLP1 binds CCT and nascent Gβ to form a stable ternary complex. Electrostatic repulsion between CK2-phosphorylated PhLP1 and CCT triggers the release of PhLP1·Gβ from CCT. The newly released PhLP1·Gβ then forms a complex with Gγ. Gα displaces PhLP1 and associates with the Gβγ dimer allowing PhLP1 to engage in another cycle of Gβγ assembly.

Post-translational modification of G proteins subunits

After chaperone-assisted protein folding of Gβ and Gγ subunits, post-translational modification of Gα and Gγ is required for the G protein subunits to be localized to membranes properly [117]. After Gβγ is assembled, the C-terminus of Gγ subunits is prenylated with 15-

carbon farnesyl or 20-carbon geranylgeranyl group through a thioester bond. This reaction is mediated by a isoprenyl transferase enzyme that targets the carboxyl terminal CaaX motif of the Gγ subunits [118]. For γ1, γ 9 and γ11, the serine at the X position codes for farnesylation, whereas the other Gγ subunits have leucine at the X position and codes for geranylgernaylation [116]. This modification greatly increases the association of Gβγ with lipid bilayers.

Gα is also anchored to the membrane through lipid modifications. Gα subunits of the $G\alpha_i$ family, including $G\alpha_i$, $G\alpha_o$, $G\alpha_z$, and $G\alpha_t$ subunits are all myristoylated, which is the attachment of the 14-carbon fatty acid myristate group to a glycine at the N-terminus of the Gα protein. This reaction is catalyzed by the enzyme N-myristoyl transferase (NMT) [119]. In addition, a 16-carbon fatty acid palmitate group is attached to one or more cysteine residues within N-terminal 20 amino acids of all the Gα subunits through a thioester bond for all Gα subunits with the exception of $G\alpha_t$. The palmitoylation is reversible, but the myristoylation is irreversible [116]. Once the Gαβγ heterotrimer is formed and post-translationally modified, the heterotrimer is trafficked to the plasma membrane, most likely in a complex with a GPCR [116].

Specificity of PhLP1-mediated Gβγ assembly

Most studies on Gβγ assembly have concentrated on a common Gβγ pair, the $G\beta_1\gamma_2$ dimer. Since there are five isoforms for Gβ and twelve isoforms for Gγ, it was not clear whether all these isoforms were assembled similarly. $G\beta_1$ and $G\beta_4$ both form dimers with all Gγs, whereas $G\beta_2$ and $G\beta_3$ only interact with specific Gγ isoforms [120]. All Gβ and Gγ subunits are obligate dimers and are irreversibly associated, with the exception of the $G\beta_5$ subunit [116]. $G\beta_5$ does not associate with Gγs but instead interacts with the RGS subfamily 7, which consists of RGS6, 7, 9 and 11 [121]. $G\beta_5$ can bind a Gγ-like (GGL) domain on RGS7 similar to the binding of other

Gβs to Gγ [7]. The $G\beta_5$-RGS complex is the principal GAP for GTP hydrolysis of Gα subunits in neuronal cells [121].

A comprehensive study was carried out to study the role of PhLP1 in assisting the assembly of different Gβγ and $G\beta_5$-RGS combinations [122]. PhLP1 binds all five isoforms of Gβ. $G\beta_{1\text{-}4}$ bound similarly to PhLP1, whereas $G\beta_5$ bound PhLP1 ~4 fold weaker than the other Gβs. Moreover, 70% siRNA-mediated PhLP1 knockdown resulted in a 70-80% decrease in assembly between $G\beta_{1\text{-}4}$ and $G\gamma_2$ [122]. Furthermore, over-expression of the dominant negative PhLP1 Δ1-75 variant has reduced the assembly between $G\beta_{1\text{-}4}$ and $G\gamma_2$ by 80-90%, supporting the idea that PhLP1 mediates the assembly of all $G\beta_{1\text{-}4}$ isoforms that dimerize with Gγs.

In reciprocal experiments, siRNA-mediated PhLP1 knockdown or PhLP1 Δ1-75 variant over-expression inhibited assembly between $G\beta_2$ and all twelve Gγ isoforms by ~80% [122]. Another recent study also showed that $G\beta_{1\text{-}4}$ can bind CCT, and the assembly of $G\beta_1\gamma_2$, $G\beta_1\gamma_3$ and $G\beta_2\gamma_3$ required CCT [113]. All this evidence supports the notion that PhLP1 functions as a co-chaperone of CCT for assembly of all Gβγ combinations. Moreover, the effects of PhLP1 did not discriminate the combinations of $G\beta_2\gamma_x$, as evidenced by the fact that siRNA knockdown or PhLP1 Δ1-75 overexpression consistently inhibited Gβγ assembly by ~80% regardless of the original extent of Gβγ dimer formation. The results of this study indicate that PhLP1 does not specify the combinations of Gβγ assembly but only assists in the association of Gβγ subunits that can form stable dimers. Moreover, the stability of $G\beta_2\gamma_x$ dimers can be classified distinctively into Gγ subfamilies, indicating that the amino acid sequence of the Gγ subunit can determine the specificity of the $G\beta_2$ and Gγ subunit interactions due to the complementarity of their binding surfaces [122].

Assembly of $G\beta_5$-RGS7 signaling complex

The GGL-domain of RGS9 occupies the same contact site on the $G\beta_5$ β-propeller as does Gγ1 [7] (Figure 1-4), suggesting that the $G\beta_5$-RGS complex may be assembled by a similar mechanism as Gβγ. However, $G\beta_5$ associates with CCT and PhLP1 with much lower affinity than $G\beta_1$ does [113, 114], suggesting that the mechanism for $G\beta_5$-RGS assembly might be significantly different from Gβγ. To test this idea, the role of PhLP1 and CCT in the process of $G\beta_5$-RGS7 assembly was assessed in the HEK-293 cell cultures [122]. A two-fold reduction in the rate of $G\beta_5$-RGS7 assembly was achieved by an 80% siRNA-mediated PhLP1 knockdown. This reduction in assembly rate was less than the five-fold decrease with $G\beta_1\gamma_2$ assembly under the same conditions [73, 114]. Moreover, 50% knockdown of CCT by siRNA has resulted in a two-fold decrease in both the assembly rates of $G\beta_5$-RGS7 and $G\beta_1\gamma_2$, suggesting that $G\beta_5$-RGS7 assembly is dependent on CCT but perhaps less dependent on PhLP1.

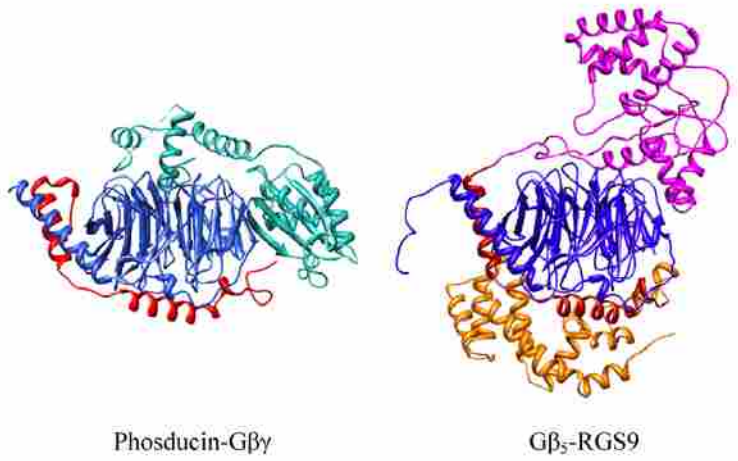

Figure 1-4. The atomic structures of Pdc-Gβγ and $G\beta_5$-RGS9 complexes.
PhLP1 is predicted to compete with the DEP/DHEX domain of the N-terminal domain in RGS9 to bind $G\beta_5$. The overlapping binding site hinders the association between PhLP1 and the $G\beta_5$-RGS dimer. Color code of individual molecules: phosducin – teal, Gβ1 – blue, Gγ – red, $G\beta_5$ – dark blue, RGS DEP/DHEX domain – magenta, RGS Gγ-like domain – dark red, RGS domain – orange. PDB numbers for the structures: Pdc-Gβγ (1A0R) [3] and $G\beta_5$-RGS9 (2PBI) [7].

Several additional experiments were performed to determine the role of PhLP1 in $G\beta_5$-RGS7 assembly. First, over-expression of wild type PhLP1 caused a ~25% reduction in the rate of $G\beta_5$-

RGS7 assembly. This effect was in contrast to the 4-fold increase in $G\beta_1\gamma_2$ assembly under the same conditions [73, 114]. Second, over-expression of PhLP1 resulted in a 10-fold increase in the amount of $G\beta_5$ binding to CCT regardless of whether RGS7 was co-expressed or not. This observation was also in contrast to the effects of PhLP1 over-expression in enhancing the release of $G\beta_1$ from CCT [114].

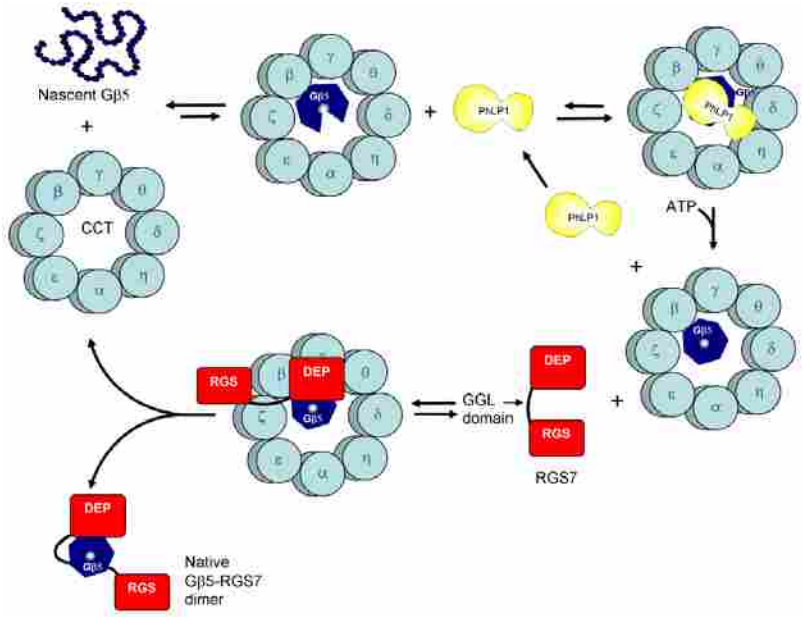

Figure 1-5. Proposed mechanism of $G\beta_5$-RGS7 assembly. $G\beta_5$ associates with CCT weakly but is not able to fold into its native state in the absence of PhLP1. PhLP1 stabilizes the $G\beta_5$-CCT complex and assists $G\beta_5$ to fold into its native state. Phosphorylation of PhLP1 and ATP hydrolysis on CCT allows PhLP1 to be released from the PhLP1-$G\beta_5$-CCT complex. After the release of PhLP1, RGS7 then interacts with the folded $G\beta_5$ on CCT via its N-terminal DEP/DHEX domain [7]. Upon association, the $G\beta_5$-RGS7 complex can be released from CCT as a functional dimer.

These differences in the roles of PhLP1 in the assembly of $G\beta_5$-RGS and $G\beta\gamma$ can be explained by the way PhLP1 is binding to these dimers. PhLP1 binds $G\beta_1\gamma_2$ and $G\beta_5\gamma_2$ with a dissociation constant of 100 nM and 440 nM, respectively, whereas the binding of PhLP1 to $G\beta_5$-RGS complex was undetectable [122]. These binding differences can be explained by structural analysis of the Pdc-$G\beta\gamma$ and $G\beta_5$-RGS9 complexes. As described previously, Pdc can bind $G\beta\gamma$ on the same contact site as $G\alpha$. This site is on the opposite side of the $G\beta$ subunit β-propeller that $G\gamma$ binds [3]. Since PhLP1 shares extensive homology with Pdc, it is likely that PhLP1 also binds $G\beta\gamma$ like Pdc. Therefore, PhLP1 can still bind $G\gamma$-associated $G\beta$. In contrast, The DEP/DHEX domain of the N-terminal lobe of RGS9 interacts with $G\beta$ at the side as PhLP1

[7], precluding the formation of a PhLP1-Gβ_5-RGS9 complex due to the overlapping binding sites. Accordingly, it appears that PhLP1 must be released from Gβ_5 subunit prior to the association of Gβ_5 with RGS.

A model based on the current data to depict the role of PhLP1 in Gβ_5-RGS assembly is shown in Figure 1-5. In both models of G$\beta\gamma$ and Gβ_5-RGS assembly, CCT is required for the folding of Gβ subunit. PhLP1 stabilizes the interaction between Gβ_5 and CCT to enhance substrate folding. PhLP1 is released from the Gβ_5-CCT complex before Gβ_5 can associate with RGS, whereas PhLP1 can still bind to Gβ in the presence of Gγ. The need for PhLP1 to stabilize the Gβ_5-CCT complex coupled with the requirement for PhLP1 release prior to Gβ_5-RGS assembly can explain why Gβ_5-RGS7 assembly was decreased by either increasing or decreasing the cellular level of PhLP1. This model also suggests that Gβ_5 can associate with RGS while binding to CCT. The basis for this prediction is the observation that RGS was recruited to CCT by Gβ_5, leading to the formation of RGS7-Gβ_5-CCT ternary complex intermediate [122]. Previous evidence has shown that RGS7 can interact with Hsc70 [123, 124], suggesting that Hsc70 can deliver nascent RGS proteins to the Gβ_5-CCT complex. After the Gβ_5-RGS complex is formed, it can be released from CCT to interact with membrane anchoring proteins and eventually becomes fully stabilized to assist in accelerating GTP hydrolysis on Gα subunits [125].

Physiological roles of other phosducin family members

The phosducin gene family is conserved among organisms ranging from single cell eukaryotes to mammals. This gene family can be classified into three subgroups [110]. Subgroup I consists of Pdc and PhLP1, subgroup II is composed of PhLP2A and PhLP2B [110, 126, 127], and subgroup III is represented by PhLPII. The physiological functions of the subgroup II and III

genes have not been thoroughly investigated. Nonetheless, PhLP2A is essential for cell growth in yeast *Saccharomyces cerevisiae* [128] and the soil amoebae *Dictyostelium discoideum* [110]. PhLP3 is believed to be involved in β-tubulin and actin folding [129, 130]. Although these members of the phosducin gene family seem to have diverse cellular functions, most evidence supports a role for PhLP1-3 as co-chaperones in protein folding while Pdc may be unique in its function in regulating Gβγ signaling in the phototransduction processes.

Conclusion

Since GPCRs regulate a large variety of physiological processes, it is vitally important to regulate GPCR signaling at different levels. Pdc and PhLP1 of the phosducin family serve different roles in regulating the GPCR signaling in the retina and other tissues in mammals. Recent studies have firmly established the physiological role and significance of PhLP1 as a molecular co-chaperone with CCT to mediate Gβγ assembly. Although a general mechanism of Gβγ assembly has been postulated, many of the mechanistic details about this process are still missing. Structural analysis of each intermediate step in CCT-assisted Gβ folding can generate snapshots of the assembly process and provide an accurate account of the mechanism beyond current understanding. Therefore, we have embarked on an endeavor to determine the structures of two key intermediates, CCT-$G\beta_1$ and CCT-$G\beta_1$-PhLP1, in the Gβγ assembly process. Structural information of these complexes will also allow us to understand the interactions between CCT, $G\beta_1$, and PhLP1 by providing the molecular details of the Gβγ assembly process. These details provide the foundation for the development of therapeutics to control Gβγ assembly and thereby regulate G protein signaling.

CHAPTER 2:
STRUCTURES OF THE $G\beta_1$-CCT AND PHLP1-$G\beta_1$-CCT COMPLEXES REVEAL INSIGHTS INTO THE MECHANISM OF $G\beta\gamma$ ASSEMBLY

Summary

G-protein coupled receptor signaling is essential for many physiological processes. Since the regulation of these responses is vitally important, GPCR signaling pathways are carefully controlled at different levels within the cascade. The phosducin-like protein 1 (PhLP1) can bind the G protein β subunit and contribute to GPCR signaling. Recent evidence has supported the concept that PhLP1 serves as a co-chaperone of the eukaryotic cytosolic chaperonin complex (CCT/TRiC) and forms a ternary complex with the $G\beta_1$-CCT complex to mediate $G\beta\gamma$ assembly. CCT/TRiC plays a crucial role in the folding of many essential proteins. Here we show three-dimensional reconstructions of the $G\beta_1$-CCT and the PhLP1-$G\beta_1$-CCT complexes assembled *in vivo.* An electron microscopic analysis reveals that $G\beta_1$, representing the WD40 repeat proteins which are a major class of CCT substrates, interacts specifically with the apical domain of CCTβ. $G\beta_1$ binding experiments with several chimeric CCT subunits confirm a strong interaction with CCTβ and map $G\beta_1$ binding to a hydrophobic core of amino acids located in α-Helix 9 and in the loop between β-strands 6 and 7, facing the chaperonin cavity. Fitting the Gβ molecule into the two 3D reconstructions ($G\beta_1$-CCT and PhLP1-$G\beta_1$-CCT) reveales that upon PhLP1 binding to $G\beta_1$-CCT, the quasi-folded Gβ molecule is constricted to a native state and shifted to an angle that can lead to the release of folded $G\beta_1$ from CCT. Moreover, mutagenesis of the CCTβ subunit suggests that PhLP1 can interact with the tip of the apical domain of the CCTβ subunit at residue S260, which is a downstream phosphorylation target site of activated

RSK and S6K from the Ras-MAPK and mTOR pathways. Together, these results reveal a novel mechanism of PhLP1-mediated Gβ folding and its release from CCT.

Introduction

GPCR signaling pathways regulate a large variety of physiological responses such as vision, cardiac rhythm, taste, growth, neuronal signals [15, 21, 22], and the malfunctioning of these signaling processes can lead to devastating diseases such as cancer, heart disease, vision impairment, neural diseases, and hypertension [16-20]. Many different ligands such as small molecule neurotransmitters, peptide hormones, chemokines, lipids, odorants and even photons of light can trigger the activation of GPCR signaling and in turn initiate the signaling processes through the intracellular G proteins. Upon binding of a ligand to the extracellular domain of a GPCR, a conformational change takes place in the packing of the seven transmembrane α-helices of the activated GPCR. This conformational change propagates to the intracellular surface of the GPCR and activates heterotrimeric G proteins that associate with the receptor. This activation process promotes the exchange of GDP for GTP on the G protein α subunit (Gα) and leads to the dissociation of Gα-GTP from the G protein βγ subunits (Gβγ). Gα-GTP and Gβγ in turn regulate the activity of effector enzymes and ion channels that mediate the cellular response to the ligand. Upon the hydrolysis of GTP to GDP, the G protein cycle terminates and the Gαβγ complex is reformed with the reassociation of Gα-GDP with Gβγ [16]. Since the regulation of these physiological responses is critical, GPCR signaling pathways are carefully controlled at different levels within the cascade. Gβγ signaling can be regulated by associating with Pdc [52-55] and PhLP1 [56, 57] to control the amount of available Gβγ to interact with Gα-GTP or with other effectors. Recent studies have shown that the PhLP1 can serve as a co-

chaperone of the chaperonin containing tailless complex polypeptide 1 (CCT) to facilitate Gβγ signaling [57, 73, 105, 114].

CCT is a group II chaperonin family. Group I chaperonins are found in prokaryotes and eukaryotic organelles of endosymbiotic origin and whose best characterized member is GroEL from *E. coli* [131]. GroEL and the rest of the Group I chaperonins have a double heptameric ring structure and assist protein folding through cooperation with a small heptameric co-chaperonin termed GroES in *E. coli* [132], which acts as a lid, isolating the unfolded protein in the chaperonin cavity. Group II chaperonins, found in eukaryotes and archaea, share an overall architecture with their bacterial counterparts, but they differ from them in several aspects [133]. First, they are composed of 1-3 different subunits and form either octameric or nonameric double ring structures. Second, they lack a co-chaperone that acts as a lid but instead rely on an additional structure, a built-in helical protrusion, which also caps the chaperonin cavity and isolates the unfolded protein in its interior.

The eukaryotic cytosolic chaperonin CCT (Chaperonin Containing TCP-1; also termed TRiC) is the most complex of all chaperonins [134]. This complexity is due not only to the fact that it is composed of 8 different but homologous subunits, but also that its mechanism seems to be very different from the other chaperonins. Whereas the folding mechanism of GroEL (and probably of the archaeal group II chaperonins, also named thermosomes) relies on non-specific, hydrophobic interactions between residues of the chaperonin apical domains and the unfolded polypeptide [80, 135], the folding mechanism of CCT seems to be based on specific interactions between charged and polar residues located in particular regions of the unfolded protein and specific CCT subunits [134]. This has been shown to be the case for the major CCT substrates, the cytoskeletal proteins actin and tubulin [85, 136]. However, recent studies have shown that hydrophobic

interactions are involved in the direct association of CCT with several substrates. This is the case for the tumor suppressor protein VHL [137] and the G protein β_1 subunit ($G\beta_1$) [102].

$G\beta_1$ is a member of the WD40 repeat family of proteins, a large group defined by the presence of a β-propeller structure. They exhibit a high degree of functional diversity, although many of them are involved in protein-protein interactions that anchor multi-subunit complexes [104]. Early proteomic studies of the yeast interactome revealed interactions of many WD40 proteins with CCT [134], and further analysis of the CCT interaction network identified a propensity for large β-sheet structures among CCT substrates, including WD40 proteins [81]. In addition to Gβ, other WD40 proteins that have been shown to be CCT substrates include Cdc20 and Cdh1, which are part of the anaphase promoting complex that plays a key role in cell cycle progression [101]. The atomic structure of Gβ is known [68] and consists of a seven-bladed β propeller, each blade formed by a WD40 motif consisting of four antiparallel β-strands, and a small N-terminal α-helix. The folding of Gβ is a complex process that is initiated by an interaction with CCT [113, 114].

Recent structural and biochemical studies have supported a model in which PhLP1 acts as a co-chaperone that is required for the release of Gβ from CCT and its subsequent association with Gγ [73, 114]. In this model, nascent Gβ polypetides bind CCT soon after polypeptide synthesis to prevent aggregation of Gβ [102]. PhLP1 then associates with Gβ-CCT to form a PhLP1-Gβ-CCT ternary complex. If PhLP1 is phosphorylated at three consecutive serine residues near its N-terminus (S18-20) by the protein kinase CK2, it releases Gβ from CCT, possibly because of electrostatic repulsion between the phosphates in S18-20 of PhLP1 and negatively charged residues on the apical domains of CCT. This repulsive force may result in the release of a PhLP1-Gβ intermediates that can associate with Gγ and form a PhLP1-Gβγ complex. The Gα

subunit then binds to the Gβγ subunits to form a heterotrimer. In this process, PhLP1 must be displaced since PhLP1 and Gα share a common binding site on the Gβγ subunits [65, 114]. The displacement of PhLP1 allows it to participate in subsequent rounds of Gβγ dimerization. Although a model of PhLP1-mediated Gβγ assembly has been postulated, the mechanism by which the Gβ subunit is assisted by PhLP1 to fold into its native state and release from CCT remains unclear.

To understand the structural basis for PhLP1-mediated Gβγ assembly, we have isolated two important intermediates in the assembly process, the $G\beta_1$-CCT and PhLP1-$G\beta_1$-CCT complexes that were assembled *in vivo* in insect cells, and have determined their structures by cryo-electron microscopy (cryo-EM). The structures show that Gβ folds into a quasi-native form in the CCT folding cavity in the absence of PhLP1 and that the association with PhLP1 closes the Gβ structure and shifts it in the CCT folding cavity, suggesting that PhLP1 stabilizes the native form of Gβ and changes its binding contacts with CCT to permit the release of Gβ from CCT.

Experimental Procedures

$G\beta_1$ and PhLP1 baculovirus preparation

Human $G\beta_1$ and PhLP1 cDNA were cloned into the pBlueBac4.5/V5-His-TOPO vector (Invitrogen Cat: K2100-20) following the manufacturer's protocol with slight modifications. In brief, PCR was used to add a C-terminal HPC4 tag (protein C epitope) along with flanking *BamHI* (5′) and *AgeI* (3′) restriction sites to the human $G\beta_1$ cDNA sequence. For PhLP1, a C-terminal His-TEV-Myc tag along with flanking *BamHI* (5′) and *XbaI* (3′) restriction sites was added to the human PhLP1 cDNA sequence (Figure 2-1). The PCR products were introduced into the pBlueBac4.5/V5-His TOPO vector at their corresponding restriction sites using standard

cloning techniques. The $G\beta_1$-HPC4-pBlueBac4.5 and the PhLP1-TEV-myc-His-pBlueBac4.5 vector were co-transfected into *Sf9* cells with the Bac-N-Blue vector (Invitrogen) to facilitate recombination for the generation of recombinant virus. The successfully recombined baculoviruses were identified by lacZ screening and were isolated using plaque assays. The presence of the $G\beta_1$-HPC4 or PhLP1-TEV-myc- His insert was confirmed by PCR and sequencing. The correct clones that express baculovirus were amplified in *Sf9* cells to produce high-titer stocks of baculovirus for expression experiments.

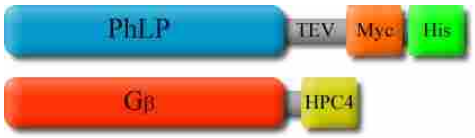

Figure 2-1. Design of PhLP1-TEV-Myc-His & $G\beta_1$-HPC4 for protein expression. The recombinant proteins PhLP1 and Gβ were co-expressed in insect cells using the baculovirus expression system. The PhLP1 construct contains the TEV protease recognition site for tag removal, the Myc-tag for potential antibody-affinity isolation and the His-tag for metal-chelate affinity purification. The Gβ construct contains the C peptide epitope sequence for the HPC4 antibody column affinity purification.

Purification of $G\beta_1$-CCT and PhLP1-$G\beta_1$-CCT complex

Hi5 cells (Invitrogen) were grown on EX405 insect cell medium (Sigma Aldrich). For expression of recombinant PhLP1 and/or $G\beta_1$ proteins, *Hi5* cells were transfected with corresponding baculovirus at an MOI of ~10 and were harvested 72-84 hrs after transfection. Portions of each sample were immunoblotted to confirm recombinant protein expression. Cells were collected by centrifugation at 3,500 g for 15 min and pellets were stored at - 80 ºC. To extract total soluble proteins for $G\beta_1$-CCT purification, cell pellets were resuspended in 3.2 ml HP-Resuspension Buffer (20 mM HEPES pH 7.5, 20 mM NaCl) per gram of cell pellet. For purification of PhLP1-$G\beta_1$-CCT complex, cell pellets were resuspended in 3.2 ml Co-resuspension Buffer (20 mM HEPES pH 8.0, 20 mM) per gram of cell pellet. Protease inhibitors (PMSF 0.5 mM and protease inhibitor cocktail 6 mg/ml (Sigma Aldrich)) were added to the solution, and the cells were lysed by two freeze-thaw cycles in liquid nitrogen and a 37 ºC water

bath (~ 10 min). 24 U/mL of Benzonase nuclease was added to cell extracts to digest genomic DNA into small fragments. Cellular debris was cleared by centrifuging at 20,000 g for 15 min. In addition, 0.05% CHAPS was added to the cell extracts to stabilize the PhLP1-Gβ_1-CCT complex. All subsequent purification steps were performed at 4 ºC.

For purification of the Gβ_1-CCT complex, the cell extract was layered on top of a sucrose cushion of 10 ml/tube 1 M sucrose in 20 mM HEPES pH 7.5, 20 mM NaCl, 0.5 mM PMSF, 6 µl/ml protease inhibitor cocktail in Beckman polyallomer ultracentrifuge tubes (26 x 77 mm). The samples were centrifuged at 93,000 g (30,000 rpm) for 2 hrs. The bottom of the tube was pierced and ~ 8 ml was collected from the sucrose layer, while the rest was discarded. This fraction was diluted 1:1 with HP-Resuspension Buffer and $CaCl_2$ (2 mM) and CHAPS (0.05%) were added. The sucrose cushion product was loaded onto a HPC4 column for further purification.

For the purification of the PhLP1-Gβ_1-CCT complex, the cell extracts were loaded directly into an equilibrated (20 mM HEPES pH 8.0, 20 mM NaCl, 0.05% CHAPS) HisPur Cobalt column. The cobalt column was then washed 3 times with Co-wash buffer (20 mM HEPES pH 8.0, 20 mM NaCl, 0.05% CHAPS). The cobalt column was eluted with 3 fractions of 1 column volume of Co-EL buffer (20 mM HEPES pH 7.5, 20 mM NaCl, 2 mM $CaCl_2$, 0.05% CHAPS, 500 mM imidazole) with 10 min. incubation time between each elution. The cobalt column product was loaded onto an HPC4 column for further purification.

The sucrose cushion product for Gβ_1-CCT purification and cobalt column product for the PhLP1-Gβ_1-CCT purification were further purified on an HPC4 affinity column. The solutions were passed twice through a 5 ml immobilized HPC4 antibody column equilibrated in HP-EQ buffer (20 mM HEPES pH 7.5, 20 mM NaCl, 2 mM $CaCl_2$, 0.05% CHAPS). For the Gβ_1-CCT

purification, the column was washed 5 times with 7 ml of HP-high salt wash buffer (20 mM HEPES pH 7.5, 500 mM NaCl, 2 mM $CaCl_2$) and one additional wash with 7 ml of HP-EQ buffer. For the PhLP1-Gβ_1-CCT purification, the HPC4 column was washed 3 times with 5 mL of HP-wash buffer (20 mM HEPES pH 7.5, 250 mM NaCl, 2 mM $CaCl_2$) and one additional wash with 5 mL of HP-EQ buffer. The product was eluted by adding 5 mL of HP-EL buffer (20 mM HEPES pH 7.5, 20 mM NaCl, 10 mM EDTA) to the column and incubating for 30 min before collection. This elution step was repeated 3 more times with 5 min incubations before each collection. The eluted complexes were concentrated to ~ 200 µl using a 15 ml (10 MWCO) Vivaspin concentrator (Sartorius Stedim Biotech), 10-20% glycerol was added and the sample was stored at – 20^{o}C until cryo-EM analysis was performed. The purified complexes usually reached 95% or higher purity as estimated by SDS-PAGE.

The composition of the insect PhLP1-Gβ_1-CCT complex was determined by mass spectrometry. A portion of the purified complex was denatured in urea, alkylated with iodoacetamide and digested with trypsin. The resulting peptides were analyzed by LCMSMS using an LTQ Orbitrap XL instrument. The MSMS data were analyzed using the Mascot search engine [138] against the Drosophila melanogaster genome database and the human Gβ_1 and PhLP1 sequences. The Drosophila genome is the closest sequenced genome to that of the *Hi5* cells, which are derived from the Cabbage Looper moth, *Trichoplusia ni.* The presence of PhLP1, Gβ_1, CCTα, β and ζ in the complex was confirmed by immunoblotting with anti-PhLP1 [139], anti-Gβ_1 antibody, or anti-CCT monoclonal antibodies (CCTα 91A, CCTβ 4E217 and CCTζ1A4). In addition, the phosphorylation state of purified PhLP1-Gβ_1-CCT was determined by treating with alkaline phosphatase and measuring the phosphorylation-dependent mobility shift in SDS-PAGE.

Preparation of cDNA constructs

The pcDNA3.1 myc-His B+ vector was used for all constructs. N-terminal myc-tagged human PhLP1 was constructed previously [73]. C-terminal FLAG-tagged human α-tubulin was constructed using standard PCR and cloning techniques. N-terminal FLAG-tagged human $G\beta_1$ was obtained from the Missouri University of Science and Technology cDNA Resource Center. Wild type human VHL, CCTβ, CCTδ were obtained from Open Biosystems. CCT constructs were internally HA-tagged (sequence including linker amino acids: GSGYPYDVPDYAGSG) at a loop on the exterior of the apical domain (after G368 of CCTβ and G383 of CCTδ) using standard PCR and cloning techniques. CCT chimeras were created by substituting amino acids of one CCT subunit with the same amino acids of another CCT subunit (see Fig. 2-7). Chimera design included some discontinuous residues to avoid disrupting secondary structure created by Pro residues. Alanine variants were created by site-directed mutagenesis using standard PCR methods.

Cell culture and transfection

HEK-293T cells were cultured in Dulbecco's modified Eagle's medium/Ham's F-12 (1:1) growth media containing 2.5 mM L-glutamine and 15 mM HEPES and supplemented w/ 10% fetal bovine serum. Cells were subcultured regularly but not beyond 25 passages. For transfection, cells were plated in 6-well plates or 60 mm dishes to 90-95% confluency and transfected using Lipofectamine 2000 (Invitrogen), according to the manufacturer's protocol. For CCT incorporation and binding experiments, cells in 60 mm dishes were transfected using 6 μg DNA (3 μg FLAG-$G\beta_1$, FLAG-α-tubulin, FLAG-VHL, Myc-PhLP1 or empty vector control as indicated and 3 μg HA-tagged CCT subunit) and 6 μl Lipofectamine 2000. Cells were fed 12-24 hours post-transfection and harvested 42-48 hours post-transfection.

Binding to CCT variants

The binding of $G\beta_1$, α-tubulin, VHL, or PhLP1 to the HA-tagged CCT variants was determined by co-immunoprecipitation. Transfected HEK-293T cells were washed twice with phosphate-buffered saline (Fisher) and harvested in immunoprecipitation (IP) buffer (phosphate-buffered saline pH 7.4, 1-2% Nonidet P-40 (Sigma Aldrich), 0.6 mM PMSF, and 6 µl/ml protease inhibitor cocktail (Sigma Aldrich P8340)). Lysates were triturated 10 times through a 25-gauge needle and centrifuged at 14,000 rpm for 10-12 min at 4°C in an Eppendorf micro-centrifuge. Protein concentrations were determined using the DC Protein Assay Kit II (Bio-Rad), and approximately equal amounts of protein were used for each sample in the immunoprecipitation. Roughly 450 µg of total protein were used for immunoprecipitation with cells from 6-well plates and 1,000 µg with cells from 60 mm dishes. Clarified lysates from 6-well plates were incubated for 1 hr at 4°C with 1 µg anti-HA antibody (clone 3F10, Roche Applied Science), followed by incubation for 1 hr at 4°C with 30 µl of a 50% slurry of Protein A/G Plus-agarose (Santa Cruz Biotechnology). Lysates from 60 mm dishes were incubated for 1-3 hrs at 4°C with 1.5 µg anti-HA and 1 hr at 4°C with 50 µl of a 50% slurry of Protein A/G Plus-agarose. Beads were then washed three times with 500 µL IP buffer, and immunoprecipitated proteins were solubilized in SDS sample buffer and resolved using 10% SDS-PAGE. For α-tubulin immunoprecipitation, an additional 250 mM NaCl was also added to buffers during incubation and wash steps. Proteins were transferred to nitrocellulose and immunoblotted using anti-PhLP1, anti-FLAG (clone M2, Sigma), anti-HA (Roche Applied Science), anti-CCTδ (AbD Serotec), or anti-CCTε (AbD Serotec) antibodies. Corresponding anti-rabbit, anti-mouse or anti-rat secondary antibodies labelled with the near infrared fluorescent dye 800 CW (LiCor Biosciences) were used, and blots were scanned using the Odyssey Infrared Imaging System (Li-

Cor Bioscience). Protein band intensities were quantified using the Odyssey software. Binding was determined by calculating the ratio of the FLAG-substrate or PhLP1 band to the HA-CCT band for each variant and normalizing the ratio to that of wild-type CCT.

Electron microscopy

For EM, 5 μl aliquots of the $G\beta_1$-CCT or PhLP1-$G\beta_1$-CCT complexes were applied to glow-discharged carbon grids for 1 min. Samples were stained for 1 min with 2% (w/v) uranyl acetate. Images were recorded at 0º tilt in a JEOL 120GX- II electron microscope, operated at 100 kV, on Kodak SO-163 film at 60,000x nominal magnification. For Cryo-EM, 5 μl aliquots of the $G\beta_1$-CCT or PhLP1-$G\beta_1$-CCT complexes were applied to glow-discharged Quantifoil 1.2 μm holey carbon grids for 1 min, blotted for 3 s and frozen rapidly in liquid ethane at -180ºC. Low-dose images (<10e- A-2) of complexes were taken on a FEI Tecnai G2 FEG200 electron microscope at 200 kV using a Gatan side-entry cryo-holder with a nominal magnification of 62,000x and 1.8-3.0 μm underfocus.

Image processing

Micrographs were digitized in a Zeiss SCAI scanner with a sampling window corresponding to 3.5 Å $pixel^{-1}$ for negatively stained samples and 4.2 Å $pixel^{-1}$ for vitrified samples. Two-dimensional classification of the negative-stain data was performed using maximum-likelihood procedures [140]. For the three-dimensional reconstruction of the frozen-hydrated data, samples were processed without any *a priori* assumption. First, images were classified into homogenous groups using reference-free methods (refine2d.py command in EMAN [141], and maximum-likelihood approaches implemented in XMIPP) and selected averages were used to build reference volume using common lines. After several rounds of refinement without symmetry imposition, an extra mass inside the CCT cavity appeared. These structures were calculated from

images selected by EMAN and were subsequently used for a further refinement using projection-matching protocols implemented in the SPIDER package [142]. The resolution of the final structures was estimated with the 0.5 criterion for the Fourier shell correlation coefficient between two independent reconstructions by using BSOFT [143]. The density map and atomic structures were visualized with UCSF Chimera [4]. The threshold was chosen to account for approximately 100% of the protein mass. The atomic structures of Pdc-Gβ_1 [3] and the CCT subunits from the open conformation of the mammalian tubulin-CCT crystal structure [1] were manually fitted with the EM density, and the handedness providing the best fit was chosen to render the EM reconstruction.

Sequence alignment

Sequence alignments of the apical domain of the eight human CCT subunits and of the CCTβ apical domain from various eukaryotes were performed using the ClustalX2 algorithm version 2.0.12 [6].

Generation of the atomic models

The atomic models of CCTβ, and CCTδ were generated with the atomic structure of mouse CCTγ (PDB code 1GML) as template, by homology modelling techniques using the program Swiss-Pdb Viewer and the SWISS-MODEL server facilities [144]. Hydrophobic surfaces were visualized with Pymol (DeLano Scientific, San Carlos, CA).

Results

Isolation of the *in vivo* assembled Gβ_1-CCT and PhLP1-Gβ_1-CCT complex

The Gβ-CCT and PhLP1-Gβ-CCT complexes are key intermediates in the process of Gβγ assembly. These complexes were isolated and their structures were determined by cryo-EM in

an effort to determine the molecular mechanism by which PhLP1 and CCT contribute to the folding and assembly of the Gβγ dimer. Both complexes were purified from insect cells using an affinity capture approach. The $G\beta_1$ cDNA was labelled at its C-terminus with an HPC4 tag, which recognizes a protein C epitope [145], and the PhLP1 cDNA was labelled at its C-terminus with an His-TEV-myc tag (Fig. 2-1). These constructs were cloned into baculovirus and expressed in insect *Hi5* cells. An immobilized HPC4 antibody column was used to purify the $G\beta_1$-CCT complex, while a tandem affinity approach using a Co^{2+}-chelate column and the HPC4 antibody column was used to isolate the PhLP1-$G\beta_1$-CCT complex. The purified products (95 % or higher purity) were analyzed by native and SDS-PAGE electrophoresis (Fig. 2-2 A & 2-3A), which revealed bands migrating at the correct molecular weights for CCT subunits, $G\beta_1$ and PhLP1. The presence of all 8 CCT subunits, $G\beta_1$, and PhLP1 in the *in vivo* assembled complexes was confirmed by immunoblotting and mass spectrometric analyses (Fig. 2-4). To determine if PhLP1 was phosphorylated at S18-20 in this complex, PhLP1-$G\beta_1$-CCT was dephosphorylated with alkaline phosphatase and the effect on the mobility in SDS-PAGE was determined. When PhLP1 is phosphorylated at S18-20 by CK2 its migration in SDS gels is retarded [114]. Alkaline phosphatase treatment caused a distinct decrease in the

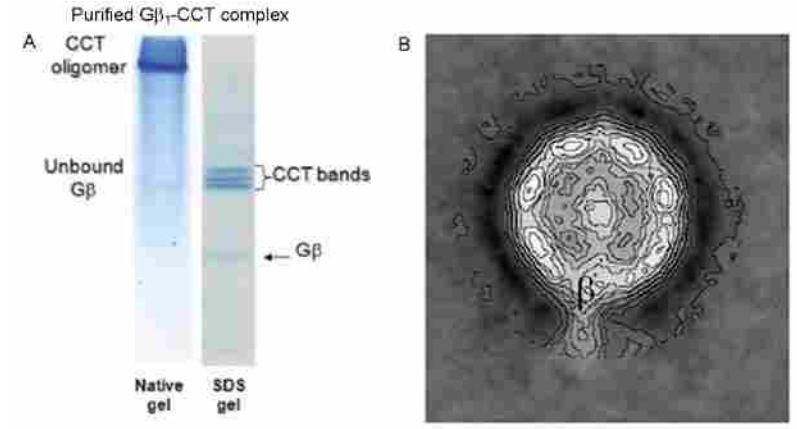

Figure 2-2. Characterization of the purified $G\beta_1$-CCT complex. (A) Electrophoretic analysis of the purified $G\beta_1$–CCT complex. The purified $G\beta_1$– CCT complex was run on both a native gel and an SDS-PAGE gel. B) The two-dimensional average cryo-image of the immuno-complexes formed by the $G\beta_1$-CCT complex and the anti-CCTβ 4E217 (1624 particles) monoclonal antibody, respectively.

mobility of the PhLP1 band (Fig. 2-3 A & B), indicating that the PhLP1 in the purified PhLP1-$G\beta_1$-CCT complex was indeed phosphorylated at S18-20. These results demonstate that the $G\beta_1$-CCT and PhLP1-$G\beta_1$-CCT intermediates in $G\beta\gamma$ assembly could be formed *in vivo* in insect cells and isolated to near homogeneity.

The CCTβ subunit is important for the binding of both $G\beta_1$ and PhLP1

Having been able to obtain very pure, *in vivo* assembled $G\beta_1$-CCT and PhLP1-$G\beta_1$-CCT complexes, we sought to characterize the nature of the interaction between the chaperonin, $G\beta_1$, and PhLP1. Aliquots of these complexes were either negatively stained or vitrified and observed by electron microscopy. For the $G\beta_1$-CCT complex, aliquots of the $G\beta_1$-CCT complex were independently incubated with monoclonal antibodies that react specifically with CCTβ (4E217) [123], and several hundred particles were again selected and used to generate the corresponding two-dimensional average image of the end-on views of the $G\beta_1$-CCT complex bound to these antibodies (Figure 2-2 B). The two average images reveal that the CCTβ subunit was involved in the interaction with $G\beta_1$, which indicate that a stable $G\beta_1$-CCT complex is formed through specific interactions with the CCTβ subunit. Similarly, an immuno-EM of negatively stained specimens of the purified

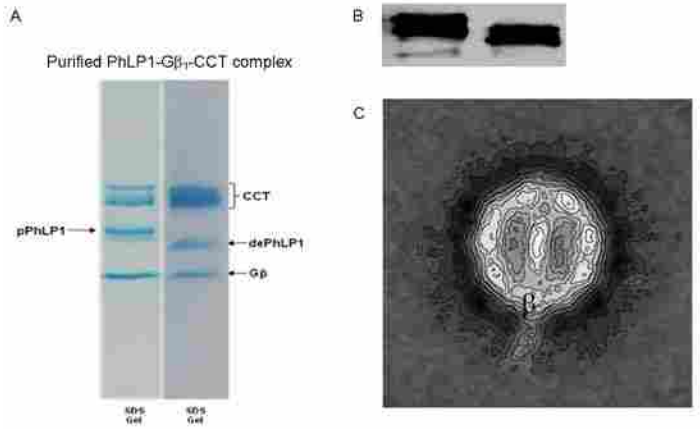

Figure 2-3. Characterization of purified PhLP1-$G\beta_1$-CCT complex.
A) SDS gels of purified PhLP1-$G\beta_1$-CCT complexes in phosphorylated (left) and dephosphorylated (right) states of PhLP1. B) Phosphorylation reaction of PhLP1 in the ternary complex. C) Immunoscopy averaged image of PhLP1-$G\beta_1$-CCT incubated with monoclonal CCTβ antibodies.

A

B

Categories	Protein Info.	Matched Peptide Profile (Bold Red)
Protein	CCT-alpha	
Accession ID	A4V391	
Mascot Score	648	
Protein	CCT-beta	
Accession ID	A4V464	
Mascot Score	667	
Protein	CCT-gamma	
Accession ID	A4V303	
Mascot Score	1663	
Protein	CCT-delta	
Accession ID	Q9VK69	
Mascot Score	340	
Protein	CCT-epsilon	
Accession ID	A1Z8U4	
Mascot Score	142	
Protein	CCT-zeta	
Accession ID	Q9VXQ5	
Mascot Score	378	
Protein	CCT-eta	
Accession ID	Q9VHL2	
Mascot Score	785	
Protein	CCT-theta	
Accession ID	Q7K3J0	
Mascot Score	102	
Protein	G-beta	
Accession ID	P62873	
Mascot Score	5168	
Protein	PhLP1	
Accession ID	Q13371	
Mascot Score	3223	

Figure 2-4. Immunoblotting and mass spectrometry analysis of purified PhLP1-Gβ_1-CCT complex. A) Immunoblots of the purified PhLP1-Gβ_1-CCT complex probed with antibodies raised against PhLP1, Gβ_1, CCTα, CCTβ, and CCTζ are shown. B) Mass spectrometry results of the PhLP1-Gβ_1-CCT complex that matched 8 subunits of CCT, human Gβ_1 and PhLP1 are shown. Amino acid sequences in red indicate peptide matches found in the mascot database.

PhLP1-Gβ_1-CCT complex was subsequently performed by incubating the purified ternary complex with CCTβ monoclonal antibodies to determine which CCT subunit is binding to PhLP1. A total of 1,968 particles were then selected to generate a two-dimensional average image of the end-on views of the PhLP1-Gβ_1-CCT complex bound to the CCTβ antibodies (Figure 2-3 C). The averaged image revealed the presence of a mass spanning the central folding cavity of CCT, interacting with 3 subunits in one side of the cavity and 2 subunits in the opposite side of the CCT complex (Figure 2-3 C). Moreover, the CCTβ subunit was indeed central to the 3 subunits that PhLP1 interacted with in one side of the CCT cavity indicating that PhLP1 also interacted with the CCTβ subunit.

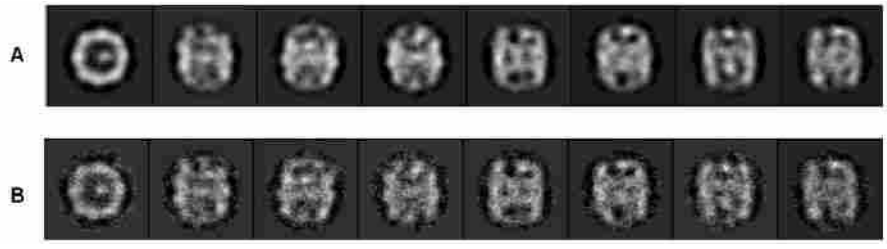

Figure 2-5. Projection of Gβ_1-CCT structure.
A) 2D Projections of the Gβ_1-CCT complex 3D model. B) Actual averaged images of the Gβ_1-CCT complex particles.

Three-dimensional structure of the Gβ_1-CCT complex

We sought to characterize in more detail the interaction between CCT, Gβ_1, and PhLP1 by cryo-EM of vitrified samples of the Gβ_1-CCT and PhLP1-Gβ_1-CCT complexes, in the absence of nucleotide. For the Gβ_1-CCT complex, 23,288 particles were selected, and a two-dimensional maximum-likelihood classification [140] (ML2D) was used to eliminate those particles deviating from the main population (Figure 2-5 A & B), which included some substrate-free particles (although the Gβ_1-CCT complex was purified using a tag on Gβ_1, some particles had lost the Gβ_1 molecule). After image classification, 17,521 homogeneous particles were used to generate a 13 Å three-dimensional reconstruction of the Gβ_1-CCT complex without imposing any symmetry

throughout the reconstruction procedure (Figure 2-6 A & B), which revealed the typical double-ring structure with one ring showing a more open conformation than the other (Figure 2-6 A & B). Inside this ring, an almost cylindrical mass was observed facing the apical region of the chaperonin and interacting mostly with one of the CCT subunits (Figure 2-6 A). This result is consistent with the two-dimensional analysis showing close proximity of $G\beta_1$ to CCTβ. The similarity between the shape of the mass inside the chaperonin cavity and the atomic structure of $G\beta_1$ [68](pdb 2TRC) prompted us to perform a docking analysis of this structure into the corresponding mass of the $G\beta_1$-CCT complex (Figure 2-6 C). Docking of the Gβ atomic structure revealed a good fit when placing the $G\beta_1$ toroidal structure almost parallel to the longitudinal axis of the apical domain, with one of the β-propeller blades facing the apical domain of the main $G\beta_1$-interacting CCT subunit. An open β-propeller conformation of $G\beta_1$ was also docked into the cylindrical mass facing the apical region of the chaperonin, giving an even better fit (Figure 2-6 D). The α-helix located at the N-terminal region of $G\beta_1$ is left outside the mass of the reconstructed $G\beta_1$ since this small mass is probably not visualized at the resolution of this reconstruction. This result suggests that $G\beta_1$ reaches a quasi-native state within the CCT folding cavity, but does not fold completely into its native state.

A similar docking analysis was carried out by fitting the atomic model of the CCTβ subunit from the tubulin-CCT crystal structure [1] into the corresponding mass of the CCT subunit interacting most closely with $G\beta_1$ (Figure 2-6 E & F). The docking shows that the CCTβ apical domain makes contact with one or two of the Gβ β-propeller blades. Optimal fitting of Gβ places β-blade 2 (numbered according to [146]) in closest proximity to CCTβ. In support of this orientation, it has been previously reported that hydrophobic residues from β-strand 3 of

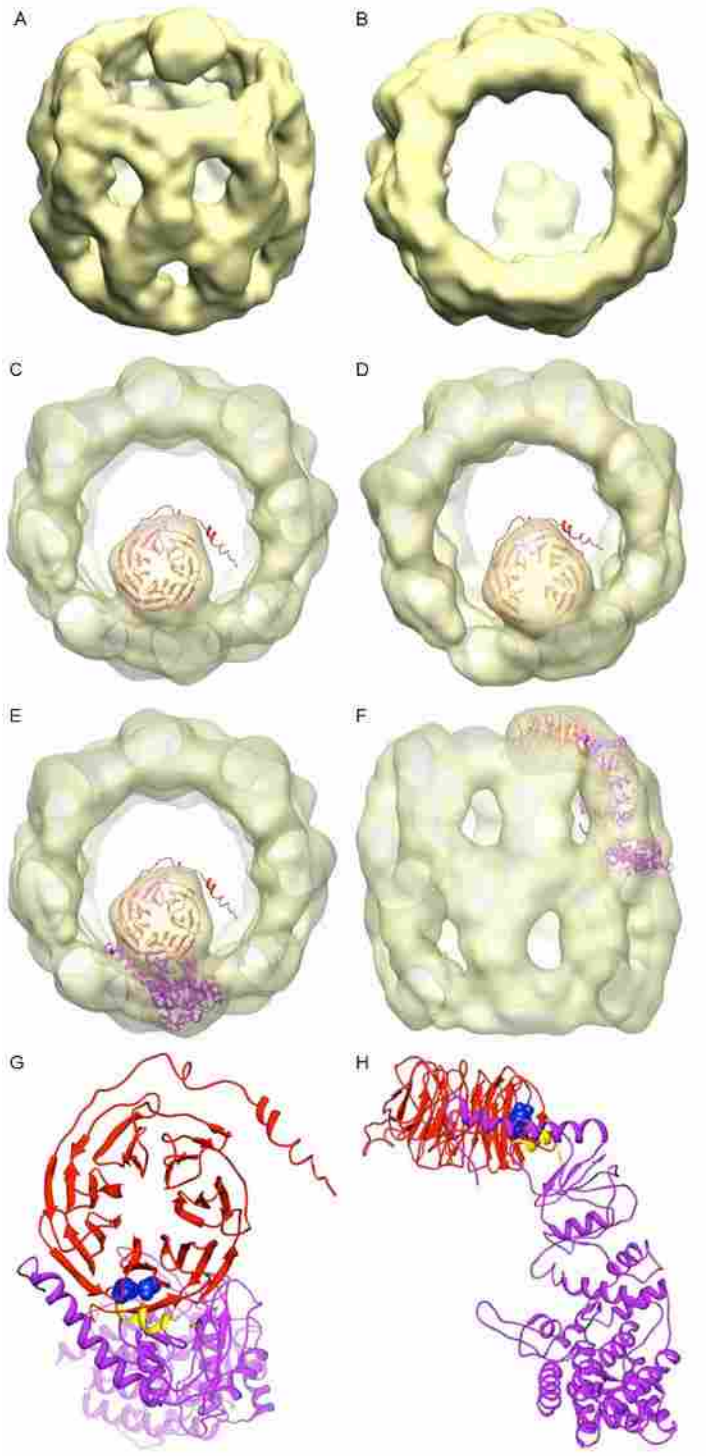

Figure 2-6. Cryo-EM reconstruction of $G\beta_1$-CCT at 13 Å.
A, B) Side and end-on views of the $G\beta_1$-CCT complex. C, D) Docking native state (C) or open β-propeller conformation (D) of $G\beta_1$ atomic structures into the cryo-EM reconstructed complex. E, F) Side and end-on views of the docking of the atomic structure of $G\beta_1$ (pdb 2QNS; in red) and the atomic model of the CCTβ subunit from the tubulin-CCT (purple) crystal structure [1] into the corresponding masses of the reconstructed $G\beta_1$-CCT complex. G, H) Close-up of the $G\beta_1$-CCTβ docking. Blue spheres and yellow ribbons identify residues involved in the proposed binding interaction.

β-blade 2 contribute to $G\beta_1$ binding to CCT [102]. Furthermore, β-blade 2 specifically pointed to α-Helix 9 and the loop connecting β-strands 6 and 7 (numbered according to [10]), suggesting that these regions (shaded blue in Fig. 2-6 E) were involved in the interaction between $G\beta_1$ and CCTβ (Fig. 2-6 G & H). The first of these two regions has already been suggested to be involved in substrate recognition [147, 148]), and both regions host a large number of hydrophobic residues in the CCTβ subunit (Fig. 2-9), which would reinforce the report that $G\beta_1$ interacts with CCT through a set of defined, hydrophobic residues located in one of the β-strands of its β-blade 2 [102] (Fig. 2-6 G & H).

Determination of $G\beta_1$ binding sites on CCTβ through mutagenesis studies

To test the role of CCTβ and the involvement of the specific regions suggested by the docking analysis in $G\beta_1$ binding, we performed a mutational analysis of the CCTβ apical domain. Sequences corresponding to Helix 9 (red in Fig. 2-7A) and the loop between β-strand 6 and 7 (blue in Fig. 2-7A) identified by the cryo-EM analysis as possible $G\beta_1$ binding sites were replaced with the corresponding sequence of other CCT subunits. Replacement sequences were chosen to maximize amino acid differences yet minimize structural perturbations. Chimeras of three additional loops that are more hydrophilic in nature were also made. These loops create a hydrophilic surface previously proposed to line the interior of the CCT folding cavity and bind substrates [10]. These chimeras included the loop preceding the helical protrusion (Chim 242, green in Fig. 2-7A), the loop between α-Helix 9 and β-strand 9 (Chim 293, purple in Fig. 2-7A) and the region encompassed by β-strand 10 and the loop between this strand and α-Helix 10 (Chim 311, orange in Fig. 2-7A). As a control, a chimera was also made of the loop after α-Helix 10 at the back of the apical domain, facing the exterior of the chaperonin, which would not

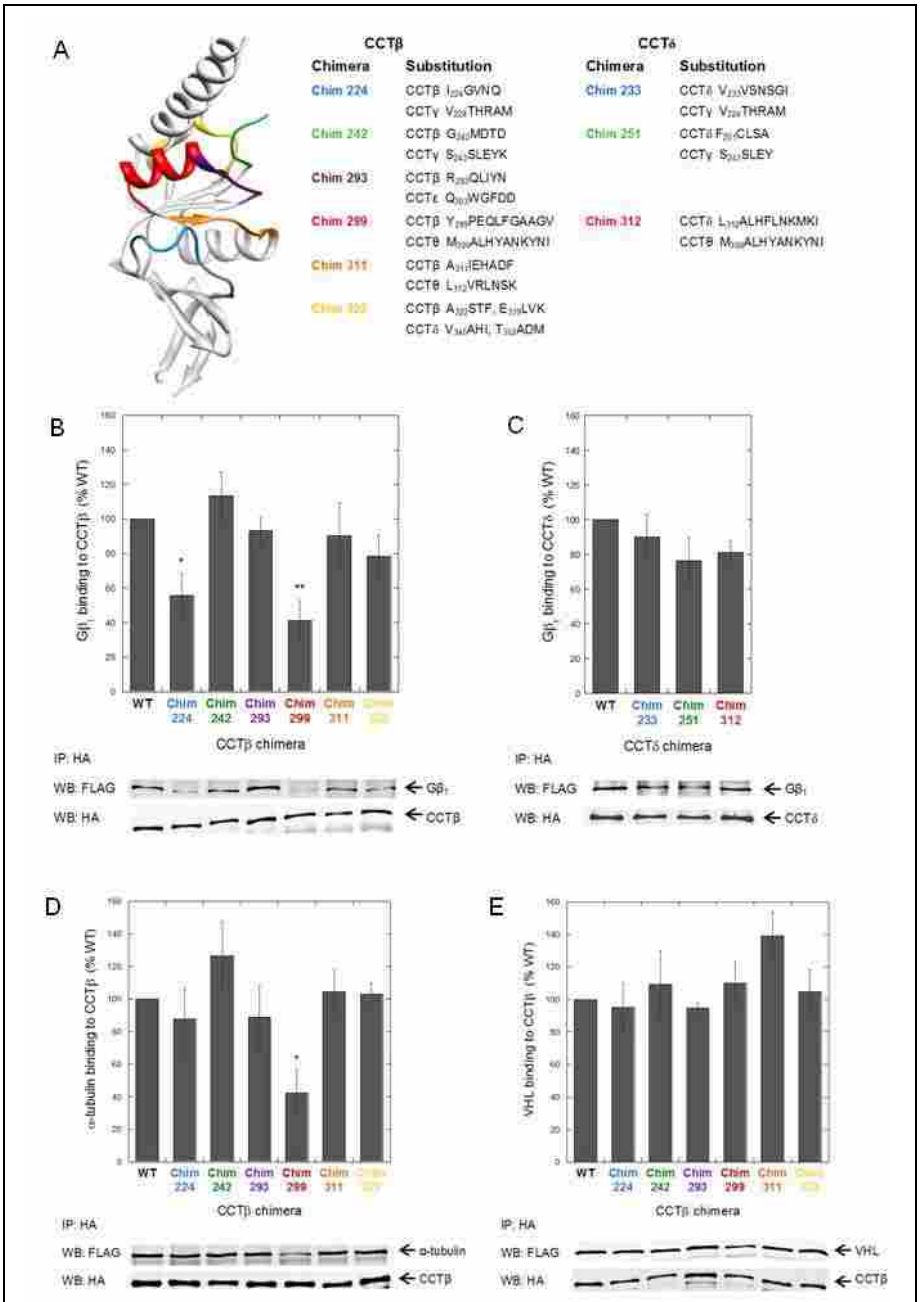

Figure 2-7. $G\beta_1$ and α-tubulin bind a hydrophobic face of CCTβ.
HEK 293T cells were transfected with HA-tagged CCTβ or δ chimeras and FLAG-tagged $G\beta_1$, α-tubulin, or VHL. CCT-substrate complexes were immunoprecipitated with anti-HA antibody, and substrate binding to CCT was measured by Western blotting. A) Design of CCT chimeras. Regions of CCTβ and δ were replaced with corresponding amino acids of other CCT subunits, as indicated in the table. Chimeric regions are mapped on the CCTγ apical domain (1GML), using UCSF Chimera [4]. Chim 322 serves as a control, as its chimeric amino acids are on the exterior of the CCT cavity. B) $G\beta_1$ binding to CCTβ chimeras. C) $G\beta_1$ binding to CCTδ chimeras. CCTδ is across from CCTβ in the folding cavity. D) α-tubulin binding to CCTβ chimeras. E) VHL binding to CCTβ chimeras. Data represent the average ± SEM of at least three experiments; * $p < 0.05$ and ** $p < 0.01$, both as compared to WT. Data from Panels A, B, D, E were provided by Rebecca Plimpton.

be expected to interfere with $G\beta_1$ binding (Chim 322, yellow in Fig. 2-7A). The $G\beta_1$ binding activity of these chimeras was tested by transfecting HEK-293T cells with $G\beta_1$ and HA-tagged versions of the chimeric CCTβ constructs or wild-type CCTβ, immunoprecipitating with an antibody to the HA tag and immunoblotting for $G\beta_1$ to quantify the amount of $G\beta_1$ bound to CCTβ. This method ensures that only the $G\beta_1$ bound to the HA-tagged chimeric subunits was measured. The results show a significant reduction in $G\beta_1$ binding only in chimeras 224 and 299, the two regions suggested by the docking analysis to be involved in $G\beta_1$ interaction (Fig. 2-7B).

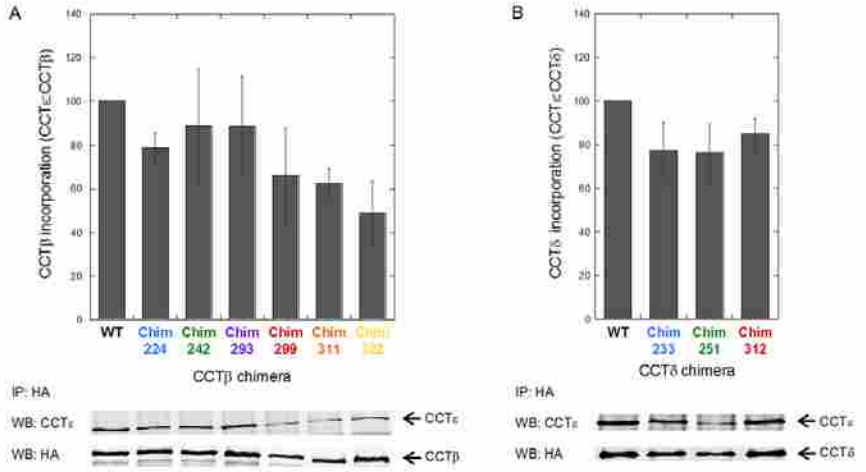

Figure 2-8. Incorporation analysis of CCTβ and CCTδ variants. CCTβ and δ variants incorporate into endogenous CCT complexes. HEK 293T cells were transfected with HA-tagged CCTβ or δ. CCT complexes were immunoprecipitated with anti-HA antibody, and incorporation was measured by Western blotting. A) Incorporation of CCTβ chimeras. B) Incorporation analysis of CCTδ chimeras. Data represent the average ± SEM of at least three experiments. Data from Panel A were provided by Rebecca Plimpton.

To determine if this reduction in $G\beta_1$ binding was specific to the CCTβ subunit, three chimeras were made to corresponding regions in CCTδ, which sits on the opposite side of the CCT toroid as CCTβ [149]. These chimeras corresponded to the two CCTβ chimeras with reduced $G\beta_1$ binding (CCTδ chimeras 233 = CCTβ chimera 224; and 312 = CCTβ chimera 299) and one additional chimera with normal $G\beta_1$ binding (CCTδ chimera 251). None of these chimeras showed a change in $G\beta_1$ binding, indicating that $G\beta_1$ does not interact with these regions of CCTδ (Fig. 2-7C).

Additional binding experiments were performed to determine if other CCT substrates interacted with these regions of the CCTβ apical domain. The binding of α-tubulin and VHL to the CCTβ chimeras was determined by co-immunoprecipitation as described for $G\beta_1$. For α-tubulin, Chim 299 showed a significant reduction in binding while the other chimeras bound similarly to wild-type CCTβ. This result is consistent with previous reports pointing to an interaction of tubulin with CCTβ [1, 136]. For VHL, there was no significant difference in binding between the wild-type CCTβ and any of the chimeras, suggesting that VHL does not interact with the apical domain of CCTβ. This result is also consistent with previous reports that VHL interacts with CCTα and CCTη [147]. In addition, these results show that the chimeric CCTβ subunits were properly folded and capable of binding substrates.

This conclusion was confirmed by measuring the incorporation of the CCTβ and δ chimeras into CCT complexes. All of the chimeras showed at least 50% incorporation compared to wild-type CCTβ, and there was no correlation between the extent of substrate binding and the degree of incorporation, indicating that reduced binding of $G\beta_1$ to the CCTβ 224 and 299 chimeras was not caused by an inability of these chimeras to fold and form viable CCT complexes (Fig. 2-8). Together, the chimera binding data demonstrate a direct interaction of $G\beta_1$ with Helix 9 and loop between β-strand 6 and 7 of the CCTβ apical domain. In addition, the Helix 9 interaction site appears to be shared with α-tubulin. These findings support a structural model that places this face of the CCT apical domains facing the chaperonin cavity in the open confirmation of CCT [150]. Moreover, these results are consistent with previous studies showing specificity in substrate binding to CCT subunits.

It has been reported that $G\beta_1$ interacts with CCT through a series of hydrophobic residues from β-propeller blade 2 [102]. This observation suggests an interaction with hydrophobic residues in the 224-228 and 299-309 regions of CCTβ. Indeed, the hydrophobic profile of these two regions reinforces this notion (Fig. 2-9; Figure 2-10 A). In particular, the 299-309 region has hydrophobic residues covering not only most of α-Helix 9 but also the cleft between this helix and α-Helix 8 (the helical protrusion) (circled in Fig. 2-9). Furthermore, this hydrophobic cleft is not conserved in CCTδ (Fig. 2-9), which is not involved in $G\beta_1$ binding (Fig. 2-7C). Additional support for the importance of the hydrophobic cleft of CCTβ in substrate binding comes from the fact that α-tubulin also interacts with this region and that a highly hydrophobic sequence of β-tubulin, which is conserved in α-tubulin, contributes significantly to CCT binding [151, 152].

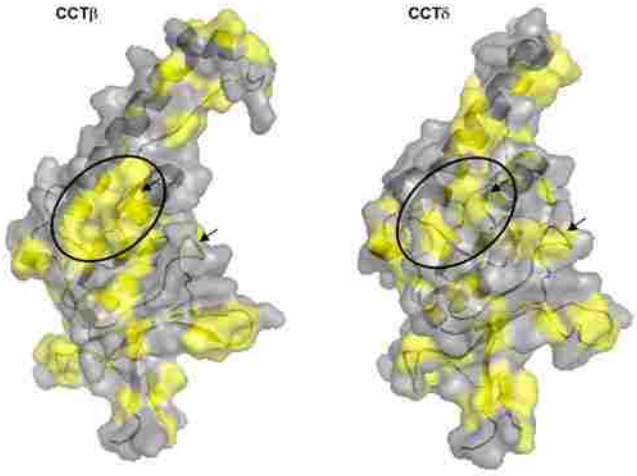

Figure 2-9. Hydrophobic regions of the apical domains of CCTβ and CCTδ.
Hydrophobic surface models of the apical domains of CCTβ and CCTδ (a non $G\beta_1$-interacting subunit) are shown. Hydrophobic residues are colored yellow. Black ellipsoids indicate the groove between α-helices 8 and 9 and arrows point to the α-Helix 9 and loop between β-strands 6 and 7 regions (left and right, respectively). Structures were generated by modeling the human sequences against the mouse CCTγ apical domain using SWISS-MODEL [8].

Three-dimensional structure of the PhLP1-$G\beta_1$-CCT complex

To better understand the role of PhLP1 in Gβ folding and assembly with Gγ, the PhLP1-$G\beta_1$-CCT complex was also isolated from insect cells and the cryo-EM structure of the complex

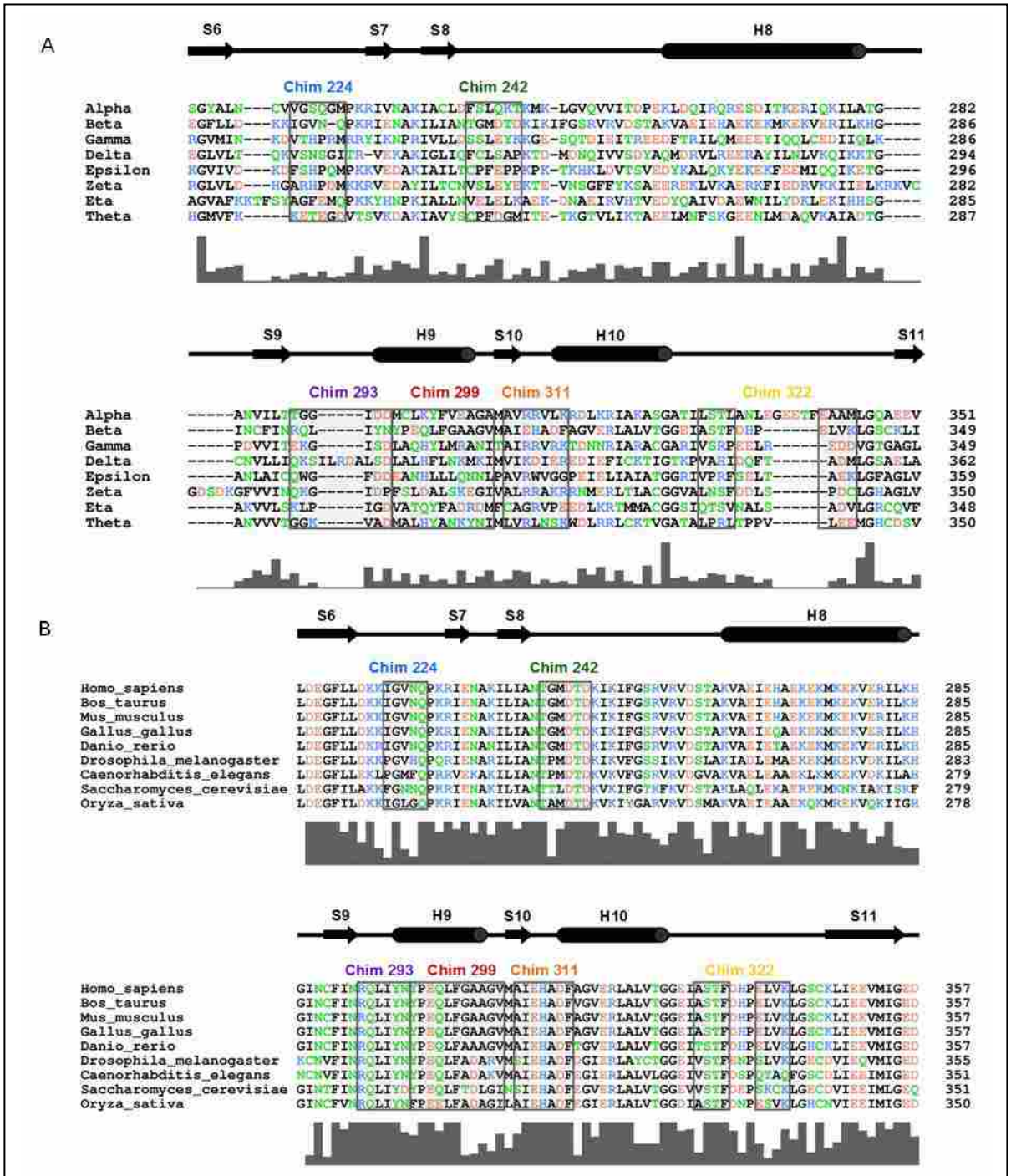

Figure 2-10. CCT sequence alignments.
A) Alignment of the eight Homo sapiens CCT subunits. B) Alignment of eukaryotic CCTβ subunits. Alignments were performed using ClustalX2, version 2.0.12 [6]. Colors indicate the chemical nature of the amino acid: nonpolar (black), polar (green), negatively charged (red), or positively charged (blue). Secondary structure was assigned from the crystal structure of the CCTγ apical domain (1GML), using UCSF Chimera [4]. Secondary structure elements are numbered as in Pappenberger et al.[10]. Chimeric regions designed for CCT substrate binding experiments are boxed.

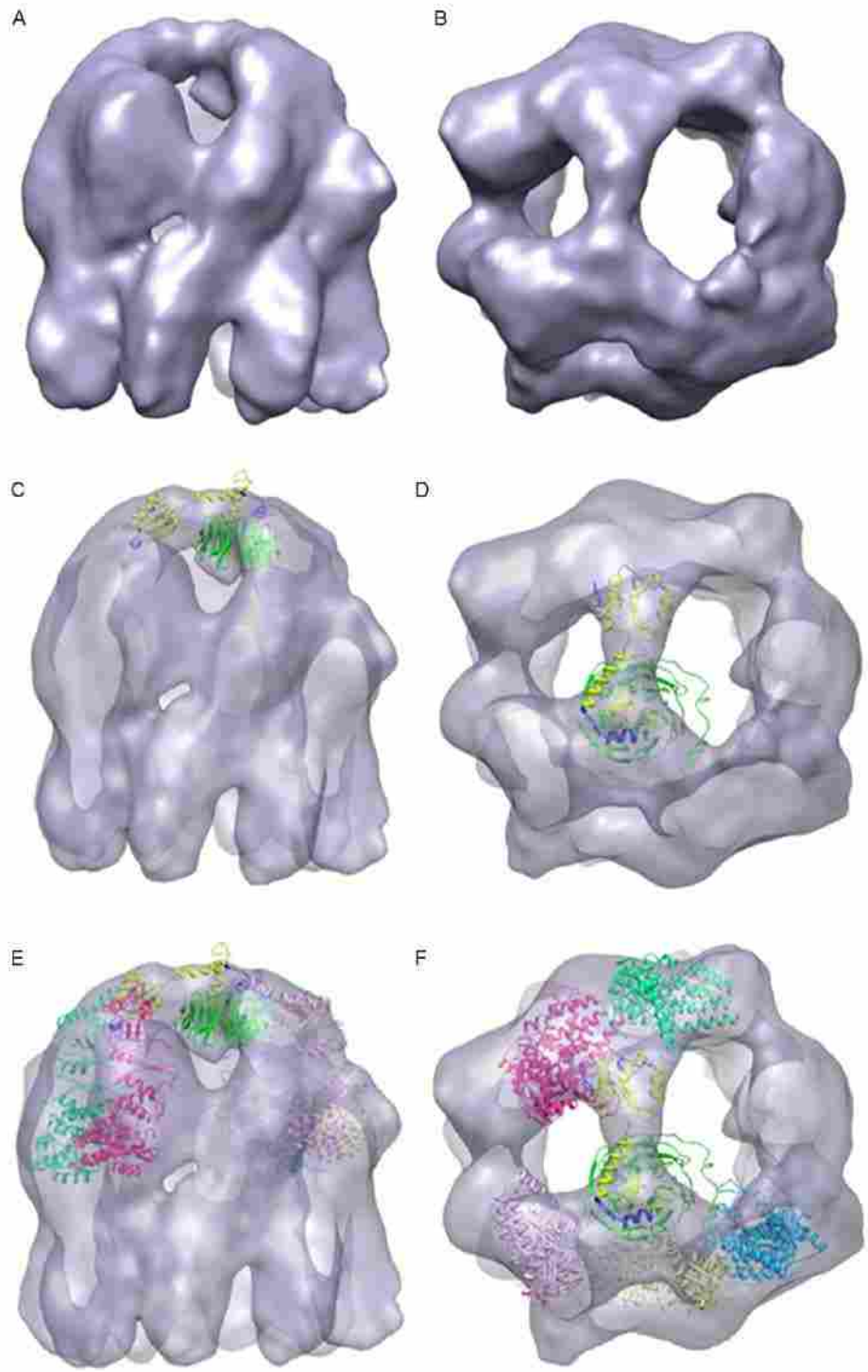

Figure 2-11. Cryo-EM reconstruction of PhLP1-Gβ_1-CCT at 18 Å.
A, B) Side and end-on views of the PhLP1-Gβ_1-CCT complex. C, D) Docking of the Pdc-Gβ_1 atomic structures into the cryo-EM reconstructed complex. E, F) Side and end-on views of the docking of the atomic structure of Pdc-Gβ_1 (pdb 2QNS; in red) and the atomic model of a CCT subunit from the tubulin-CCT crystal structure (pdb 2XSM; in magenta, dark green, purple, dark yellow and blue) into the corresponding masses of the reconstructed PhLP1-Gβ_1-CCT complex.

was determined. The cryo-EM analysis revealed some heterogeneity in the PhLP1-Gβ_1-CCT sample with several sub-populations that could be classified into CCT alone, Gβ_1-CCT and PhLP1-Gβ_1-CCT complexes, suggesting that the PhLP1-Gβ_1-CCT complex is somewhat unstable. This instability is consistent with the observation that PhLP1 enhances the release of Gβ_1 from CCT [114]. After sorting the complexes, a total of 11,634 homogeneous PhLP1-Gβ_1-CCT particles were used to generate a ~18 Å three-dimensional reconstruction of the complex without imposing any symmetry throughout the reconstruction procedure (Figure 2-11 A & B). The structure resembles that of the PhLP1-CCT complex [105] with a mass spanning the CCT folding cavity, interacting with three subunits on one side of the cavity and two on the opposite side. There is an additional mass deep within the folding cavity that was not seen in the PhLP1-CCT structure. Docking of the Pdc- Gβ_1 atomic structure [3] into the cryo-EM structure gives a good fit with Gβ_1 oriented in the mass inside the folding cavity and Pdc oriented above Gβ_1 in the mass spanning the cavity (Figure 2-11 C & D). In this structure, it is very likely that Gβ_1 retains its binding contacts with CCTβ. If so, the docking places the N-terminal, Gβ-binding domain of PhLP1 in close proximity to CCTβ, γ and ζ on one side of the cavity and the C-terminal domain of PhLP1 in close proximity to CCTδ and η on the opposite side of the cavity. This same orientation of PhLP1 was observed in the PhLP1-CCT structure [105]. Additional docking of the atomic structure of these CCT subunits [1] into the cryo-EM structure gives a good fit with CCTβ coming into close contact with Gβ_1 and the N-terminal domain of PhLP1 (Fig. 2-11 E&F).

There are some important differences in the position of Gβ_1 and PhLP1 in the PhLP1- Gβ_1-CCT complex compared to the Gβ_1-CCT and PhLP1-CCT complexes. First, in the Gβ_1-CCT reconstruction, the Gβ_1 electron density is larger than the native Gβ_1 β-propeller in the absence

of PhLP1 (Figure 2-6 D), suggesting a more open form of the β-propeller. In the presence of PhLP1, the Gβ$_1$ β-propeller is more narrow (Fig. 2-12 A-B), implying that PhLP1 binding constricts the β-propeller into a more native conformation. Second, the position of Gβ on CCT is shifted to the left in the presence of PhLP1, indicating a change in binding contacts between Gβ$_1$ and CCTβ upon PhLP1 binding (Fig. 2-12 A-B). This change in binding contacts may be responsible for the release of Gβ from CCT upon PhLP1 binding. Third, PhLP1 sits much lower on CCT, more into the folding cavity in the presence of Gβ$_1$. This reorientation of PhLP1 is likely a result of the binding of PhLP1 to Gβ$_1$ in the folding cavity.

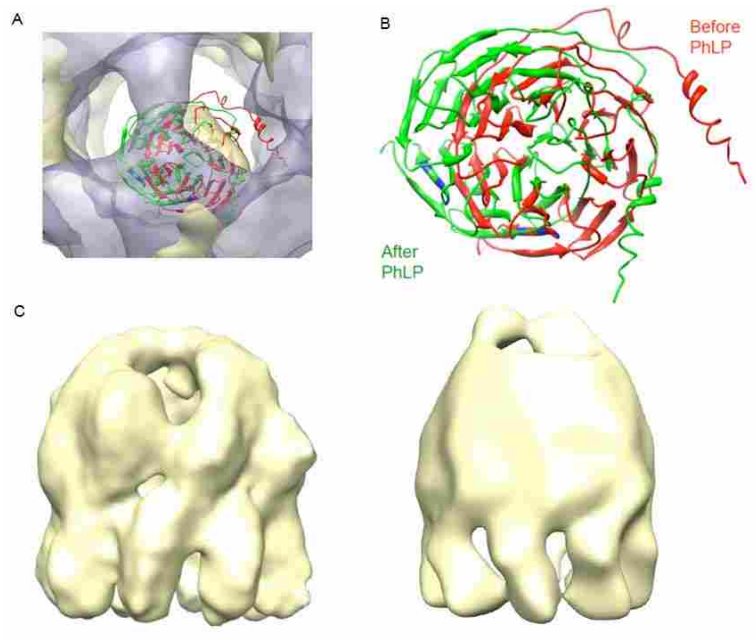

Figure 2-12. A proposed mechanism of PhLP1-mediated Gβ$_1$ folding and release from CCT.
A, B) Shows the comparison of Gβ$_1$ positions before (red) and after (green) PhLP1 binding. PhLP1 binding shifts the position of the folded Gβ$_1$ by ~10 Å. This shift results in a change in contacts between Gβ$_1$ and CCTβ, which is most likely responsible for the release of PhLP1-Gβ$_1$ from the CCT complex C) Differences in the position of PhLP1 in the PhLP1-Gβ$_1$-CCT complex (left) compared to the PhLP1-CCT complex (right) suggest that PhLP1 sits down deeper into the folding cavity of CCT to reach Gβ$_1$. This reorientation of PhLP1 allows PhLP1 to bind Gβ$_1$ while maintaining contacts with CCT subunits in both sides of the folding cavity.

Mutagenesis studies reveal a binding site for PhLP1 on CCTβ

The docking analysis of PhLP1-Gβ$_1$-CCT points to an interaction between PhLP1 and CCTβ in addition to the interaction of Gβ$_1$ with CCTβ. One would predict that the residues of CCTβ involved in an interaction with PhLP1 would lie above those residues of CCTβ involved

in $G\beta_1$ binding since PhLP1 sits above $G\beta_1$ in the CCT folding cavity. The only region of the CCTβ apical domain that sits above the Helix 9 $G\beta_1$ binding site is the helical extension of Helix 8 (Fig. 2-7A). Therefore, we substituted residues in the helical extension and measured their effect on PhLP1 binding to CCTβ. Unexpectedly, many amino acid substitutions in the helical extension yielded variants with very poor incorporation into the CCT complex (data not shown), with the exception of S260 substitutions. The S260 site on CCTβ sits at the very top of the helical extension (Fig. 2-13) and has previously been shown to be phosphorylated by the p90 ribosomal S6 kinase (RSK) and the p70 ribosomal S6 kinase (S6K) that are activated by the extracellular signal-regulated kinase (ERK) and mammalian target of rapamycin (mTOR) signalling pathways [153]. These signaling pathways can regulate a range of cellular responses including cell proliferation and growth [154]. An S260A substitution had no effect on PhLP1 binding to CCTβ, but a phosphorylation-mimicking S260D substitution reduced PhLP1 binding to CCTβ by approximately 50% (Figure 2-13 B). Both of these variants showed normal incorporation into CCT complexes (Fig. 2-13 C), indicating that they were folding normally and that the decreased binding of PhLP1 to the S260D

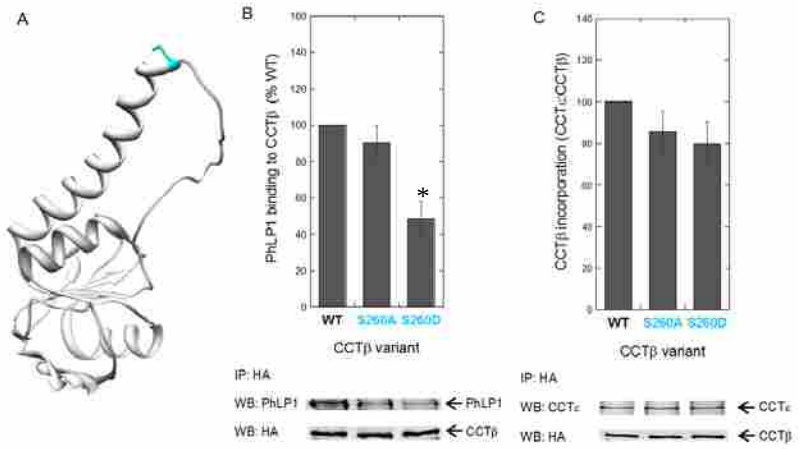

Figure 2-13. PhLP1 binding to CCTβ S260 mutants.
A) S260 residue is located at the tip of CCTβ apical domain. B) PhLP1-CCTβ S260A/D binding data. C) Incorporation data of CCTβ S260A/D variants. PhLP1 interacts with a serine in the CCTβ helical protrusion. HEK 293T cells were transfected with HA-tagged CCTβ S260 variants and Myc-tagged PhLP1. PhLP1-CCT complexes were immunoprecipitated with anti-HA antibody, and binding was measured by Western blotting. The S260 residue is indicated (blue) in the apical domain of the CCTβ structure (3KTT), using UCSF Chimera [4]. Incorporation of CCTβ S260 variants are shown in C). Data represent the average ± SEM of at least three experiments; * $p < 0.05$, as compared to WT.

variant was most likely the result of direct disruption of an interaction of PhLP1 with CCTβ. From this result, two important observations can be made. First, an important PhLP1-CCT interaction site is found near the tip of the CCTβ helical extension, supporting the docking analysis that pointed to an interaction of the N-terminal domain of PhLP1 with CCTβ. Second, PhLP1 binding to CCT and thus Gβγ assembly may be regulated by RSK and S6K phosphorylation.

Discussion

CCT can fold single monomers of an oligomeric complex and maintain their assembly competent state until the oligomeric complex assembly occurs [81]. Therefore, some of these substrates are only released from CCT in the presence of their binding partners [101, 155, 156]. In this way, CCT can serve as a reservoir for their stabilization against aggregation or degradation until complex assembly takes place [100]. This may be the case for the assembly process of the heterotrimeric G protein αβγ complex, which is important for the propagation of GPCR signaling. The CCT-assisted assembly of Gβ and Gγ into the Gβγ dimer is particularly challenging. Nascent polypeptides of Gβ and Gγ emerging from a translating ribosome face a propensity to aggregate since neither of these subunits is stable on its own. Moreover, the folding process of Gβ is complicated because it must bring together regions that are far removed from each other in the primary sequence to form the β-propeller structure. As a result, Gβ folding requires CCT and an essential co-chaperone, PhLP1, which catalyzes Gβγ assembly by binding to Gβ in the CCT folding cavity and releasing Gβ from CCT [114]. To better understand the mechanism of this assembly process, we have characterized two important intermediates, $G\beta_1$-CCT and PhLP1-$G\beta_1$-CCT complexes, through cryo-electron microscopy analysis and site-

directed mutagenesis. These complexes are unique in that they were isolated directly from cells. As such, the $G\beta_1$-CCT and PhLP1-$G\beta_1$-CCT structures should be good representations of the complexes as they exist *in vivo*.

Binding of $G\beta_1$ to CCT

The immuno-microscopy and cryo-EM analysis of the $G\beta_1$-CCT complex reveals that $G\beta_1$ interacts specifically with CCTβ in the folding cavity (Fig. 2-2 B; Fig. 2-6 E & F). Docking analysis of the $G\beta_1$-CCT structure suggests that $G\beta_1$ has achieved a quasi-folded state with an open β-propeller structure while bound to CCT (Fig. 2-6 C & D). Moreover, optimal docking indicates that β-propeller blade 2 of $G\beta_1$ specifically points to α-Helix 9 and the loop between β-strands 6 and 7 of the CCTβ apical domain (Fig 2-6 E-H). Both of these regions of the CCTβ apical domain face the interior of the chaperonin cavity [150] and together form a hydrophobic face (Fig. 2-9). In the atomic model, these regions of CCT are 3.4 Å apart and they are in close proximity to the β-blade 2 of $G\beta_1$, the $G\beta_1$ blade containing the amino acids proposed to be involved in CCT binding [102]. This proposed interaction was confirmed by the mutagenesis results which showed that chimeras of these regions of CCTβ had significantly reduced $G\beta_1$ binding (Fig. 2-7 C). Since there is considerably more hydrophobicity of these regions in CCTβ compared to the same region of any other CCT subunits (Fig. 2-9; 2-10 A), it seems likely that $G\beta_1$ interacts with these regions of the apical domain of CCTβ through a set of defined, hydrophobic residues located in one of the β-strands of β-blade 2 (Fig. 2-6 G-H).

One of the β-strands in VHL interacts specifically with the hydrophobic residues of Helix 9 of CCTα [147]. The general hydrophobicity of Helix 9 is conserved in both CCTα and β but the positions of charged and hydrophilic residues are not (Fig. 2-10 A). Thus, the binding specificity

of $G\beta_1$ and VHL appears to come from the specific structural environment of the CCT apical domains in the region surrounding Helix 9. Interestingly, the analogous region of GroEL is also responsible for binding its substrates [148, 157]. These observations suggest that many CCT substrates with β-sheet structures might bind in the Helix 9 region and that the amino acid sequence diversity of the CCT apical domains in this region provides the specificity of substrate recognition. This is in contrast to the non-specific hydrophobic interactions described for GroEL and its substrates [157-159].

Role of PhLP1 in the folding and release of Gβ from CCT

As described earlier, CCT is a more complex chaperonin than the rest of the family and uses a plethora of co-factors or co-chaperones in folding its substrates [106, 123]. CCT-assisted folding and release of Gβ proteins require interaction with PhLP1 [57, 73, 114], and we have used cryo-EM analysis to determine the PhLP1-$G\beta_1$-CCT structure, in which the PhLP1 is in its phosphorylated state (Figure 2-11 A-B). Several important insights regarding the mechanistic details of the PhLP1-mediated Gβγ assembly process can be drawn from the structural analysis of this complex. First, the cryo-EM analysis suggests that the N-terminal domain of PhLP1 binds above $G\beta_1$ in the folding cavity simultaneously contacting the CCTβ, γ and ζ on one side of the cavity, while the C-terminal domain of PhLP1 interacts with CCTδ and η on the opposite side of the cavity (Fig. 2-3 C; Fig. 2-11 E & F). Moreover, the docking analysis indicates that $G\beta_1$ retains binding contacts with CCTβ while binding to PhLP1 (Fig. 2-11 E & F). Second, differences in the position of PhLP1 in the PhLP1-$G\beta_1$-CCT complex compared to the PhLP1-CCT complex suggest that PhLP1 sits down deeper into the folding cavity of CCT to reach $G\beta_1$ (Fig. 2-12 C). This reorientation of PhLP1 allows PhLP1 to bind $G\beta_1$ while maintaining contacts

with CCT subunits in both sides of the folding cavity (Fig. 2-12 C). Third, a comparison between the electron densities of $G\beta_1$ in the $G\beta_1$-CCT and PhLP1- $G\beta_1$-CCT structures reveals that in the presence of PhLP1, the $G\beta_1$ β-propeller is more narrow (Fig. 2-12 A & B), implying that PhLP1 binding constricts the $G\beta_1$ β-propeller strands, probably completing its folding and stabilizing the native conformation of $G\beta_1$. Fourth, PhLP1 binding shifts the position of the folded $G\beta_1$ by ~10 Å. This shift must result in a change in contacts between $G\beta_1$ and CCTβ, which is most likely responsible for the release of PhLP1-$G\beta_1$ from the CCT complex (Fig. 2-12 A & B). Finally, the stability of the $G\beta_1$-CCT complex shows that $G\beta_1$ cannot be released by the normal ATP binding and hydrolysis cycle of CCT. Moreover, the structure of the PhLP1- $G\beta_1$-CCT complex indicates that it is very unlikely that PhLP1 can remain bound in the closed, ATP-hydrolysis transition state of CCT. Therefore, it appears that PhLP1 binds $G\beta_1$-CCT in the open form and releases PhLP1-$G\beta_1$ prior to ATP binding and hydrolysis.

The heterogeneity of the PhLP1- $G\beta_1$-CCT complex reflects its relative instability compared to the $G\beta_1$-CCT complex. In fact, our ability to purify the complex was greatly enhanced by the absence of over-expressed Gγ in our insect cell expression system. In the presence of Gγ, Gβ release from CCT is accelerated, not because Gγ binds Gβ in the CCT folding cavity, but most likely because Gβ assembly with Gγ drives the equilibrium toward the dissociation of the PhLP1-$G\beta_1$-CCT complex by irreversible formation of the Gβγ dimer. In this manner, the stable Gβγ complex is brought together from its unstable subunits for subsequent association with the Gα subunit to form a heterotrimer and release PhLP1 to participate in subsequent rounds of Gβγ dimerization.

PhLP1 binds CCT at the tip of the helical protrusion

Docking of the Pdc-G$\beta_1\gamma_1$ atomic structure [3] onto the PhLP1-Gβ_1-CCT structure places a region of Pdc corresponding to an important CCT binding site of PhLP1 in contact with CCTβ (Fig. 2-11 E & F). Our mutagenesis data has provided evidence that PhLP1 can interact with residue S260 of CCTβ, which is located at the tip of the helical protrusion of the apical domain [150, 160] (Figure 2-13 A). Interestingly, both RSK of the ERK signalling pathway and S6K from the PI3K-mTOR signalling pathway can phosphorylate CCTβ subunit at this residue [153]. Based on the fact that the phosphorylation mimicking S260D substitution decreases the binding of PhLP1 to CCT, and that S260 is phosphorylated by RSK and S6K, it is possible that the Gβγ assembly may be regulated by the ERK and mTOR pathways. Since phosphorylation by CK2 at S18-20 in N-terminus of PhLP1 can enhance the release of Gβ from CCT, it also seems possible that these phosphorylation events on PhLP1 and CCTβ can work in concert to enhance the release of Gβ_1 from CCT due to their mutual electrostatic repulsion. In this way, Gβγ assembly may be regulated by signals that activate the ERK or mTOR pathways. This is an intriguing possibility that merits further investigation.

In conclusion, we have analyzed the process of PhLP1-mediated Gβγ assembly and determined using cryo-electron microscopy the first structures of two *in vivo* assembled intermediates in this process, Gβ_1-CCT and PhLP1-Gβ_1-CCT. This study shows the exquisite way in which CCT and PhLP1 work together to fold and assemble Gβγ, and it also suggests possible novel ways of regulating Gβγ assembly.

CHAPTER 3:
ROD-SPECIFIC PHOSDUCIN-LIKE PROTEIN 1 (PHLP1) CONDITIONAL KNOCKOUT MICE REVEAL THE ROLE OF PHLP1 FOR Gβγ SUBUNIT ASSEMBLY *IN VIVO*

Summary

G proteins play a vital role in cellular signal transduction processes [15, 21, 22]. Our lab and others have recently shown that the nascent Gβ polypeptide requires the assistance of the cytosolic chaperonin complex (CCT) to fold correctly into its native tertiary structure [113, 114]. Folding of Gβ also requires a co-chaperone, phosducin-like protein 1 (PhLP1), which interacts with the CCT apical domains to form a PhLP1-Gβ-CCT ternary complex that subsequently breaks down and releases PhLP1-Gβ from CCT for association with Gγ and formation of the Gβγ dimer [73, 114]. This mechanism of PhLP1-mediated Gβγ assembly is derived from cell culture experiments and structural data, but has yet to be tested *in vivo*. Here we report the first *in vivo* study of PhLP1 function from a retinal rod photoreceptor-specific PhLP1 conditional knockout mouse. This mouse provides a model in which the physiological consequences of the loss of PhLP1 function can be characterized in the G protein signaling system of mammalian vision. In this mouse, all G protein subunits that express in the rod photoreceptor cells were significantly down-regulated, resulting in severely impaired photoresponses. Moreover, significant down-regulation of $G\beta_5$ and RGS9-1 was also observed, indicating that PhLP1 plays as important role in $G\beta_5$-RGS dimer formation as it does in the Gβγ assembly process. These findings demonstrate that PhLP1 is required for the folding and assembly of Gβγ *in vivo* and extend this essential role of PhLP1 to $G\beta_5$-RGS9 dimers as well.

Introduction

G protein signaling is essential for regulating a large variety of physiological processes such as cardiac rhythm and output, neuronal signaling, immune responses and sensory detection [15, 21, 22]; and the malfunctioning of these signaling processes can lead to devastating diseases such as cancer, heart disease, vision impairment, neural diseases, and hypertension [16-20]. Many different ligands such as small molecule neurotransmitters, peptide hormones, chemokines, lipids, odorants and even photons of light can trigger the activation of GPCR signaling, which is is particularly important in the phototransduction cascade. The light-activated GPCR rhodopsin associates with the heterotrimeric G protein transducin $\alpha\beta\gamma$ subunits (G_t) and catalyzes the exchange of GDP to GTP on the transducin α subunit ($G\alpha_t$). As $G\alpha_t$-GTP dissociates from the activated receptor and $G_t\beta\gamma$ dimers, it interacts with the cGMP phosphodiesterase (PDE) and activates the cGMP hydrolysis activity of PDE. The rapidly decreased cytoplasmic cGMP concentration results in the closure of cGMP-gated cation channels in the plasma membrane of the photoreceptor outer segment and hyperpolarizes the membrane potential to signal a light response. The RGS9-1/$G\beta_5$-L/R9AP GAP complex accelerates the hydrolysis of GTP in $G\alpha_t$ to GDP resulting in the dissociation of $G\alpha_t$-GDP from PDE and the G protein cycle terminates. The $G\alpha\beta\gamma$ complex is then reformed by the association between $G\alpha t$-GDP and $G\beta\gamma$ subunits [16].

To perform these essential functions, the G protein heterotrimer must be assembled from its nascent α, β and γ polypeptides. This is no small task given the fact that $G\beta$ and $G\gamma$ are unstable proteins on their own, but must associate and form the $G\beta\gamma$ dimer to achieve a stable quarternary structure. Our lab and others have recently shown that the nascent $G\beta$ polypeptide requires the assistance of the cytosolic chaperonin complex (CCT) to fold correctly into its native tertiary

structure [113, 114]. Folding of Gβ also requires a co-chaperone, phosducin-like protein 1 (PhLP1), which interacts with the CCT apical domains to form a PhLP1-Gβ-CCT ternary complex that is an important intermediate in Gβγ assembly [73, 114]. If PhLP1 is phosphorylated in this complex, it triggers the release of Gβ from CCT in what is believed to be a phospho-PhLP1-Gβ dimer that can then interact with the Gγ subunit to form the Gβγ dimer [114].

The mechanism of PhLP1-mediated Gβγ assembly has been studied extensively in cell culture experiments and structural studies. The next important step in testing this hypothesis is to investigate the function of PhLP1 *in vivo*. A previous study has revealed the dominant effect of PhLP1 by using transgenic expression of the PhLP1 Δ1-83 mutant in the mouse rod photoreceptor cells [161]. Since PhLP1 binds the Gβ subunit with its N-terminal domain, deletion of PhLP1 N-terminal domain resulted in impaired Gβ subunit folding. Moreover, the over-expressed PhLP1 Δ1-83 mutant formed a stable complex with trapped Gβ and CCT in the rod photoreceptor cells, leading to the unavailability of CCT to other protein substrates. Although the expression of G protein transducin β and γ subunits were essentially eliminated in this study, supporting the current thesis that PhLP1 is important for Gβγ assembly, a large disturbance of cellular functions in the rod photoreceptor cells resulted due to the impaired functions of CCT. Since the loss of many other important visual proteins such as rhodopsin and PDEαβ may not be a direct result from the loss of PhLP1 function, it was difficult to interpret the actual physiological roles of PhLP1. As a result, it is imperative to make an actual knockout of PhLP in order to assess the physiological functions of PhLP1 *in vivo*. However, it is important to do a conditional knockout instead of a whole animal knockout because if PhLP1 is required

for Gβγ assembly, then a whole animal knockout would be expected to be embryonically lethal. This prediction stems from the fact that the Gβ knockout is embryonically lethal [162].

The *Cre-Lox* recombination system has been widely used for the development of conditional knockout mice by initiating site-specific recombination in genomic DNA [163]. *Cre* recombinase is able to catalyze the recombination of DNA between two *loxP* sequences. When cells that have *loxP* sites in their genome express Cre, a recombination event will occur between the *loxP* sites so that the double-stranded DNA between the *loxP* sites is excised and the surrounding DNA is ligated back together by the Cre protein. Therefore, expression of Cre recombinase under the control of a tissue-specific promoter can facilitate the cleavage of any genes flanked by two *LoxP* sequences oriented in the same direction in a tissue-specific manner.

Therefore, we used the *Cre*-LoxP system to conditionally knockout the *PhLP1* gene in the photoreceptor cells of the retina to determine the effects of PhLP1 deletion on Gβγ expression and G protein signaling. Photoreceptor cells are an ideal model system for these experiments because the process by which they convert light into a neuronal response (called phototransduction) is a well-studied G protein-dependent pathway [15]. We have prepared gene-targeted mice in which the PhLP1 gene was flanked by two *loxP* sites. We subsequently crossed these mice with iCre75 mice in which the *Cre* recombinase is expressed only in retinal rod photoreceptor cells under the control of the rhodopsin promoter. The resulting mice lack PhLP1 only in their rod photoreceptors. The loss of PhLP1 led to profound consequences on the ability of these rods to detect light as a result of a significant reduction in the expression of transducin (G_t) subunits. Expression of other G protein subunits as well as $G\beta_5$-RGS9-1 complexes was also greatly decreased, yet all of this occurs without causing rapid degeneration of the photoreceptor

cells. These results show for the first time the essential nature of PhLP1 for Gβγ and $G\beta_5$-RGS dimer assembly *in vivo*, confirming and extending results from cell culture and structural studies.

Experimental Procedures

Development of PhLP1-LoxP targeting vector

The development and construction of PhLP1-LoxP targeting vector were performed based on a previously described protocol [164]. The detailed experimental procedures are described here.

Preparation of Red-competent BAC containing *E. coli*

E. coli containing the PhLP1 BAC clones (BACPAC Resource Center; Cat: RP23-464H12) were inoculated into 5 mL of SOB, 20 mg ml^{-1} chloramphenicol, and grown at 30–32°C overnight. The cells were made electro-compotent using the following protocol. Cells were by centrifuged at 2000 g for 5 min at 4°C. The supernatant was discarded, the cells were resuspended in 1 ml of 10% ice cold glycerol, transferred into a 1.7-ml Eppendorf tube and centrifuged at 8,000g at 4°C in a microcentrifuge for 10 s. The supernatant was discarded, the cells were resuspended again in 1 mL of 10% (vol/vol) ice cold glycerol and centrifuged again as before. The supernatant was again discarded, the cells were resuspended in 100 μl of 10% (vol/vol) ice cold glycerol and divided into two 50-ul aliquots. A total of 10 ng of the Red recombinase-expressing plasmid pKD46 was transformed to one tube of the freshly made electro-competent cells by electroporation under the default setting. A total of 300 μL of SOC medium was added immediately after the pulse, and the cells were transferred into an Eppendorf tube. Without additional incubation, 50 μl of the cells were spread onto LB-agar plates containing 100 mg ml^{-1} ampicillin and 20 mg ml^{-1} chloramphenicol. The plates were then incubated at 30–32°C for 24–30 hrs. After incubation, a single colony was picked and grown in a 15-ml tube containing 5 ml of SOB medium containing ampicillin and chloramphenicol and was

incubated at 30–32°C overnight. An appropriate amount of the culture was inoculated into a 250-mL flask containing 50 ml of SOB medium containing ampicillin and chloramphenicol to reach a final OD_{600} of about 0.1–0.2. To induce the expression of the Red recombinase, L-arabinose (powder or freshly made liquid stock) was added to a final concentration of 0.1%, and the bacterial culture was incubated at 30–32°C. When the OD_{600} was between 0.4–0.8, the culture was transferred into a 50-mL conical tube and left on ice for 10 min with occasional swirling. The cells were centrifuged for 15 min at 2,000g at 4°C, and the supernatant was discarded. The cells were resuspended gently in 50 mL of ice cold 10% glycerol and centrifuged as before. The supernatant was again discarded, and the cells were resuspended gently in 25 mL of ice cold 10% glycerol and were centrifuged as before. After the centrifugation, the supernatant was discarded, and the cells were resuspended gently in 25 mL of ice cold 10% glycerol and centrifuged as before. Finally, the supernatant was discarded and any remaining liquid was removed by pipetting. Approximately 100 μl of fresh ice cold 10% (vol/vol) glycerol was added and the pellet was resuspended. The cells were then divided into 50-100 μl aliquots. These aliquots were either used immediately or stored at -80°C for later use.

Preparation of chemically competent DH5α cells

DH5α *E. coli* were inoculated onto an LB-agar plate and incubated at 37°C overnight. A single colony was picked and grown in 5 ml SOB medium at 37°C overnight. After determining the OD_{600}, 1 ml was transferred into 250 ml of SOB medium in a 2-L flask to obtain OD_{600} of approximately 0.01–0.02. The cell culture was incubated at 21–24°C with shaking (200–300 rpm). When the OD_{600} of the cells reached approximately 0.5–0.6, the culture was transferred into a large centrifuge tube and left on ice for 10–20 min with occasional shaking. The cells were centrifuged at 2,500g at 4°C for 10 min. The cell pellet was gently resuspended in 80 ml of ice

cold 10% glycerol and was left on ice for 10 min. The cells were again centrifuged as before. The pellet was then resuspended gently in 20 ml of ice cold 10% glycerol. A total of 1.4 ml of DMSO was added to the tube and mixed well, and the tube was kept on ice for 10 min. The competent cells were divided into 50 μl aliquots and frozen in liquid nitrogen and were stored at 80 °C until used.

Preparation of Red-competent DH5α/pKD46 cells

A total of 50 μl of chemically competent DH5α cells were transformed with pKD46 (~10 ng) by 42°C heat shock for 1 min. Right after heat shock, the transformed cells were directly spread onto an LB-agar plate with 100 mg ml^{-1} ampicillin and grown at 30–32°C for ~24 to 30 hrs. Several colonies were picked and grown in 20 ml of SOB medium overnight at 30–32°C. After determining the OD_{600}, appropriately 10 ml of culture were inoculated into a 1-L flask containing 250 ml of SOB medium to reach an OD_{600} of ~0.1–0.2. A total of 0.25 g (0.1%) L-arabinose powder was added to the culture, and the culture was incubated at 30–32°C with shaking (200–300 rpm) for another 2 to 4 hrs. When the OD_{600} of the cells reaches ~0.4–0.8, the culture was transferred into a large centrifuge tube and was left on ice for 10–20 min with occasional shaking. The cells were centrifuged for 5 min at 4,000g at 4°C. The supernatant was discarded, and the pellets were resuspended gently in 200 ml of ice cold 10% (vol/vol) glycerol. The cells were again centrifuged as above and the supernatant was discarded. The pellets were gently resuspended in 200 ml of ice cold 10% (vol/vol) glycerol and centrifuged again as above. The supernatant was again discarded, and the pellet was resuspended gently in 100 ml of ice cold 10% (vol/vol) glycerol. The cells were centrifuged again as before and the supernatant was discarded. The pellet was gently resuspended in a fresh 0.5 ml of ice cold 10% (vol/vol) glycerol. The cells were then divided into 50 μl aliquots and snap frozen in liquid nitrogen.

Subcloning of the PhLP1 genomic fragment into the pStart-K vector

Two oligonucleotides were designed for PCR amplification of the pStartK vector for construction of the targeting vector with the PhLP1 gene. The upstream oligo sequence was: TGAAGTGCTTATTACTTTAATAGTTTCAAAGTCATGGATCTATTTGATGAgccgcactcgag atatctagaccca; and the downstream oligo sequence was: AGGCAAGAGCTGGAGTGGAGA AAAACTCAAATGGGACCTGGGGCTTTTCCcgactgaattggttcctttaaagc. Sequences in capital letters share 50-bp homologous sequences with the targeting regions of the BAC plasmid. Sequences in lowercase anneal to the backbone of pStartK. These two primers were used to amplify the template pStartK by PCR (5 x 25-μl reactions: pStart-K, 50 ng; 10x buffer, 12.5 μl; 25 mM $MgCl_2$, 10 μl; primers, 2.5 μl each at 10 mM; 10 mM dNTP, 2.5 μl; Pfx Taq, 1.25 μl; H_2O was added to a total volume of 125 μl; PCR conditions: 94°C 2 min; 30 cycles of 94°C 30 s, 59°C 30 s and 68°C 90 s; 68°C 7 min.). The amplified PCR products were combined and purified using a QIAprep PCR purification column following the manufacturer's instructions and eluted with 100 μl H_2O. The eluted DNA was digested with 2 μl (20 U) of DpnI for 1–2 h at 37°C. The reaction was re-purified on a QIAprep column and eluted with 40 μl H_2O. The purified PCR product (5-10 μl) was electroporated into 50 μl of the Red-competent *E. coli* previously transformed with the targeting BAC plasmid. One ml of SOC medium was used for rescue immediately after the pulse, and the cells were transferred into a 1.7-ml Eppendorf tube and incubated at 37°C for 1 h. The cells were plated onto LB-agar plates with 50 μg ml^{-1} kanamycin. Eight colonies were picked and grown in 5 ml of SOB medium at 37°C overnight for DNA preparation using QIAprep spin columns. Purified DNA was digested by restriction enzymes (5 μl DNA digested with 0.2 μl of restriction enzyme in 25 μl reaction, incubated at 37°C for 2 hrs) and was separated on a 1% agarose gel to identify clones with the successfully

captured genomic fragment of the PhLP1 gene into the pStartK plasmid. pStartK-PhLP1 was designated for clones with expected restriction patterns. Several clones of pStartK-PhLP1 were sequenced to confirm junction regions of the captured sequences.

Insertion of the 1st LoxP site into the Targeting Vector

Two primers were designed to insert a LoxP site at 10 bp upstream of the transcription initiation site of the PhLP1 gene (exon 2) and concomitantly introduce an AflII site for Southern blot screening and an AscI restriction enzyme site for subsequent cloning. The upstream oligo sequence was CATGTCTTCCTTGCTCAAGCTAGCAAAAAATCCTTGATACATTTTTC TTTataacttcgtatagcatacattatacgaagttatcttaagggcgcgccagcattacacgtcttgagcgattgt; and the downstream oligo sequence was GTAATTTCTCCCCCAGTAACTTATCATCCAGGGTT GTCATGGTGCCTGGAggcgcgcccacttaacggctgacatgggaatta. The uppercase sequences shared 50-bp homologous sequences with the genomic DNA of PhLP1 intron 1 for Red-recombination. Sequences in lowercase are for introducing the LoxP site, restriction sites, and amplification of the chloramphenicol resistance gene (cat) in the plasmid pKD3. PCR was performed using these primers to amplify the chloramphenicol resistance gene (5 x 25- μl reactions: pKD3, 50 ng; 10x buffer, 12.5 μl; 25 mM $MgCl_2$, 10 μl; primers, 2.5 μl each at 10 mM; 10 mM dNTP, 2.5 μl; Pfx Taq, 1.25 μl; H_2O is added to a total volume of 125 μl. PCR conditions: 94°C 2 min; 30 cycles of 94°C 30 s, 59°C 30 s and 68°C 60 s; 68°C 7 min). PCR products were combined and purified through a QIAprep spin column and eluted with 100 μl H_2O. The eluted DNA was digested with 2 μl (20 U) of DpnI for 2 hrs at 37°C. The reaction was re-purified on a QIAgen column and eluted with 40 μl H_2O. The purified PCR product (5 μl, 500 ng) was electroporated along with pStartK-PhLP1 (5 μl, 500 ng) into 50 μl of Red-competent DH5α/pKD46 cells. The electroporated cells were rescued in 1 ml of SOC medium and incubated at 37°C for 1 hr. Cells

were centrifuged briefly at 14,000 rpm in a microfuge for 10 s at 23^{o}C. The supernatant was discarded, and the pellet was resuspended in approximately 100 μl of the remaining media. Cells were plated on LB-agar plates with 30 mg ml^{-1} chloramphenicol and incubated at 37°C overnight. Several colonies were picked and grown in 5 ml of SOB medium at 37°C overnight for DNA preparation. DNA were purified and digested to identify correct clones. Clones with correct restriction patterns were sequenced at the junction regions to confirm successful homologous recombination. The resulting plasmid was designated pStartK-PhLP1-LoxP-AflII. Five μg of pStartK-PhLP1-LoxP-AflII plasmid was cut in a 50 μl reaction with 1 μl (10 U) of the AscI restriction enzyme and incubated at 37°C for 2 hrs. The reaction mix was loaded and separated on a 1% agarose gel for DNA purification using a QIAgen column and was eluted with 48 μl H_2O. A standard ligation reaction was set up to perform self-ligation of the above purified DNA plasmid as follows: 5 μl (500 ng) of purified DNA plasmid, 2 μl of T4 DNA ligase buffer and 1 μl of T4 DNA ligase in a total volume of 20 μl for ligation reaction at 23^{o}C for 2 hrs. Chemically competent DH5α cells were transformed with 20 μl of the above ligation reaction mixture by heat shock at 42°C for 1 min. One mL of SOC medium was added for rescue and incubated at 37°C for 1 h. Cells were centrifuged briefly at 14,000 rpm in a microfuge for 10s at 23^{o}C. The supernatant was discarded, and the pellet was resuspended in the remaining liquid of 100 μl. Cells were plated on LB-agar plates with 50 μg ml^{-1} kanamycin. Several colonies were picked for culture and DNA isolation. Restriction digestion and sequencing were used to confirm successful ligation. Clones with correct sequences and restriction patterns were designated pStark-PhLP1-LoxP1-AflII.

Insertion of the 2nd LoxP site and Neo positive selection cassette into the Targeting Vector

Two primers were designed to insert the second LoxP site downstream of the exon 3 of PhLP1 gene and concomitantly introduce an AflII site for Southern blot screening and an MfeI restriction enzyme site for subsequent cloning at this position. The upstream oligo sequence was GATCACTTTGACTGGGGAATGATTTTAGGTCATAAAACCTAGACAAAAGCcaattgagcatt acacgtcttgagcgattgt, and the downstream oligo sequence was CTTGAGACTCTCCCGCCTAGC TGATGTGACTGGGTCTTTTAGGTGATACAataacttcgtataatgtatgctatacgaagttatcttaagcaattgcac ttaacggctgacatgggaattag. The uppercase sequences shared 50-bp homology sequences with genomic DNA of PhLP1 intron 3 for red-recombination. Sequences in lowercase are for introducing the second LoxP site, addition of restriction sites, and amplification of the chloramphenicol resistance gene in the plasmid pKD3. PCR was performed using these primers to amplify the chloramphenicol resistance gene (5 x 25- μl reactions: pKD3, 50 ng; 10x buffer, 12.5 μl; 25 mM $MgCl_2$, 10 μl; primers, 2.5 μl each at 10 mM; 10 mM dNTP, 2.5 μl; Pfx Taq, 1.25 μl; H_2O is added to a total volume of 125 μl. PCR conditions: 94°C 2 min; 30 cycles of 94°C 30 s, 59°C 30 s and 68°C 60 s; 68°C 7 min). PCR products were combined and purified through a QIAprep spin column, and the column was eluted with 100 μl H_2O. The eluted DNA was digested with 2 μl (20 U) of DpnI for 2 hrs at 37°C. The reaction was re-purified on a QIAgen column and eluted with 48 μl H_2O. The purified PCR product (5 μl , 500 ng) was electroporated with pStartK-PhLP1-LoxP-AflII (5 μl, 500 ng) into 50 μl of Red-competent DH5α/pKD46 cells. The electroporated cells were rescued in 1 ml of SOC medium and incubated at 37°C for 1 hr. Cells were centrifuged briefly at 14,000 rpm in a microfuge for 10 s at 23°C. The supernatant was discarded, and the pellet was resuspended in approximately 100 μl of the remaining media. Cells were plated on LB-agar plates with 30 mg ml^{-1} chloramphenicol

and incubated at 37°C overnight. Several colonies were picked and grown in 5 ml of SOB medium at 37°C overnight for DNA preparation. DNA were purified and digested to identify correct clones. Clones with correct restriction patterns were sequenced at the junction regions to confirm successful homologous recombination. The resulting plasmid was designated pStartK-PhLP1-LoxP2-AflII.

Two primers were designed to amplify a PCR product that contained the neomycin resistant gene with two flanking FRT sites. This PCR product was used to ligate with the MfeI-digested pStark-PhLP1-LoxP-AflII plasmid to insert the NeoR gene in the intron 3 of PhLP1. The upstream oligo sequence was ATGCATCAATTGGAAGTTCCTATTCTCTAGAAAGTATAG GAACTTCaggtctgaagaggagtttacgtccag, and the downstream oligo sequence was TAGTCACAA TTGATTATGTACCTGACTGATGAAGTTCCTATACTTTCTAGAGAATAGGAACTTCgaag ggttccgcaagctctagtcgag. Sequences in uppercase were for introducing the MfeI site to the PCR product. Sequences in lowercase were for annealing to the PL451 plasmid and amplification of the neomycin resistance gene (Neo) and the FRT sequences in the plasmid PL451. PCR was performed using these primers to amplify the chloramphenicol resistance gene (5 x 25- μl reactions: PL451, 50 ng; 10x buffer, 12.5 μl; 25 mM $MgCl_2$, 10 μl; primers, 2.5 μl each at 10 mM; 10 mM dNTP, 2.5 μl; Pfx Taq, 1.25 μl; H_2O is added to a total volume of 125 μl. PCR conditions: 94°C 2 min; 30 cycles of 94°C 30 s, 59°C 30 s and 68°C 60 s; 68°C 7 min). PCR products were combined and purified through a QIAprep spin column, which was eluted with 100 μl H_2O. The eluted DNA was digested with 2 μl (20 U) of DpnI for 2 hrs at 37°C. The reaction was re-purified on a QIAgen column and was eluted with 48 μl H_2O.

Five μg of pStartK-PhLP1-LoxP2-AflII plasmid was cut in a 50 μl reaction with 1 μl (10 U) of MfeI restriction enzyme and incubated at 37°C for 2 hrs. The reaction mix was purified using

a QIAgen column and eluted with 48 μl H_2O. The eluted DNA was dephosphorylated by CIAP enzyme at 37°C for 30 min and re-purified with QIAgen spin column. A standard ligation reaction was set up to insert a pre-cut MfeI-FRT-Neo-FRT-MfeI cassette into the MfeI-digested pStartK-PhLP1-LoxP2-AflII plasmid as follows: 12 μl (~500 ng) of pStartK-PhLP1-LoxP2-AflII recipient DNA, 5 μl (200 ng) of pre-cut MfeI-FRT-Neo-FRT-MfeI cassette, 2 μl of T4 DNA ligase buffer and 1 μl of T4 DNA ligase in a total volume of 20 μl for ligation reaction at 23^{o}C for 2 hrs. Chemically competent DH5α cells were transformed with 20 μl of the above ligation reaction mixture by heat shock at 42°C for 1 min. One mL of SOC medium was added for rescue and incubated at 37°C for 1 h. Cells were centrifuged briefly at 14,000 rpm in a microfuge for 10s at 23^{o}C. The supernatant was discarded, and the pellet was resuspended in the remaining liquid of 100 μl. Cells were plated on LB-agar plates with 50 mg ml^{-1} kanamycin. Several colonies were picked for culture and DNA isolation. Restriction digestion and sequencing were used to confirm successful ligation. Clones with correct sequences and restriction patterns were designated pStark-PhLP1-LoxP2-Neo plasmid.

Gateway recombination: adding the negative selection tk cassette

HSV-TK genes were introduced into the targeting vector using Gateway recombination reaction. The reaction mixture was set up as follows: LR reaction buffer (5x), 1 μl; pStartK-PhLP1-LoxP2-Neo, 2 μl; pWS-TK2 linearized with SalI, 1 μl; LR clonase enzyme mix, 1 μl, incubated at 25°C for 1 hr, 0.5 μl of proteinase K was added to the solution and the solution mix was incubated for 10 min at 37°C. Chemically competent DH5α cells were transformed with 2 μl of the above reaction mixture by heat shock at 42°C for 1 min. Cells were spread on LB-agar plates with 100 μg ml^{-1} ampicillin. The plates were incubated at 30–32°C for 20 to 30 hrs. Several colonies were picked and grown in 5 ml of SOB medium at 30–32°C for 20 hrs for DNA

isolation. Correct clones were confirmed by restriction digestion analysis and sequencing. Correct clones were designated pStartK-PhLPl-LoxP-TK2 (Fig. 3-1 A).

Preparation of DNA for electroporation of ES cells

pStartK-PhLPl-LoxP-TK2 targeting vectors were linearized for electroporation of ES cells. Approximately 100–150 μg of clean DNA were prepared by digesting 200 μg of targeting vector DNA with NotI restriction enzyme at 1–2 U per μg DNA in a total volume of 500 μl reaction for ~ 4 h. About 50 ng of digested DNA along with 50 ng of uncut targeting vector and ladder were run on a 0.8% agarose gel in Tris-acetate-EDTA (TAE) buffer at 100 V for 1 hr to determine the completeness of the digestion. To purify the 500 μl DNA digest, 1 volume of phenol and 1 volume of chloroform were added, and the tube was hand-shaken vigorously for 1 min. The tube was centrifuged at 20,000g for 3–5 min at 23^{o}C in a bench-top centrifuge. The supernatant was transferred into a new tube, and an equal volume of chloroform was added. The tube was hand-shake vigorously and was centrifuged again at 20,000g for 3-5 min at 23^{o}C. The supernatant was transferred into a new Eppendorf tube. Approximately 1.6-2 volumes of 100% ethanol were added. The tube was mixed by gentle inversion to form web-like DNA. The tube was centrifuged at 3,000g for 2 min, and the supernatant was discarded. The DNA pellet was rinsed with 0.5 ml of 70% ethanol by shaking. Then the tube was centrifuged at 3,000g for 2 min. The supernatant was again discarded. The tube was centrifuged briefly at 3,000g for 10 s, and the residual liquid was removed by pipetting. The linearized DNA pellet was required to be fully dissolved by gentle pipetting up and down in 100 μl of Tris-EDTA (TE) buffer (pH 7.5, filtered). The linearized DNA was stored at 4°C until use or at -20°C for long-term storage.

Gene targeting in mouse ES cells

Two reactions of G4-derived ES cell lines were prepared for electroporation at 250V with or without 30 μg of the NotI-linearized pStark-PhLP1-LoxP2-TK2 targeting vector. The electroporation cuvettes were kept on ice immediately after electroporation for 20 minutes. A negative control with the same amount of G4 ES cells was treated with the electroporation procedure without the addition of targeting vector DNA. The electroporated mixture were then plated onto two separate 10-cm dishes with mitomycinC-treated (mitoC-treated) NeoR (Neomycin resistant) mouse embryonic fibroblasts (MEFs) and grown in ES media (15% Fetal bovine Serum (FBS), 100 μM MEM Non Essential amino acids, 100 μM β-Mercaptoethanol, 2 mM L-Glutamine, 50 μg/mL Pen/Strep, LIF 10E3) for 24 hours. After the incubation, the media was replaced with ES media containing 300 μg/mL of G418 and 2 μM FIAU. The media was replaced with fresh media about every 2-3 days. Within approximately 7-9 days, all colonies missing the neomycin gene had cleared off and the Neomycin-positive colonies were still viable in the presence of the selective media. Non-differentiated well-shaped colonies were picked with a 200-μl pipette and transferred into a 48-well plate containing approximately 100 μl trypsin/EDTA in each well. After a set of colonies had been picked, the plate was incubated at 37°C for 10 min. Approximately equal volume of ES media (with G418 and FIAU) was added to each well to inactivate the trypsin. The ES cells were triturated in each well with a multi-channel pipetman and were transferred to a 48-well plate of mitoC-treated NeoR MEFs. Additional 400 μl of media were added to each well after the transfer. The media was changed upon visible detection of depleted nutrients. When the ES cells became confluent (from several days to 2 weeks at the most) and populated most of the area in the well, the ES cells were replica-plated for storage. For replica plating of these ES cells, the media from each well was aspirated and

washed with 1X PBS twice. Then, 100 μl of trypsin/EDTA was added and incubated at 37°C for 10 minutes. After incubation, 100 μl of ES media was added to each well, and the ES cells were triturated ~20 times. Approximately 100 μl of ES cells were transferred into two separate 48-well plates with mitoC-treated MEFs for master plate storage and DNA preparation. Approximately 400 μl of additional media were added to each well. When the ES cells had populated most of the area of the master plate, the wells were washed with 1X PBS and added with 100 μl trypsin / EDTA and incubated at 37°C for 10 minutes. After incubation, 100 μl of ES media was added and triturated. Approximately 200 μl of 2X freezing media (ES medium with 30% FBS and 20% DMSO) was added to each well and mixed. The entire mixture was transferred into a cryo-storage tube and placed into a freezing box to store at -80°C. For the DNA plates, the media was aspirated and washed with 1X PBS once when the ES cells had populated most of the area of the wells. The ES cells were lysed with 300 μl of DNA lysis buffer and transferred to a 1.7-mL Eppendorf tube. Approximately 5 μl of proteinase K was added to each tube and incubated at 37°C overnight. Extraction procedures of genomic DNA from these ES cells were described in the following section.

Preparation of genomic DNA from ES cells for Southern blot or PCR

To prepare DNA from ES cells for Southern blot analysis or PCR, ES cells were lysed in 1.7-ml Eppendorf tubes in ~500 μl of ES cell lysis buffer. About 5 μl of proteinase K (from 20 mg ml^{-1} stock) was added to a final concentration 0.2 mg ml^{-1} and incubated at 37°C for 4 hrs without shaking. About 25 μl of additional proteinase K (from 20 mg ml^{-1} stock) was added and incubated at 55°C overnight. An equal volume of phenol:chloroform mix was added to each tube. The tubes were shaken vigorously for 2 min and centrifuged at 20,000g for 5 min at RT.

The supernatant was transferred into a new Eppendorf tube, and ~1 ml 100% isopropanol was added along with 1 μl of glycoblue and 1/10 volume 3 M sodium acetate solution. The DNA was spun down at 20,000g for 15 min at 23^{o}C and washed with 0.5 of 70% ethanol once. DNA was again spun down at 20,000g for 5 min and was dissolved in 50 μl TE buffer (pH 7.5) by incubating at 55°C for 30 min.

Southern blotting screening of stem cell

The screening of ES cells was carried out by Southern blotting. Radioactive-labeled probes were prepared using the Ready-To-Go DNA labeling beads (Amersham) following the manufacturer's instructions. Probes were purified with G50 columns (ProbeQuant G-50 Micro Columns from Amersham). Genomic DNA from ES cells were digested with the following set up: 5–10 μg of genomic DNA in ~15 μl were digested with AflII (10–20 U) in a 25 μl reactions in the presence of 4 mM spermidine for 12–20 hrs at 37°C. The digested DNA were separated by adding 10 μl of 6X loading dye, heated at 65°C for 10 min and loaded onto a 0.7% agarose gel in 1 x TAE buffer. An appropriate amount of 1 kb DNA ladder was also included in a control lane. The samples were run at 20-50 V for about 4-5 hrs. The gel was then photographed under UV light and exposed under extended UV irradiation for a total of 5 mins. The DNA was transferred into Hybond N+ nylon membrane (Amersham) by downward capillary transfer using a protocol described previously [165]. The gel was denatured in 3 M NaCl, 0.4 M NaOH for 1 hr, and DNA was blotted onto a Hybond N+ membrane in 3 M NaCl, 8 mM NaOH for approximately 4 hrs. The nylon membrane was neutralized in 0.2 M sodium phosphate, pH 6.5 and UV-crosslinked with a UV Stratalinker 1800 for 3 mins. The membrane was placed in a sealed plastic bag for prehybridization in an oven set at 42°C with 7.5 mL of hybridization solution (Millipore). After approximately 1.5 to 2 hrs, the radioactive probe was added to the plastic bag, and the bag was

re-sealed. The probed was boiled for 10 mins and snapped cooled on ice prior to use. The hybridization reaction was incubated at 42°C for 18-40 hrs. After hybridization, the membrane was washed twice in 2X SSC, 0.1% SDS at 23^{o}C for 15 min and once in 0.2 X SSC, 0.1% SDS at 42°C for 10–15 min. The membrane was placed into a phosphor imaging cassette at 23^{o}C for approximately 18-40 hrs and visualized using a Phosphor-Imager system.

Karyotyping and microinjection

Karyotyping and microinjection were performed in the University of Utah Transgenic Mice Core facility. Successfully generated chimeric embryos were implanted into the uteri of surrogate mothers. The chimeric offspring were further inbred to produce homozygous mice that carried the *PhLP1-loxP* mutation. The *neo* gene that was needed for positive selection was removed by crossing the PhLP1-loxP mice with FLP transgenic mice. The progeny were screened for the *neo* gene deletion by PCR for identifying complete *neo* excision strains.

The mice containing the fully processed *PhLP1-loxP* gene were then bred with the *Rhodopsin*-Cre (iCre75) mice and further inbred to produce homozygous PhLP1-loxP$^{+/+}$ iCre75$^{+/-}$ mice, designated PhLP1$^{F/F}$Cre^{+} mice. The reduction in PhLP1 expression in rod cells of these mice was confirmed by immunocytochemistry and immunoblotting of protein extracts. PhLP1 expression levels were compared to littermates lacking the PhLP1-LoxP mutation.

Genotyping of PhLP1 knockout mice

Genotyping of knockout mice was carried out by Southern blotting for germline transmission confirmation, and PCR was used for routine genotyping of mice from subsequent breeding. Approximately 0.5 cm tail tissue was put in a 1.7-mL Eppendorf tube containing 480 μl of tail lysis buffer for the isolation of genomic DNA. About 25 μl of proteinase K (from 20 mg ml^{-1}

stock) was added and incubated at 55°C overnight. An equal volume of phenol:chloroform mix was added to each tube. The tubes were shaken vigorously for 2 min and centrifuged at 20,000g for 5 min at RT. The supernatant was transferred into a new Eppendorf tube, and ~1 ml 100% isopropanol was added along with 1 μl of glycoblue and 1/10 volume of 3 M sodium acetate solution. DNA was spun down at 20,000g for 15 min at 23^{o}C and washed with 0.5 of 70% ethanol once. DNA was again spun down at 20,000g for 5 min and was dissolved in 200 μl TE (pH 7.5) by incubating at 55°C for 30 min. For quick preparation of DNA for PCR genotyping, a small mouse ear clip tissue was boiled in 75 ul Hotshot lysis solution [164] for 1 hr and neutralized with 75 μl of 40 mM Tris-Cl. Approximately 3 μl of the mixture was used for PCR genotyping in a 25 μl reaction.

Several primers were designed to genotype these mice. P3: GATCACTTTGACTGGGGAA TGATTTTAGGT; P4: GAGGTGGTAAGCAGGTGTACTGGCTGGTTT; P_Neo: GGCGGCA TCAGAGCAGCCGATTGTCTGTTGTGCCCAGTCATAGCCGAATA. Multiplex PCR reactions for genotyping were set up at follows: (25-μl reactions: DNA, 3 μl; 10x amplification buffer, 5 μl; PCR enhance, 5 μl; 25 mM $MgCl_2$, 0.5 μl; primers, 1.25 μl each at 10 mM; 10 mM dNTP, 0.75 μl; Pfx Taq, 0.2 μl; H_2O was added to a total volume of 25 μl. PCR conditions: 94°C 5 min; 30 cycles of 94°C 30 s, 50°C 30 s and 68°C 60 s; 68°C 7 min). PCR products were loaded and separated on 1% agarose gels. Presence of a band size of 844 bp indicated the presence of the neomycin gene in the intron 3 of the PhLP1 gene. After crossing with Flp-mice, the disappearance of this band indicated the removal of neomycin from the genome. Subsequently, genotypes of PhLP1$^{F/F}$ (704 bp), PhLP1$^{F/+}$ (704 bp, 600 bp) and PhLP1$^{+/+}$ (600 bp) were determined according to the presence of corresponding band sizes (Figure 3-2 E). Genotyping for determination of the presence of Flp and Cre genes in these mice were performed according to

the Jackson Lab web protocol (http://jaxmice.jax.org; strain: 129S4/SvJaeSor-Gt(ROSA) 26Sor$^{tm1(FLP1)Dym}$/J) and [166], respectively.

Assessment of photoresponse by ERG

Prior to ERG recordings, age-matched mice were dark-adapted overnight and anesthetized by intraperitoneal injection using 60 mg ketamine and 10 mg xylazine per kilogram of body weight. Pupils were dilated by adding a drop of 1% tropicamide for 10-15 min to the eyes. A recording electrode was placed on the cornea with a reference electrode inserted subcutaneous above the skull. ERG responses were measured using a UTAS E-3000 (LKC Technologies, Inc., Gaithersburg, MD) apparatus according to [167]. Scotopic ERG recordings of both PhLP1$^{F/F}$Cre^{+} and controls were performed with different intensities of light flashes between -40 to 20 dB. The recovery time of the scotopic ERG between each flash varied from 10 sec to 60 sec (depending on the flash intensities) at low intensities $\leq$ 0.39 log cdS m^{-2}. For flash intensities > 0.39 log cdSm^{-2}, the recovery intervals between two flashes was 2-5 min. Photopic ERGs recordings were performed under a background light of 1.48 log cdS m^{-2} and the stimulating flash intensities varied from -0.61 to 2.89 log cdS m^{-2}. The recovery time of photopic ERG between each flash varied from 10 sec to 2 min depending on the flash intensities. The amplitudes of the a-wave and b-wave at different light intensities were compared between the PhLP1$^{F/F}$Cre^{+} and controls.

Immunohistochemistry and assessment of photoreceptor degeneration

The expression levels of PhLP1 and transducin subunits in rod photoreceptors in these mice were tested by immunocytochemistry as described previously [167-169]. Briefly, superior hemisphere of eyes from age-matched PhLP1$^{F/F}$Cre^{+} and control mice were cautery-marked for orientation. These eyes were enucleated under ambient illumination without adaptation and were immersion-fixed for 2 hr using freshly prepared 4% paraformaldehyde in 0.1 M phosphate buffer

(pH 7.4) and cryo-protected overnight in 30% sucrose in 0.1 M phosphate buffer (pH 7.4). The cornea and lens were then removed, and the eyecups were embedded in optimal cutting temperature (OCT) compound and cryosectioning was performed. Cryosections of 12 μm were cut through the optic nerve head along the vertical meridian and were placed on superfrost microscope slides. For immunohistochemistry, sections were rinsed in 0.1 M PBT, and blocked for 1 hr using 10% normal goat serum, 0.1% Triton X-100 in 0.1 M phosphate buffer (pH 7.4). Primary antibodies to PhLP1 (1:250 dilution), $G\alpha_{t1}$ (1:50, Santa Cruz Biotechnology), $G\beta_1$ (1:200, Santa Cruz Biotechnology) and $G\gamma_1$ (1:50, Santa Cruz Biotechnology) were applied to each group of four sections in a humidified chamber overnight at 4°C. After rinsing in three 10-min PBT washes, rhodamine- or fluorescein isothiocyanate-conjugated secondary antibodies (Jackson ImmunoResearch Laboratories, West Grove, PA; catalog no. 711-295-152 and 715-096-150) at a 1:200 dilution were applied for 2 hrs at room temperature. The sections were viewed using a Zeiss LSM 510 inverted Laser Scan confocal microscope with a 60x, 1.3 numerical aperture oil objective lens and an optical slit setting of <0.9 μm. Images were taken consistently inferior to the optic nerve of each section.

Cryosections with intact morphology were used for further analysis to determine photoreceptor degeneration as described previously [170] . These sections were labeled with 100 ng/ml 4'6 diamidino-2-phenylindole dihydrochloride (DAPI) nuclear stain for 30 minutes in the dark and were then mounted and coverslipped. Digital images were then acquired and were used to measure the outer nuclear layer thickness in the superior central retina approximately 100 μm from the edge of the optic nerve head.

Determination of G_t subunit and PhLP1 expression

Whole retina extracts were prepared from eyes of age-matched PhLP1$^{F/F}$Cre^{+} mice and controls under ambient illumination [171]. These retinas were harvested and placed in ice-cold RIPA buffer (1x PBS with 2% NP-40 and 6 μl/mL Sigma Protease inhibitor cocktail). The retinas were then passed through an 18G needle 20 times and a 25G needle 10 times to release the proteins. Extracts were centrifuged at 13,800 rpm for 10 min at 4°C to remove cellular debris. Protein concentrations were determined by BCA protein assay, and extracts with equal amounts of protein were loaded and separated by electrophoresis on 10% polyacrylamide gels and transferred onto nitrocellulose membranes using an iBlot transfer apparatus (Invitrogen). After blocking with Licor Blocking buffer for 1 hr, membranes were immunoblotted for each of the transducin subunits as well as other visual proteins as indicated. The amounts of each protein in the immunoblots were quantified using a LICOR Odyssey near-infrared imaging system and compared to controls.

Results

Generation of rod-specific PhLP1 conditional knockout mice

The design of the targeting vector for inserting the loxP sequences into the PhLP1 gene is shown in Fig. 3-1. The circular DNA plasmid contains the PhLP1 gene flanked by two homologous arms of approximately 2.9 kb and 5kb in length with loxP sequences in introns 1 and 3 (Figure 3-1 A-C). At these positions, the loxP sequences did not cause a frame shift in the amino acid sequence of PhLP1. Thus, the endogenous PhLP1 gene was replaced with the PhLP1-LoxP construct without affecting the native PhLP1 function until the Cre recombinase was expressed to disrupt the expression of PhLP1. This targeting vector also contained neomycin

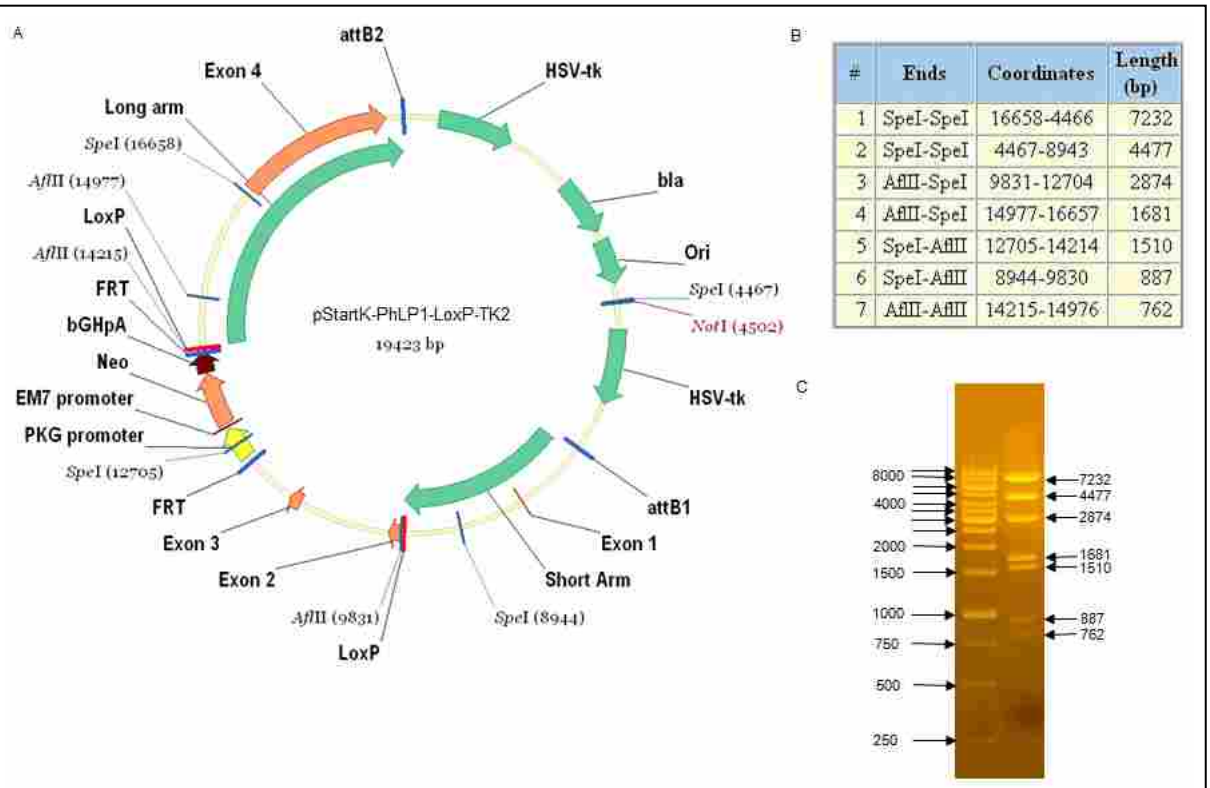

#	Ends	Coordinates	Length (bp)
1	SpeI-SpeI	16658-4466	7232
2	SpeI-SpeI	4467-8943	4477
3	AflII-SpeI	9831-12704	2874
4	AflII-SpeI	14977-16657	1681
5	SpeI-AflII	12705-14214	1510
6	SpeI-AflII	8944-9830	887
7	AflII-AflII	14215-14976	762

Figure 3-1. Design of pStartK-PhLP1-LoxP-TK2 targeting vector.
A) Vector map for the conditional deletion of PhLP in mouse rod photoreceptor cells is depicted here. The main components of the targeting vector for developing the conditional knockout mouse are shown. B) The number of bands, cleavage ends, sequence coordinates, and length (bp) for the AflII-SpeI restriction digestion of the final targeting vector are shown. This table was generated using NEB cutter v2.0 (http://tools.neb.com/NEBcutter2/index.php) C) Validation of the final targeting vector by AflII and SpeI restriction digestion. Lane 1: 1kb DNA ladder Lane 2: AflII-SpeI digested final targeting vector. Band sizes are indicated.

resistance (neo) and thymidine kinase (TK) genes for the positive and negative selection (Figure 3-1 A).

Electroporation of ES cells, positive/negative selection

The targeting vector was linearized with the NotI restriction enzyme and purified with phenol/ chloroform/isopropanol precipitation. The linearized targeting vector was electroporated into G4 hybrid ES cells lines to substitute for the endogenous *pdcl* gene by homologous recombination. G418 and FIAU were used to carry out positive and negative selection on the electroporated ES cells, respectively. The correctly targeted ES cell clones were screened by Southern blotting. Fig. 3-2 A-D shows different genotypes of the ES cell lines indicated by the

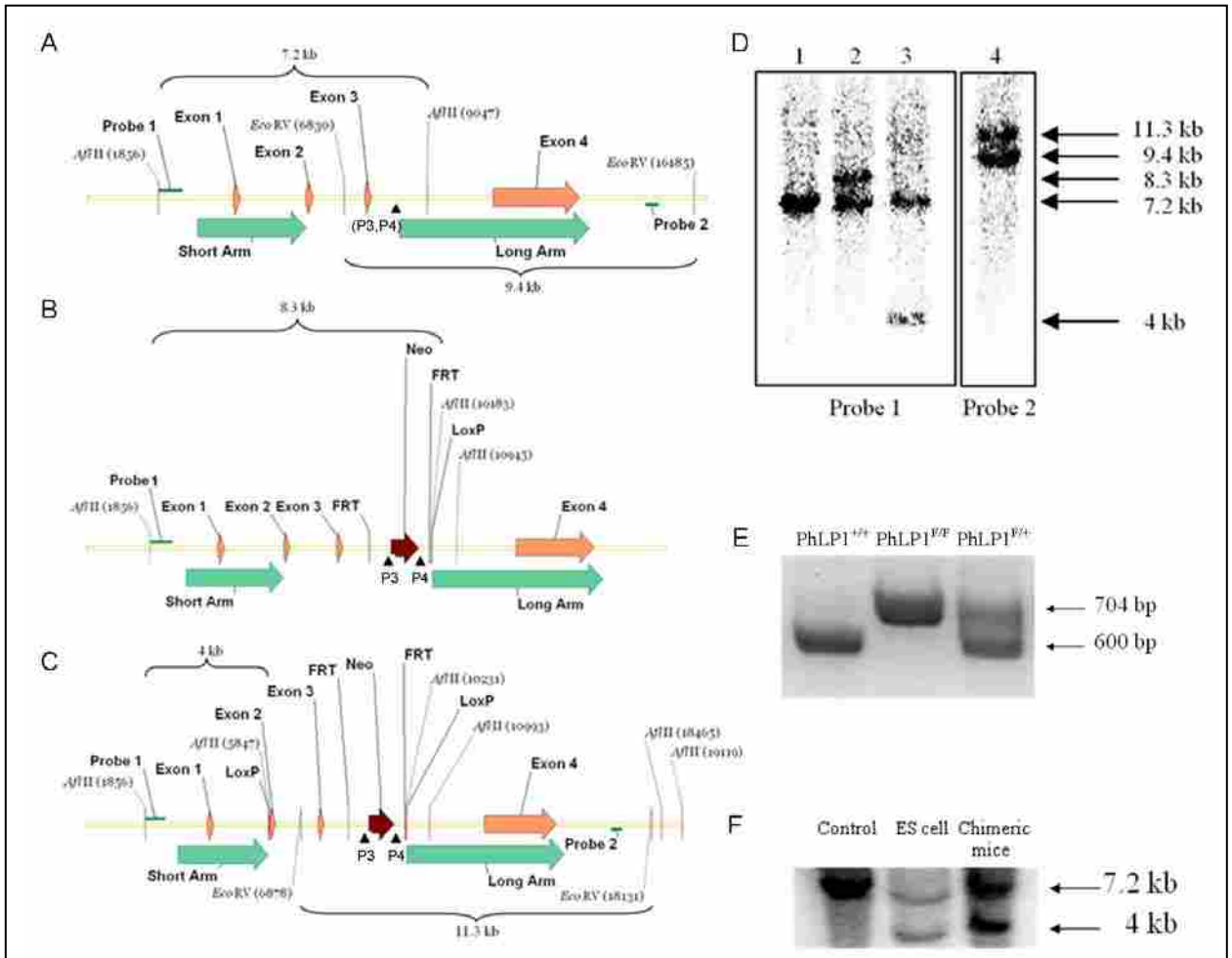

Figure 3-2. Southern blot and genotyping analysis of ES cells and chimeric mice.
A-C) The maps of wild type (A), incomplete incorporation B) and complete incorporation C) of LoxP sites in the pdcl gene along with the restriction site of AflII and EcoRV are shown. The annealing site of probe 1 and 2 are indicated in each map. For 5' end (upstream) probing in the Southern analysis, ES cell DNA were digested with AflII restriction enzyme and were hybridized with probe 1. The predicted band sizes for wild type, incomplete incoporation and complete incorporation were 7.2 kb, 8.3 kb, and 4 kb, respectively. For 3' end (downstream) probing, ES cell DNA were digested with EcoRV restriction enzyme and were hybridized with probe 2. The predicted bands size for wild type and targeted (both incomplete incoporation and complete incorporation) are 9.4 kb and 11.3 kb, respectively. D) Southern blot analysis of DNA from selected G4 mice ES cell lines after positive and negative selection is shown. Lanes 1-3 show the results from 5' end probing using AflII digestion and probe 1 hybridization. Lane 4 shows the results from 3' end probing using EcoRV digestion and probe 2 hybridization. Lane 1 and 2 show the patterns for the genotype of wild type and an incorrectly targeted allele. Lanes 3 and 4 show the patterns for the genotype of correctly targeted allele. E) Genotyping of PhLP1 CKO mice by PCR. Two primers (P3, P4) were used in the PCR to amplify the 600 bp product from the PhLP1 gene and/or the 704 bp product from the PhLP1-LoxP allele containing residual sequences from the removal of the neomycin resistance cassette. Genomic DNA was extracted from mouse ear clip tissues as described in text. F) Southern blot analysis of DNA obtained from 1) tail tissue of a B6 mouse 2) ES cells that were used for blastocyst implantation, 3) tail tissue of a blastocyst implantation-generated PhLP1-loxP chimeric mouse.

map and their corresponding Southern blotting results. Among 121 ES cell clones that were screened, 16 were targeted at the *pdcl* allele with 2 having correct incorporation of both loxP sites at the right location of the *pdcl* locus. Therefore, the efficiency for selecting correctly recombined ES cells was approximately 2%.

Karyotyping, Generation of Chimeric mice and Genotyping

Karyotyping revealed that a clone with the desired mutation termed G2B1 contained ES cells with 84% having 40 chromosomes, 12% having 39 chromosomes, and 4% having 41 chromosomes. Blastocyte microinjections were performed on these ES cells, and they successfully generated 15 chimeric mice that carried the desired PhLP1-LoxP construct. Genotyping by PCR and Southern blot were performed on these mice and confirmed successful insertion of the PhLP1-LoxP in place of the *pdc1* gene (Figure 3-2 E-F). Breeding with Flp and iCre75 mice have produced PhLP1 conditional knockout mice in retinal rod photoreceptor cells. Only the mice with $PhLP1^{F/F}Cre^{+}$, $PhLP1^{F/+}Cre^{+}$, and $PhLP1^{+/+}Cre^{+}$ genotypes were used in subsequent experiments for characterization.

Assessment of photoresponse by ERG

Electroretinography (ERG) was used to assess the effects of PhLP1 deletion in the retinal function. ERG technology is based on the recording of complex field potentials initiated in the retina by light responses detected by placing an electrode on the cornea [172]. The initial negative deflection, designated as the a-wave, reflects the light-dependent current suppression in the rod/cone outer segments [173], and the subsequent positive deflection, designated as the b-wave, measures the depolarization from the bipolar cells functioning downstream of the photoreceptor cells in the retinal phototransduction process [174].

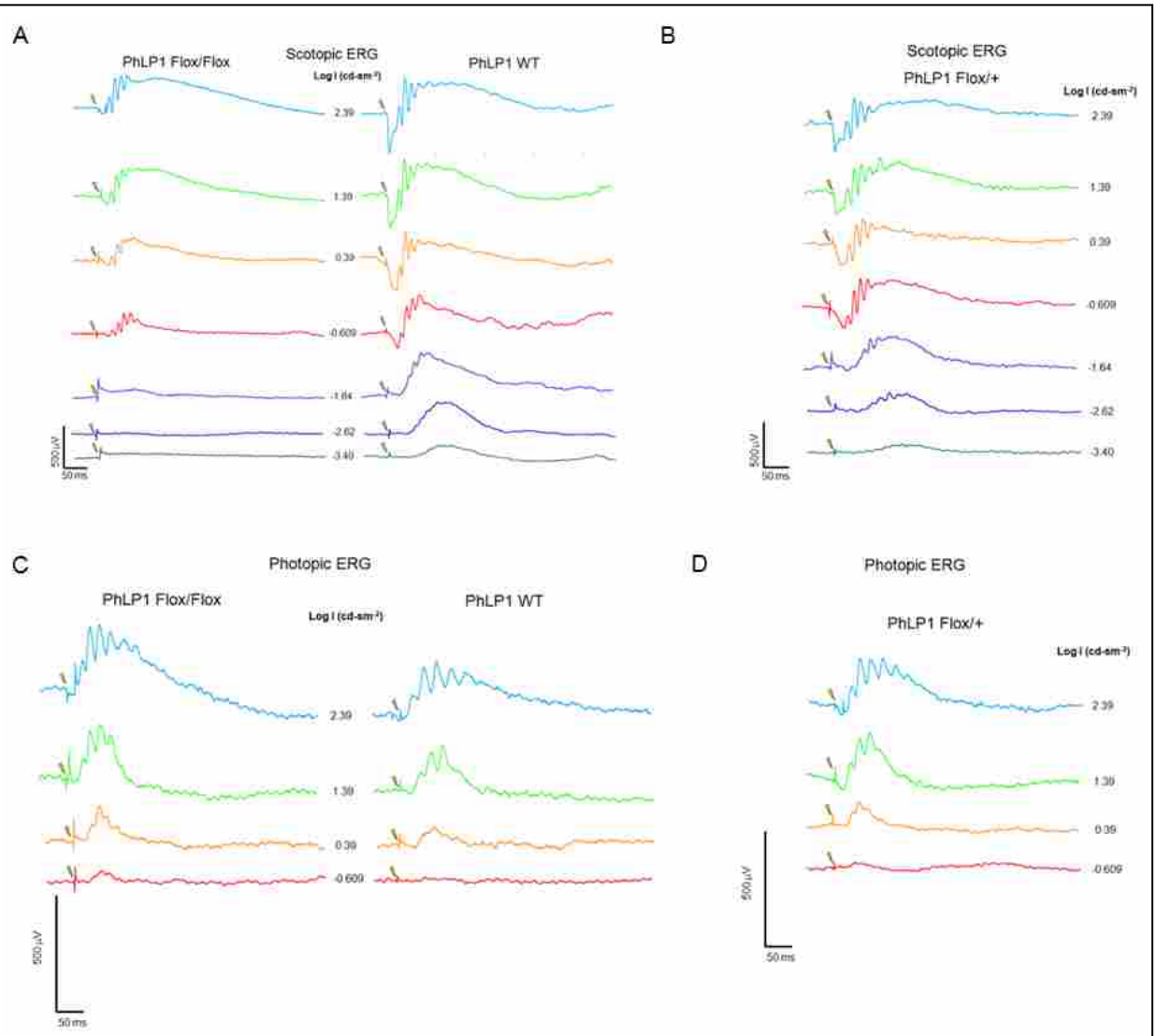

Figure 3-3. Scotopic and photopic ERG analysis of 33- to 37-d-old mice.
A, B). Scotopic ERG recordings were obtained from dark-adapted PhLP1$^{F/F}$Cre^{+}, PhLP1$^{F/+}$Cre^{+}, and PhLP1$^{+/+}$Cre^{+} mice under increasing intensities of flash stimuli. C, D) Photopic ERG recordings were obtained from light-adapted mice under increasing intensities of flash stimuli. Traces are shown in log scale and measured in cdSm^{2}.

ERGs of 5 week old PhLP1$^{F/F}$Cre^{+} mice and controls were recorded under various conditions. Under a low intensity flash, a prominent b-wave was detected in dark-adapted (scotopic) WT mice. However, no detectable b-wave was found in the scotopic ERG of PhLP1$^{F/F}$Cre^{+} mice under the same conditions, indicating a significant defect in the rods and/or in the rod bipolar cells. Under higher light intensities, a characteristic a-wave was detected in dark-adapted control mice. In contrast, the a-wave was largely absent in dark-adapted PhLP1$^{F/F}$Cre^{+} mice (Figure 3-3

A and B), suggesting that the rod cells of these PhLP1$^{F/F}$Cre^{+} mice were unresponsive to light. Although these mice showed b-wave signals under high intensity flashes, these photoresponses were closely similar to the murine cone b-wave [173, 175] suggesting that under bright lights, only cone bipolar cells were activated (Figure 3-3 A and B). The maximal amplitude of the scotopic b-wave, which was dominated by the responses from rod bipolar cells, was also reduced by approximately 50 – 60% in dark-adapted PhLP1$^{F/F}$Cre^{+} mice, which is consistent with the observed a-wave reduction. To test whether these PhLP1$^{F/F}$Cre^{+} mice retain normal cone functions, they were exposed to a background light that suppresses over 95% of the rod circulating current [173]. Under this rod-saturating background, PhLP1$^{F/F}$Cre^{+} mice and controls showed very similar photopic ERG responses (Figure 3-3 C and D), further indicating that the recorded responses from these PhLP1$^{F/F}$Cre^{+} mice originated from cone-driven bipolar cells.

Immunohistochemistry and assessment of photoreceptor degeneration

Results of immunohistochemistry showed that PhLP1 was successfully knockout in the rod cells (Figure 3-4 A-H). The signals from PhLP1 antibodies were mostly absent in the outer and inner segment of the photoreceptor cells since 97% of these cells are rods in mice. PhLP1 was also absent in the outer nuclear layer. Detectable amount of PhLP1 was found in the outer plexiform layer, which is mainly composed of biopolar cells and horizontal cells and the synaptic nerves of the photoreceptors (Figure 3-4 A-B). This observation was expected because the knockout only targeted the rod cells. The signals from the $G\alpha_{t1}$, $G\beta_1$ and $G\gamma_1$ subunits were all significantly diminished in the PhLP1$^{F/F}$Cre^{+} mice (Figure 3-4 C-H). Since $G\beta_1$ is expressed to some extent in all cell types of the retina, it was seen in the cells of the inner retina, but its expression is drastically reduced in the photoreceptor cell layer. In addition, both $G\alpha_{t1}$ and $G\gamma_1$, which are only expressed in photoreceptors, showed similarly decreased expression levels. This

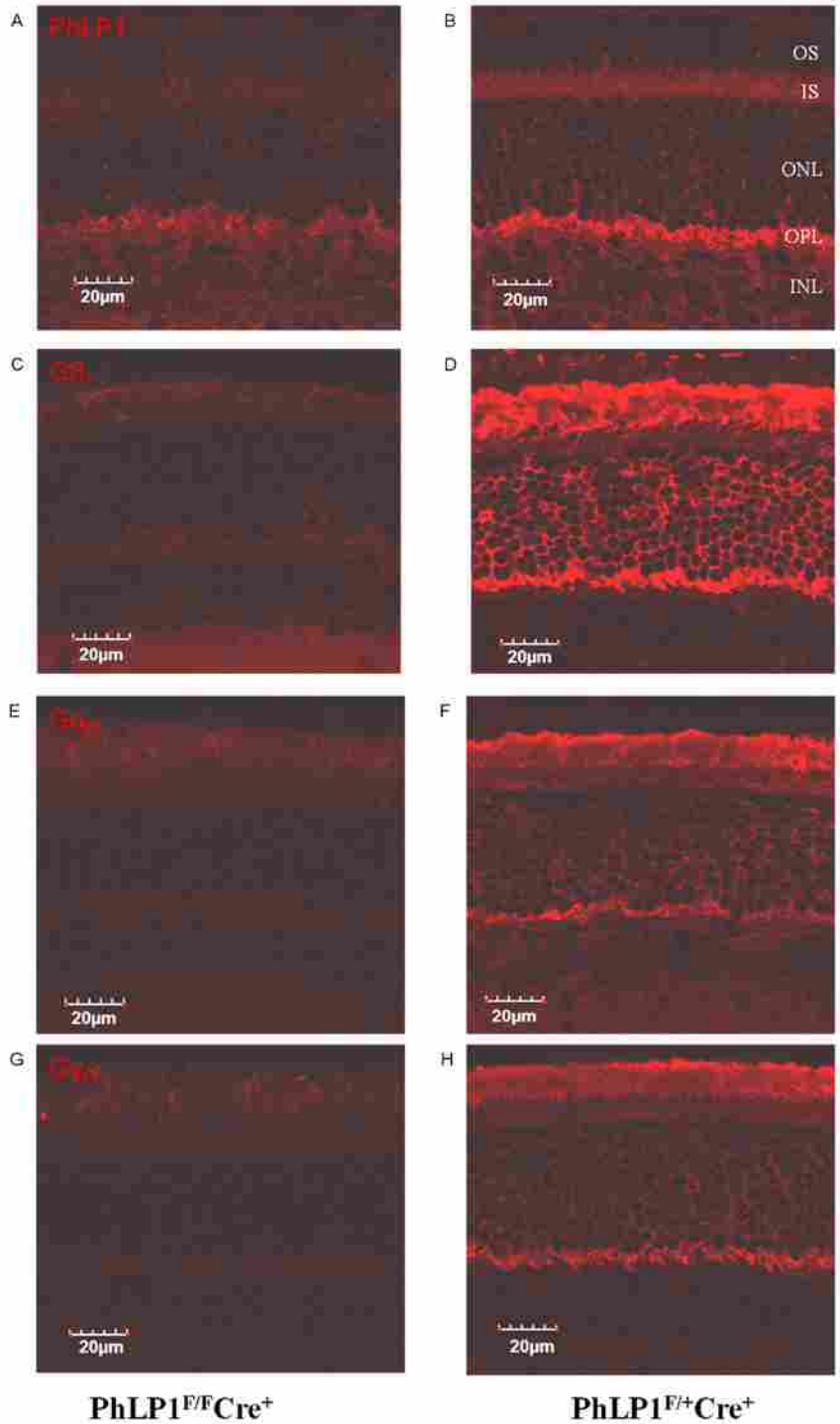

Figure 3-4. Immunohistochemical analysis of PhLP1 and transducin subunits.

A-H) Expression of PhLP1 and G protein transducin αβγ subunits are shown as indicated. Proteins were detected with a rhodamine-conjugated seconday antibody (fluorescent red). Scale bar = 20 μm. The outer segment (OS), inner segment (IS), outer nuclear layer (ONL), outer plexiform layer (OPL) and inner nuclear layer (INL) are labeled in panel B.

marked decrease in G_t subunits explains the lack of the a-wave in the ERG experiments because in the absence of G_t, phototransduction cannot occur [171].

Morphological analysis of 5 week old PhLP1$^{F/F}$Cre^{+} retinas (Fig. 3-4) showed normal maturation of photoreceptor cells and retinal development. The outer nuclear layer that consists of photoreceptor nuclei can serve as a gauge for the number of rods present in the photoreceptor cells, and at 5 weeks of age, the outer-nuclear-layer thickness of PhLP1$^{F/F}$Cre^{+} mice was similar to controls. The thickness of the outer nuclear layers measured in the 5-week old PhLP1$^{F/F}$Cre^{+} mice and controls were approximately 100 μm indicating that the loss of PhLP1 in rods did not severely hinder the health of the photoreceptor cells, and there are negligible changes in the thickness of the outer nuclear layer. This result indicated that PhLP1 is not essential for the viability of the rod outer segments.

Determination of PhLP1 and G_t subunit expression

Whole retina extracts from PhLP1$^{F/F}$Cre^{+} mice and controls were used to analyze the effects of PhLP1 knockout on protein content. The protein expression of PhLP1 and all three G_t subunits were dramatically reduced (Figure 3-5 A and B; 3-6 A and B). PhLP1 expression in the whole retina was reduced to 25% of wild-type. The remaining PhLP1 comes from retinal cell types other than rods which are known to express PhLP1. $G\alpha_{t1}$ and $G\gamma_1$, which are only expressed in rods, were reduced to 32% and 16% of wild-type, respectively. $G\beta_1$, which like PhLP1 is found in other retinal cell types [176], was reduced to 35% of wild-type. This finding demonstrates that G_t subunit expression in rods is dependent on PhLP1 *in vivo*. Interestingly, retinal expression of other Gβ and Gγ subunits is also reduced in the PhLP1$^{F/F}$Cre^{+} mice. $G\beta_4$ expression was reduced by 95% and $G\gamma_3$ expression was reduced by 80%. In contrast, $G\beta_3$ expression is not reduced in the PhLP1$^{F/F}$Cre^{+} mice, which is consistent with the observation that $G\beta_3$ is expressed in murine

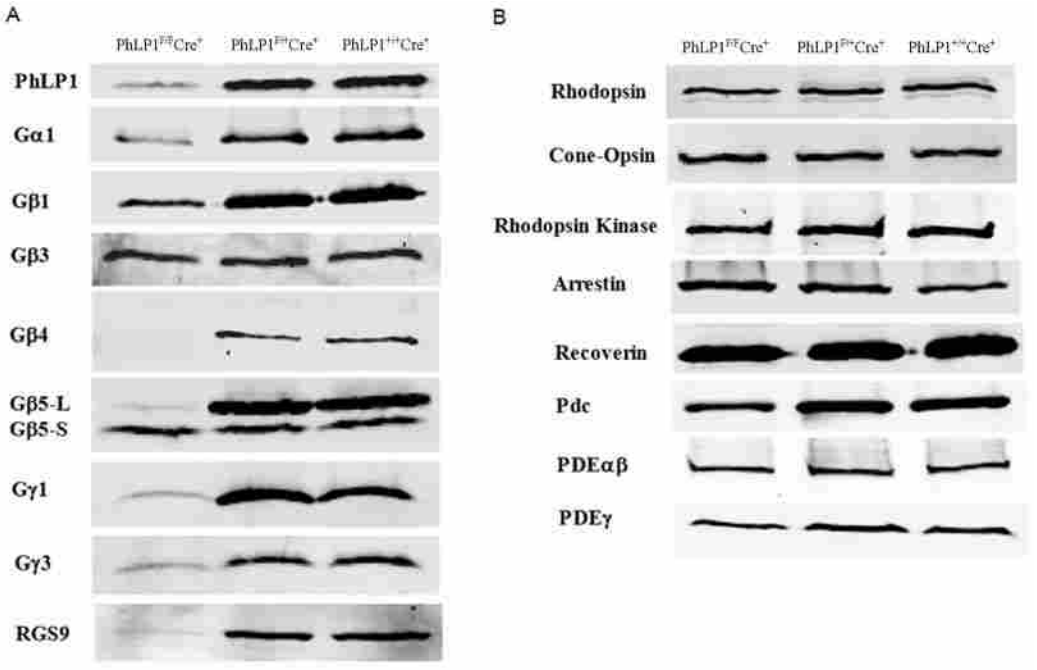

Figure 3-5. Immunoblots of whole retina extracts from 33- to 37-d-old mice.
A) Immunoblots of retina lysates probed with antibodies raised against PhLP1, RGS9 and major G protein subunits expressed in retina. B) immunoblots of other important photoreceptor proteins. Retina lysates obtained from PhLP1$^{F/F}$Cre^{+}, PhLP1$^{F/+}$Cre^{+}, and PhLP1$^{+/+}$Cre^{+} mice are indicated.

cones and bipolar cells, but not in rods [177, 178]. Interestingly, the expression of the rod specific Gβ_5L-RGS9-1 complex which is the Gα_t GTPase that sets the rate of recovery of the photoresponse, is dramatically reduced in the PhLP1$^{F/F}$Cre^{+} mice, while the Gβ_5S isoform, which is not expressed in rods, is not reduced. These findings demonstrate that PhLP1 plays an important role in the expression of G$\beta\gamma$ and Gβ_5L-RGS9-1 dimers in rod photoreceptors.

Most other visual proteins were not affected by the knockout of PhLP1 in rods indicating that the down regulation of PhLP1 was specifically affecting G protein dimer assembly (Figure 3-5 B; 3-6 B). One exception was Pdc, which is a known G$\beta\gamma$ binding partner in rods and has been shown to be reduced when G$\beta\gamma$ levels are reduced [174, 176]. The fact that rhodopsin and other proteins that localize to the rod outer segment are not reduced in the absence of PhLP1 indicates that the rods are not degenerating and that the outer segments do not have serious defects. This

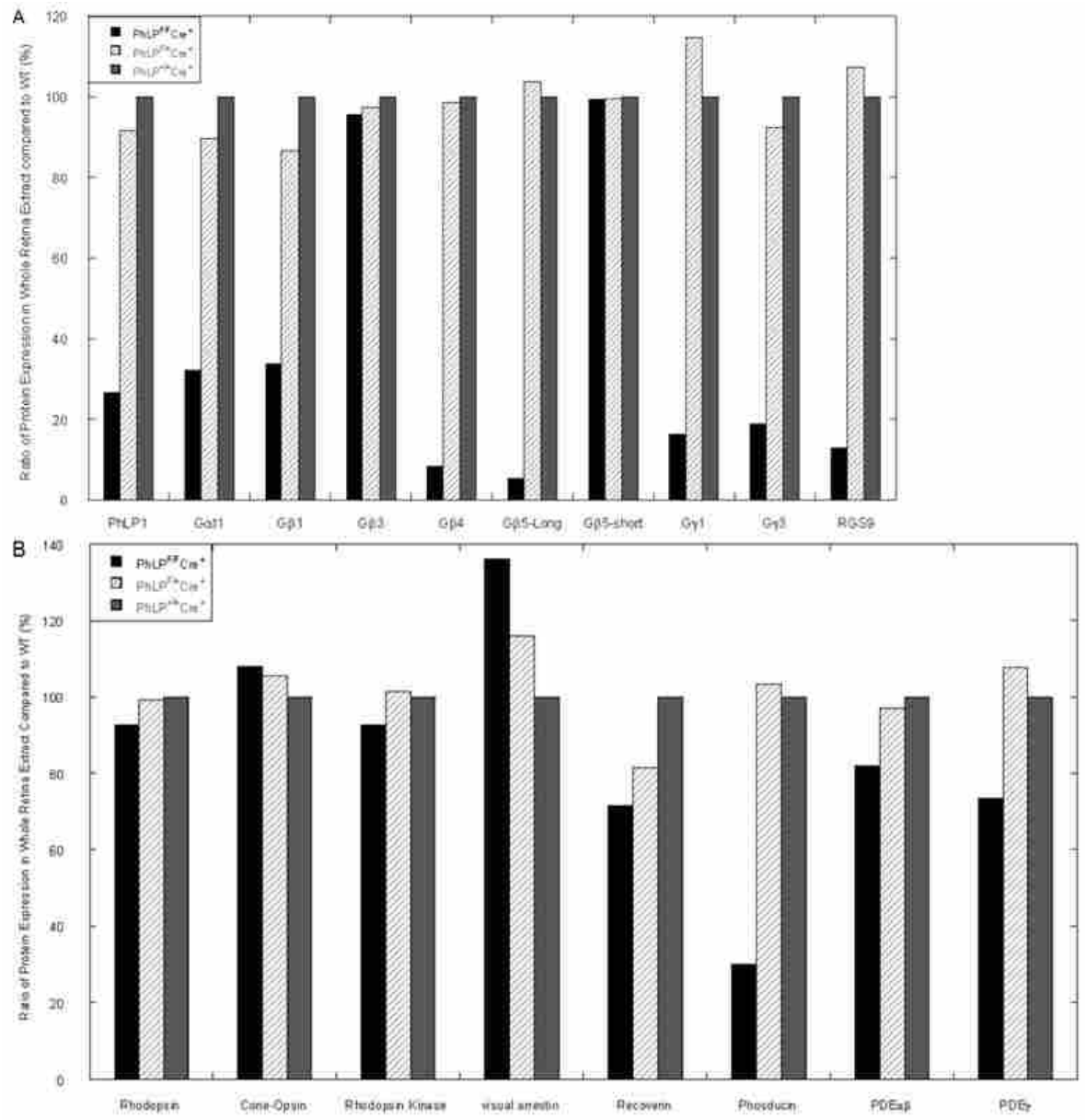

Figure 3-6. Retinal protein expression levels in 33- to 37-d-old mice.
Levels of protein expression in PhLP1$^{F/F}$Cre^{+} and PhLP1$^{F/+}$Cre^{+} retina extracts were compared to PhLP1$^{+/+}$Cre^{+} for normalization. A) Percentages of protein expression levels of PhLP1, RGS9 and major G protein subunits expressed in retina are shown in graph corresponding to the immunoblots that were shown in Figure 3-5 A. B) Protein expression levels of other important photoreceptor proteins expressed in retina are presented here corresponding to the immunoblots that were shown in Figure 3-5 B.

observation is consistent with the normal morphology of retina under light microscope observations (Figure 3-4) and shows that the rod specific PhLP1 depletion is not causing a global disruption of rod function, at least at 5 weeks of age, as was seen with the transgenic over-expression of the PhLP1 Δ1-83 variant [161]. This evidence for normal rod morphology

indicates that the loss of G protein subunit expression is a direct effect of the absence of PhLP1 and is not an indirect effect of photoreceptor degeneration or malformation of the rod outer segments.

Discussion

An essential role of PhLP1 as a co-chaperone with CCT in Gβγ dimer assembly has emerged from a significant body of evidence accumulated from genetic deletion studies in single-celled organisms [110, 179], structural studies of the PhLP1-CCT complex [105] and biochemical studies in cell culture [57, 73, 111, 112, 114, 122]. However, this proposed role of PhLP1 has not been examined in a mammalian system *in vivo*. As a result, we used mouse gene targeting strategies to assess the physiological function of PhLP1 *in vivo*. We reasoned that a whole animal deletion strategy would be less informative because disruption of the $G\beta_1$ gene was embryonically lethal [162] and if PhLP1 was essential for Gβγ assembly, its deletion in the whole animal would be lethal as well. Therefore, we chose a conditional gene targeting method to specifically delete PhLP1 from mouse retinal rod cells. We expected the rod-specific PhLP1 conditional knockout mouse to be an ideal system to analyze the effects of PhLP1 on Gβγ assembly *in vivo* because both Gβγ subunits and PhLP1 are abundantly expressed in the photoreceptor cells [139, 180] and the effects of PhLP1 deletion can render readily observable changes in phototransduction.

Lack of severe photoreceptor degeneration upon PhLP1 deletion

A major concern in making this knockout mouse was that loss of PhLP1 would cause the rods to degenerate. Like other neurons, photoreceptors are susceptible to degeneration from perturbation of their protein chaperone systems. This was the case with the rhodopsin promoter-

driven transgenic over-expression of the PhLP1 Δ1-83 dominant negative variant in rods. Malformation of outer segments and rapid degeneration of the photoreceptors occurred [161]. Fortunately, the conditional PhLP1 knockout mouse did not display this same severe degeneration phenotype. The immunohistochemistry experiments showed that the photoreceptor layer thickness was not decreased at 5 weeks when the ERG and protein expression analysis was performed (Fig. 3-4). Moreover, there was no decrease in expression of rhodopsin or other non-G protein outer segment proteins at this age (Fig. 3-5, 3-6), indicating that the outer segments were normal. The most likely reason for the lack of severe degeneration in the conditional PhLP1 knockout compared to the PhLP1 Δ1-83 transgenic is that the over-expressed PhLP1 dominant negative interferes with other CCT functions by blocking the binding of important CCT substrates like actin and tubulin, whereas PhLP1 deletion only interferes with the co-chaperone functions of PhLP1. Therefore, we can conclude that the effects of PhLP1 deletion on G protein subunit expression and phototransduction were a direct result of loss of PhLP1 and not an indirect result of outer segment malformation or photoreceptor degeneration.

Effects of PhLP deletion on the photoresponse

The complete loss of the scotopic (dark-adapted) a-wave upon PhLP1 deletion was a surprise. This total lack of responsiveness has only been observed in the $G\alpha_t$ knockout [171]. There are two separate $G\gamma_1$ knockout mouse models and both showed reduced scotopic a-waves, but not a complete loss of the rod light response [174, 176]. In the $G\gamma_1$ knockouts, $G\alpha_t$ and $G\beta_1$ expression was reduced by a similar amount to what we observed in the PhLP1 conditional knockout. Thus, there was residual $G\alpha_t$, and it was proposed that this $G\alpha_t$ was able to interact with rhodopsin and initiate phototransduction in the absence of $G\beta\gamma$, albeit at a much reduced rate [174, 176]. This conclusion is brought into question by the total loss of rod light sensitivity

in the PhLP1 knockout, in which 30% of the normal $G\alpha_t$ complement still remains. A major difference between the $G\gamma_1$ knockouts and the PhLP1 knockout is that expression of other Gβ and Gγ subunits found in rods, such as $G\beta_4$ and $G\gamma_3$ are also reduced in the PhLP1 knockout (Fig. 3-5 and 3-6), whereas in the $G\gamma_1$ knockout they are not reduced [176]. This observation suggests that the residual phototransduction observed in the $G\gamma_1$ knockout mice resulted from compensatory coupling of $G\alpha_t$ to rhodopsin by $G\beta_4\gamma_3$ or another Gβγ combination found in the rod outer segments and not coupling of $G\alpha_t$ by itself to rhodopsin. The contribution of Gβγ to activation of Gα by receptors has been a question in the G protein signaling field for 30 years. Our results suggest that Gβγ is absolutely required for activation of $G\alpha_t$ by rhodopsin *in vivo*.

The modestly reduced b-waves at high scotopic light intensities and the near normal b-waves in photopic (light-adapted) conditions suggest that cone phototransduction is not affected by PhLP1 deletion in the rods and that coupling to cone bipolar cells is normal. Rod responses are shut-down under light-adapted conditions, so only the cone responses are seen in the photopic ERG. This result indicates that there is no loss of cone function and that the PhLP1 knockout was correctly targeted to the rods. Moreover, rod degeneration leads to cone degeneration as well, so normal cone function supports the idea that the loss of the a-wave is not the result of rod degeneration but of the loss of properly assembled G_t heterotrimers.

Decreased G protein subunit expression supports the model of Gβγ assembly

The model of Gβγ assembly presented in Chapter 1 proposes that PhLP1 is essential for the release of Gβ from CCT and its association with Gγ. The reduced expression of $G\alpha_t$, $G\beta_1$, and $G\gamma_1$ in the PhLP1 knockout rods is fully consistent with this notion and extends the proposed role of PhLP1 to the *in vivo* situation. Moreover, the reduced expression of $G\beta_4$ and $G\gamma_3$ supports the

conclusion from cell culture studies [122] that PhLP1 is required for assembly of all Gβγ subunit combinations. Importantly, the drastic reduction in $G\beta_5$L and RGS9-1 expression in rods upon PhLP1 deletion shows that $G\beta_5$-RGS dimer formation is more PhLP1 dependent than proposed from the cell culture studies. In those studies, an 80% siRNA-mediated knockdown of PhLP1 resulted in only a two-fold reduction in the rate of $G\beta_5$-RGS7 assembly [122]. One possible explanation for this difference is that in the cell culture work $G\beta_5$S and RGS7 were both over-expressed and that the higher concentration of subunits resulted in a decreased dependence on PhLP1 for assembly. Another possibility is that the $G\beta_5$L-RGS9-1 dimer is more dependent on PhLP1 than the $G\beta_5$S-RGS7 dimer. Whatever the reason, the drastic reduction in $G\beta_5$L and RGS9-1 in the PhLP1 knockout demonstrates that PhLP1 is essential for $G\beta_5$-RGS9-1 assembly in rods *in vivo*.

Another observation worth noting is the 70% reduction in Pdc expression. A very similar reduction in Pdc expression was observed in the two Gγ1 knockout models [174, 176]. In addition, a similar reduction in $G\beta_1$ expression was observed in the Pdc knockout [181]. This result indicates that Pdc and Gβγ mutually stabilize each other from ubiquitin-mediated degradation [182], which supports the idea that the role of Pdc in photoreceptors is to chaperone Gβγ as it shuttles between the outer and inner segment of the photoreceptor under bright light conditions [76, 181]. The stark differences between the effect of PhLP1 knockout on phototransduction observed here compared to the lack of effect of the Pdc knockout on phototransduction observed previously [181, 182] underlines the fact that although PhLP1 shares a high degree of homology with Pdc and they both bind Gβγ, the fundamental role of PhLP1 is very different from that of Pdc.

Conclusion

Decreased expression of G protein subunits and significant impairment of phototransduction in the rod cells of PhLP1 conditional knockout mouse provides strong *in vivo* evidence that PhLP1 is required for Gβγ assembly. In addition, the dramatic decrease in $G\beta_5$Land RGS9-1 in rods indicates that the $G\beta_5$L-RGS9-1 dimer, whose GTPase activity on $G\alpha_t$ plays such a critical role in turning off the light response, also requires PhLP1 for its assembly. These results provide sufficient impetus for studies to identify small molecule inhibitors of the Gβγ and $G\beta_5$-RGS assembly processes. These molecules could be designed to disrupt the PhLP1-Gβ interaction that is essential for formation of both of these dimers. If such molecules could be found, they could prove extremely valuable as therapeutics in treating the myriad of diseases caused by excessive signaling through G protein pathways. For example, lysophosphatidic acid (LPA) is a major mitogen that contributes to the transformation phenotype of many cancers [183]. LPA is known to signal through a G protein-coupled receptor. However, good antagonists of the LPA receptor are lacking. Inhibition of G protein signaling with therapeutics that block Gβγ assembly would perform the same function as an LPA receptor antagonist by blocking G protein signaling downstream of the receptor and could thus block LPA-mediated cancer growth and metastasis. Importantly, the results of this study show that specific inhibition of PhLP1 function can shut down all downstream Gβγ signaling without affecting the overall health of the cells that are being targeted. Therefore, this unique power of PhLP1 can be harnessed for designing therapeutic means to alleviate the diseases associated with pathological Gβγ signaling. By showing that PhLP1 is mediating Gβγ assembly *in vivo*, this study has established an essential part of an important research effort that has the potential for broad reaching benefits to human health and well-being.

REFERENCES

1. Munoz, I.G., et al., *Crystal structure of the open conformation of the mammalian chaperonin CCT in complex with tubulin.* Nature Structural & Molecular Biology, 2011. **18**(1): p. 14-+.
2. Rasmussen, S.G., et al., *Crystal structure of the beta2 adrenergic receptor-Gs protein complex.* Nature, 2011. **477**(7366): p. 549-55.
3. Gaudet, R., A. Bohm, and P.B. Sigler, *Crystal structure at 2.4 angstroms resolution of the complex of transducin betagamma and its regulator, phosducin.* Cell, 1996. **87**(3): p. 577-88.
4. Pettersen, E.F., et al., *UCSF chimera - A visualization system for exploratory research and analysis.* Journal of Computational Chemistry, 2004. **25**(13): p. 1605-1612.
5. *The Retina, an Approachable Part of the Brain - Dowling,Je.* Perceptual and Motor Skills, 1987. **65**(2): p. 679-679.
6. Larkin, M.A., et al., *Clustal W and Clustal X version 2.0.* Bioinformatics, 2007. **23**(21): p. 2947-8.
7. Cheever, M.L., et al., *Crystal structure of the multifunctional Gbeta5-RGS9 complex.* Nat Struct Mol Biol, 2008. **15**(2): p. 155-62.
8. Bordoli, L., et al., *Protein structure homology modeling using SWISS-MODEL workspace.* Nature Protocols, 2009. **4**(1): p. 1-13.
9. Lambright, D.G., et al., *The 2.0 A crystal structure of a heterotrimeric G protein.* Nature, 1996. **379**(6563): p. 311-9.
10. Pappenberger, G., et al., *Crystal structure of the CCT gamma apical domain: Implications for substrate binding to the eukaryotic cytosolic chaperonin.* Journal of Molecular Biology, 2002. **318**(5): p. 1367-1379.
11. Masland, R.H., *The functional architecture of the retina.* Sci Am, 1986. **255**(6): p. 102-11.
12. Noel, J.P., H.E. Hamm, and P.B. Sigler, *The 2.2 A crystal structure of transducin-alpha complexed with GTP gamma S.* Nature, 1993. **366**(6456): p. 654-63.
13. Jeon, C.J., E. Strettoi, and R.H. Masland, *The major cell populations of the mouse retina.* Journal of Neuroscience, 1998. **18**(21): p. 8936-8946.
14. Dyer, M.A. and C.L. Cepko, *Regulating proliferation during retinal development.* Nat Rev Neurosci, 2001. **2**(5): p. 333-42.
15. Arshavsky, V.Y., T.D. Lamb, and E.N. Pugh, Jr., *G proteins and phototransduction.* Annu Rev Physiol, 2002. **64**: p. 153-87.
16. Cabrera-Vera, T.M., et al., *Insights into G protein structure, function, and regulation.* Endocrine Reviews, 2003. **24**(6): p. 765-781.
17. Spiegel, A.M. and L.S. Weinstein, *Inherited diseases involving g proteins and g protein-coupled receptors.* Annu Rev Med, 2004. **55**: p. 27-39.
18. Spiegelberg, B.D. and H.E. Hamm, *Roles of G-protein-coupled receptor signaling in cancer biology and gene transcription.* Current Opinion in Genetics & Development, 2007. **17**(1): p. 40-44.
19. Melien, O., *Heterotrimeric G proteins and disease.* Methods Mol Biol, 2007. **361**: p. 119-44.
20. Malbon, C.C., *G proteins in development.* Nat Rev Mol Cell Biol, 2005. **6**(9): p. 689-701.

21. Rockman, H.A., W.J. Koch, and R.J. Lefkowitz, *Seven-transmembrane-spanning receptors and heart function.* Nature, 2002. **415**(6868): p. 206-12.
22. Gainetdinov, R.R., et al., *Desensitization of G protein-coupled receptors and neuronal functions.* Annu Rev Neurosci, 2004. **27**: p. 107-44.
23. Foord, S.M., et al., *International Union of Pharmacology. XLVI. G protein-coupled receptor list.* Pharmacol Rev, 2005. **57**(2): p. 279-88.
24. Schoneberg, T., et al., *Mutant G-protein-coupled receptors as a cause of human diseases.* Pharmacol Ther, 2004. **104**(3): p. 173-206.
25. Cabrera-Vera, T.M., et al., *Insights into G protein structure, function, and regulation.* Endocr Rev, 2003. **24**(6): p. 765-81.
26. Fu, Y. and K.W. Yau, *Phototransduction in mouse rods and cones.* Pflugers Arch, 2007. **454**(5): p. 805-19.
27. Lem, J., et al., *Morphological, physiological, and biochemical changes in rhodopsin knockout mice.* Proc Natl Acad Sci U S A, 1999. **96**(2): p. 736-41.
28. Humphries, M.M., et al., *Retinopathy induced in mice by targeted disruption of the rhodopsin gene.* Nat Genet, 1997. **15**(2): p. 216-9.
29. Yau, K.W., *Phototransduction mechanism in retinal rods and cones. The Friedenwald Lecture.* Invest Ophthalmol Vis Sci, 1994. **35**(1): p. 9-32.
30. Chen, C., K. Nakatani, and Y. Koutalos, *Free magnesium concentration in salamander photoreceptor outer segments.* J Physiol, 2003. **553**(Pt 1): p. 125-35.
31. Cornwall, M.C. and G.L. Fain, *Bleached pigment activates transduction in isolated rods of the salamander retina.* J Physiol, 1994. **480 (Pt 2)**: p. 261-79.
32. Surya, A., K.W. Foster, and B.E. Knox, *Transducin activation by the bovine opsin apoprotein.* J Biol Chem, 1995. **270**(10): p. 5024-31.
33. Okada, T., et al., *Activation of rhodopsin: new insights from structural and biochemical studies.* Trends Biochem Sci, 2001. **26**(5): p. 318-24.
34. Baehr, W., M.J. Devlin, and M.L. Applebury, *Isolation and Characterization of Cgmp Phosphodiesterase from Bovine Rod Outer Segments.* Journal of Biological Chemistry, 1979. **254**(22): p. 1669-1677.
35. Hurley, J.B. and L. Stryer, *Purification and Characterization of the Gamma-Regulatory Subunit of the Cyclic-Gmp Phosphodiesterase from Retinal Rod Outer Segments.* Journal of Biological Chemistry, 1982. **257**(18): p. 1094-1099.
36. Karpen, J.W., et al., *Gating Kinetics of the Cyclic-Gmp-Activated Channel of Retinal Rods - Flash-Photolysis and Voltage-Jump Studies.* Proceedings of the National Academy of Sciences of the United States of America, 1988. **85**(4): p. 1287-1291.
37. Wilden, U., S.W. Hall, and H. Kuhn, *Phosphodiesterase Activation by Photoexcited Rhodopsin Is Quenched When Rhodopsin Is Phosphorylated and Binds the Intrinsic 48-Kda Protein of Rod Outer Segments.* Proceedings of the National Academy of Sciences of the United States of America, 1986. **83**(5): p. 1174-1178.
38. Kuhn, H. and U. Wilden, *Deactivation of Photoactivated Rhodopsin by Rhodopsin-Kinase and Arrestin.* Journal of Receptor Research, 1987. **7**(1-4): p. 283-298.
39. Kawamura, S., *Light-Sensitivity Modulating Protein in Frog Rods.* Photochemistry and Photobiology, 1992. **56**(6): p. 1173-1180.
40. Kawamura, S., *Rhodopsin Phosphorylation as a Mechanism of Cyclic-Gmp Phosphodiesterase Regulation by S-Modulin.* Nature, 1993. **362**(6423): p. 855-857.

41. Chen, C.K., et al., *Ca(2+)-dependent interaction of recoverin with rhodopsin kinase.* J Biol Chem, 1995. **270**(30): p. 18060-6.
42. Klenchin, V.A., P.D. Calvert, and M.D. Bownds, *Inhibition of rhodopsin kinase by recoverin. Further evidence for a negative feedback system in phototransduction.* J Biol Chem, 1995. **270**(27): p. 16147-52.
43. McBee, J.K., et al., *Confronting complexity: the interlink of phototransduction and retinoid metabolism in the vertebrate retina.* Prog Retin Eye Res, 2001. **20**(4): p. 469-529.
44. He, W., C.W. Cowan, and T.G. Wensel, *RGS9, a GTPase accelerator for phototransduction.* Neuron, 1998. **20**(1): p. 95-102.
45. Makino, E.R., et al., *The GTPase activating factor for transducin in rod photoreceptors is the complex between RGS9 and type 5 G protein beta subunit.* Proc Natl Acad Sci U S A, 1999. **96**(5): p. 1947-52.
46. Hu, G. and T.G. Wensel, *R9AP, a membrane anchor for the photoreceptor GTPase accelerating protein, RGS9-1.* Proc Natl Acad Sci U S A, 2002. **99**(15): p. 9755-60.
47. Makino, C.L., X.H. Wen, and J. Lem, *Piecing together the timetable for visual transduction with transgenic animals.* Curr Opin Neurobiol, 2003. **13**(4): p. 404-12.
48. Cowan, C.W., et al., *High expression levels in cones of RGS9, the predominant GTPase accelerating protein of rods.* Proceedings of the National Academy of Sciences of the United States of America, 1998. **95**(9): p. 5351-5356.
49. Zhang, X., T.G. Wensel, and T.W. Kraft, *GTPase regulators and photoresponses in cones of the eastern chipmunk.* Journal of Neuroscience, 2003. **23**(4): p. 1287-1297.
50. Ross, E.M. and T.M. Wilkie, *GTPase-activating proteins for heterotrimeric G proteins: regulators of G protein signaling (RGS) and RGS-like proteins.* Annu Rev Biochem, 2000. **69**: p. 795-827.
51. Krispel, C.M., et al., *RGS expression rate-limits recovery of rod photoresponses.* Neuron, 2006. **51**(4): p. 409-16.
52. Lee, R.H., B.S. Lieberman, and R.N. Lolley, *A novel complex from bovine visual cells of a 33,000-dalton phosphoprotein with beta- and gamma-transducin: purification and subunit structure.* Biochemistry, 1987. **26**(13): p. 3983-90.
53. Lee, R.H., et al., *Regulation of retinal cGMP cascade by phosducin in bovine rod photoreceptor cells. Interaction of phosducin and transducin.* J Biol Chem, 1992. **267**(35): p. 25104-12.
54. Bauer, P.H., et al., *Phosducin is a protein kinase A-regulated G-protein regulator.* Nature, 1992. **358**(6381): p. 73-6.
55. Yoshida, T., et al., *The phosphorylation state of phosducin determines its ability to block transducin subunit interactions and inhibit transducin binding to activated rhodopsin.* J Biol Chem, 1994. **269**(39): p. 24050-7.
56. Barhite, S., C. Thibault, and M.F. Miles, *Phosducin-like protein (PhLP), a regulator of G beta gamma function, interacts with the proteasomal protein SUG1.* Biochim Biophys Acta, 1998. **1402**(1): p. 95-101.
57. McLaughlin, J.N., et al., *Regulation of angiotensin II-induced G protein signaling by phosducin-like protein.* J Biol Chem, 2002. **277**(38): p. 34885-95.
58. Reig, J.A., L. Yu, and D.C. Klein, *Pineal transduction. Adrenergic----cyclic AMP-dependent phosphorylation of cytoplasmic 33-kDa protein (MEKA) which binds beta gamma-complex of transducin.* J Biol Chem, 1990. **265**(10): p. 5816-24.

59. Miles, M.F., et al., *Phosducin-like protein: an ethanol-responsive potential modulator of guanine nucleotide-binding protein function.* Proc Natl Acad Sci U S A, 1993. **90**(22): p. 10831-5.
60. Schroder, S. and M.J. Lohse, *Quantification of the tissue levels and function of the G-protein regulator phosducin-like protein (PhlP).* Naunyn Schmiedebergs Arch Pharmacol, 2000. **362**(4-5): p. 435-9.
61. Thibault, C., et al., *Cloning and characterization of the rat and human phosducin-like protein genes: structure, expression and chromosomal localization.* Biochim Biophys Acta, 1999. **1444**(3): p. 346-54.
62. Abe, T., et al., *The sequence of the mouse phosducin-encoding gene and its 5'-flanking region.* Gene, 1993. **133**(2): p. 179-86.
63. Sparkes, R.S., et al., *Assignment of the phosducin (PDC) gene to human chromosome 1q25-1q32.1 by somatic cell hybridization and in situ hybridization.* Genomics, 1993. **18**(2): p. 426-8.
64. Danner, S. and M.J. Lohse, *Phosducin is a ubiquitous G-protein regulator.* Proc Natl Acad Sci U S A, 1996. **93**(19): p. 10145-50.
65. Savage, J.R., et al., *Functional roles of the two domains of phosducin and phosducin-like protein.* J Biol Chem, 2000. **275**(39): p. 30399-407.
66. Humrich, J., et al., *Regulation of phosducin-like protein by casein kinase 2 and N-terminal splicing.* J Biol Chem, 2003. **278**(7): p. 4474-81.
67. Ford, C.E., et al., *Molecular basis for interactions of G protein betagamma subunits with effectors.* Science, 1998. **280**(5367): p. 1271-4.
68. Sondek, J., et al., *Crystal structure of a G-protein beta gamma dimer at 2.1A resolution.* Nature, 1996. **379**(6563): p. 369-74.
69. Hawes, B.E., et al., *Determination of the G beta gamma-binding domain of phosducin. A regulatable modulator of G beta gamma signaling.* J Biol Chem, 1994. **269**(47): p. 29825-30.
70. Tanaka, H., et al., *Analysis of the T beta gamma-binding domain of MEKA/phosducin.* Neurochem Int, 1997. **31**(4): p. 625-34.
71. Tanaka, H., et al., *MEKA/phosducin attenuates hydrophobicity of transducin beta gamma subunits without binding to farnesyl moiety.* Biochem Biophys Res Commun, 1996. **223**(3): p. 587-91.
72. Loew, A., et al., *Phosducin induces a structural change in transducin beta gamma.* Structure, 1998. **6**(8): p. 1007-19.
73. Lukov, G.L., et al., *Phosducin-like protein acts as a molecular chaperone for G protein betagamma dimer assembly.* EMBO J, 2005. **24**(11): p. 1965-75.
74. Higgins, J.B. and P.J. Casey, *In vitro processing of recombinant G protein gamma subunits. Requirements for assembly of an active beta gamma complex.* J Biol Chem, 1994. **269**(12): p. 9067-73.
75. Schmidt, C.J. and E.J. Neer, *In vitro synthesis of G protein beta gamma dimers.* J Biol Chem, 1991. **266**(7): p. 4538-44.
76. Willardson, B.M., et al., *Regulation of phosducin phosphorylation in retinal rods by Ca2+/calmodulin-dependent adenylyl cyclase.* Proc Natl Acad Sci U S A, 1996. **93**(4): p. 1475-9.
77. Schroder, S. and M.J. Lohse, *Inhibition of G-protein betagamma-subunit functions by phosducin-like protein.* Proc Natl Acad Sci U S A, 1996. **93**(5): p. 2100-4.

78. Stoldt, V., et al., *Review: the Cct eukaryotic chaperonin subunits of Saccharomyces cerevisiae and other yeasts.* Yeast, 1996. **12**(6): p. 523-9.
79. Liou, A.K.F. and K.R. Willison, *Elucidation of the subunit orientation in CCT (chaperonin containing TCP1) from the subunit composition of CCT micro-complexes.* Embo Journal, 1997. **16**(14): p. 4311-4316.
80. Hartl, F.U. and M. Hayer-Hartl, *Molecular chaperones in the cytosol: from nascent chain to folded protein.* Science, 2002. **295**(5561): p. 1852-8.
81. Yam, A.Y., et al., *Defining the TRiC/CCT interactome links chaperonin function to stabilization of newly made proteins with complex topologies.* Nat Struct Mol Biol, 2008. **15**(12): p. 1255-62.
82. Thulasiraman, V., C.F. Yang, and J. Frydman, *In vivo newly translated polypeptides are sequestered in a protected folding environment.* EMBO J, 1999. **18**(1): p. 85-95.
83. Kim, S., K.R. Willison, and A.L. Horwich, *Cystosolic chaperonin subunits have a conserved ATPase domain but diverged polypeptide-binding domains.* Trends Biochem Sci, 1994. **19**(12): p. 543-8.
84. Melki, R., et al., *Cytoplasmic chaperonin containing TCP-1: structural and functional characterization.* Biochemistry, 1997. **36**(19): p. 5817-26.
85. Llorca, O., et al., *The 'sequential allosteric ring' mechanism in the eukaryotic chaperonin-assisted folding of actin and tubulin.* EMBO J, 2001. **20**(15): p. 4065-75.
86. Ditzel, L., et al., *Crystal structure of the thermosome, the archaeal chaperonin and homolog of CCT.* Cell, 1998. **93**(1): p. 125-38.
87. Meyer, A.S., et al., *Closing the folding chamber of the eukaryotic chaperonin requires the transition state of ATP hydrolysis.* Cell, 2003. **113**(3): p. 369-81.
88. Hynes, G.M. and K.R. Willison, *Individual subunits of the eukaryotic cytosolic chaperonin mediate interactions with binding sites located on subdomains of beta-actin.* J Biol Chem, 2000. **275**(25): p. 18985-94.
89. Frydman, J., et al., *Function in protein folding of TRiC, a cytosolic ring complex containing TCP-1 and structurally related subunits.* EMBO J, 1992. **11**(13): p. 4767-78.
90. Gao, Y.J., et al., *A Cytoplasmic Chaperonin That Catalyzes Beta-Actin Folding.* Cell, 1992. **69**(6): p. 1043-1050.
91. Llorca, O., et al., *3D reconstruction of the ATP-bound form of CCT reveals the asymmetric folding conformation of a type II chaperonin.* Nature Structural Biology, 1999. **6**(7): p. 639-642.
92. I, R., C. Smith, and R.G. Yount, *The active site of myosin.* Annual Review of Physiology, 1996. **58**: p. 671-702.
93. Sprang, S.R., *G protein mechanisms: Insights from structural analysis.* Annual Review of Biochemistry, 1997. **66**: p. 639-678.
94. Melki, R. and N.J. Cowan, *Facilitated Folding of Actins and Tubulins Occurs Via a Nucleotide-Dependent Interaction between Cytoplasmic Chaperonin and Distinctive Folding Intermediates.* Molecular and Cellular Biology, 1994. **14**(5): p. 2895-2904.
95. Kafri, G. and A. Horovitz, *Transient kinetic analysis of ATP-induced allosteric transitions in the eukaryotic chaperonin containing TCP-1.* Journal of Molecular Biology, 2003. **326**(4): p. 981-987.
96. Kafri, G., K.R. Willison, and A. Horovitz, *Nested allosteric interactions in the cytoplasmic chaperonin containing TCP-1.* Protein Science, 2001. **10**(2): p. 445-449.

97. Roobol, A., et al., *Disassembly of the cytosolic chaperonin in mammalian cell extracts at intracellular levels of K+ and ATP.* Journal of Biological Chemistry, 1999. **274**(27): p. 19220-19227.
98. Liou, A.K.F., E.A. McCormack, and K.R. Willison, *The chaperonin containing TCP-1 (CCT) displays a single-ring mediated disassembly and reassembly cycle.* Biological Chemistry, 1998. **379**(3): p. 311-319.
99. Brackley, K.I. and J. Grantham, *Activities of the chaperonin containing TCP-1 (CCT): implications for cell cycle progression and cytoskeletal organisation.* Cell Stress & Chaperones, 2009. **14**(1): p. 23-31.
100. Spiess, C., et al., *Mechanism of the eukaryotic chaperonin: protein folding in the chamber of secrets.* Trends Cell Biol, 2004. **14**(11): p. 598-604.
101. Camasses, A., et al., *The CCT chaperonin promotes activation of the anaphase-promoting complex through the generation of functional Cdc20.* Mol Cell, 2003. **12**(1): p. 87-100.
102. Kubota, S., H. Kubota, and K. Nagata, *Cytosolic chaperonin protects folding intermediates of Gbeta from aggregation by recognizing hydrophobic beta-strands.* Proc Natl Acad Sci U S A, 2006. **103**(22): p. 8360-5.
103. Tian, G., et al., *Specificity in chaperonin-mediated protein folding.* Nature, 1995. **375**(6528): p. 250-3.
104. Smith, T.F., et al., *The WD repeat: a common architecture for diverse functions.* Trends Biochem Sci, 1999. **24**(5): p. 181-5.
105. Martin-Benito, J., et al., *Structure of the complex between the cytosolic chaperonin CCT and phosducin-like protein.* Proc Natl Acad Sci U S A, 2004. **101**(50): p. 17410-5.
106. Martin-Benito, J., et al., *Structure of eukaryotic prefoldin and of its complexes with unfolded actin and the cytosolic chaperonin CCT.* EMBO J, 2002. **21**(23): p. 6377-86.
107. Ho, Y., et al., *Systematic identification of protein complexes in Saccharomyces cerevisiae by mass spectrometry.* Nature, 2002. **415**(6868): p. 180-3.
108. Gavin, A.C., et al., *Functional organization of the yeast proteome by systematic analysis of protein complexes.* Nature, 2002. **415**(6868): p. 141-7.
109. Plaxco, K.W., et al., *Simplified proteins: minimalist solutions to the 'protein folding problem'.* Curr Opin Struct Biol, 1998. **8**(1): p. 80-5.
110. Blaauw, M., et al., *Phosducin-like proteins in Dictyostelium discoideum: implications for the phosducin family of proteins.* EMBO J, 2003. **22**(19): p. 5047-57.
111. Humrich, J., et al., *Phosducin-like protein regulates G-protein betagamma folding by interaction with tailless complex polypeptide-1alpha: dephosphorylation or splicing of PhLP turns the switch toward regulation of Gbetagamma folding.* J Biol Chem, 2005. **280**(20): p. 20042-50.
112. Knol, J.C., et al., *The phosducin-like protein PhLP1 is essential for G{beta}{gamma} dimer formation in Dictyostelium discoideum.* Mol Cell Biol, 2005. **25**(18): p. 8393-400.
113. Wells, C.A., J. Dingus, and J.D. Hildebrandt, *Role of the chaperonin CCT/TRiC complex in G protein betagamma-dimer assembly.* J Biol Chem, 2006. **281**(29): p. 20221-32.
114. Lukov, G.L., et al., *Mechanism of assembly of G protein betagamma subunits by protein kinase CK2-phosphorylated phosducin-like protein and the cytosolic chaperonin complex.* J Biol Chem, 2006. **281**(31): p. 22261-74.
115. Clapham, D.E. and E.J. Neer, *G protein beta gamma subunits.* Annu Rev Pharmacol Toxicol, 1997. **37**: p. 167-203.

116. Marrari, Y., et al., *Assembly and trafficking of heterotrimeric G proteins.* Biochemistry, 2007. **46**(26): p. 7665-77.
117. Wedegaertner, P.B., *Lipid modifications and membrane targeting of G alpha.* Biol Signals Recept, 1998. **7**(2): p. 125-35.
118. Lane, K.T. and L.S. Beese, *Structural biology of protein farnesyltransferase and geranylgeranyltransferase type I.* Journal of Lipid Research, 2006. **47**(4): p. 681-699.
119. Farazi, T.A., G. Waksman, and J.I. Gordon, *The biology and enzymology of protein N-myristoylation.* Journal of Biological Chemistry, 2001. **276**(43): p. 39501-39504.
120. Dingus, J., et al., *G Protein betagamma dimer formation: Gbeta and Ggamma differentially determine efficiency of in vitro dimer formation.* Biochemistry, 2005. **44**(35): p. 11882-90.
121. Anderson, G.R., E. Posokhova, and K.A. Martemyanov, *The R7 RGS protein family: multi-subunit regulators of neuronal G protein signaling.* Cell Biochem Biophys, 2009. **54**(1-3): p. 33-46.
122. Howlett, A.C., et al., *Specificity of Phosducin-like protein1-mediated G proteinbg and Gb5-RGS protein dimer formation.* Journal of Biological Chemistry, 2009. **submitted**.
123. Cuellar, J., et al., *The structure of CCT-Hsc70 NBD suggests a mechanism for Hsp70 delivery of substrates to the chaperonin.* Nat Struct Mol Biol, 2008. **15**(8): p. 858-64.
124. Posokhova, E., V. Uversky, and K.A. Martemyanov, *Proteomic identification of Hsc70 as a mediator of RGS9-2 degradation by in vivo interactome analysis.* J Proteome Res, 2010. **9**(3): p. 1510-21.
125. Gospe, S.M., et al., *Membrane Attachment Is Key to Protecting Transducin GTPase-Activating Complex from Intracellular Proteolysis in Photoreceptors.* Journal of Neuroscience, 2011. **31**(41): p. 14660-14668.
126. Wilkinson, J.C., et al., *VIAF, a conserved inhibitor of apoptosis (IAP)-interacting factor that modulates caspase activation.* J Biol Chem, 2004. **279**(49): p. 51091-9.
127. Lopez, P., et al., *A novel germ line-specific gene of the phosducin-like protein (PhLP) family. A meiotic function conserved from yeast to mice.* J Biol Chem, 2003. **278**(3): p. 1751-7.
128. Flanary, P.L., et al., *Functional analysis of Plp1 and Plp2, two homologues of phosducin in yeast.* J Biol Chem, 2000. **275**(24): p. 18462-9.
129. Lacefield, S. and F. Solomon, *A novel step in beta-tubulin folding is important for heterodimer formation in Saccharomyces cerevisiae.* Genetics, 2003. **165**(2): p. 531-41.
130. Stirling, P.C., et al., *PhLP3 modulates CCT-mediated actin and tubulin folding via ternary complexes with substrates.* J Biol Chem, 2006. **281**(11): p. 7012-21.
131. Braig, K., et al., *The crystal structure of the bacterial chaperonin GroEL at 2.8 A.* Nature, 1994. **371**(6498): p. 578-86.
132. Xu, Z.H., A.L. Horwich, and P.B. Sigler, *The crystal structure of the asymmetric GroEL-GroES-(ADP)(7) chaperonin complex.* Nature, 1997. **388**(6644): p. 741-750.
133. Gutsche, I., L.O. Essen, and W. Baumeister, *Group II chaperonins: new TRiC(k)s and turns of a protein folding machine.* Journal of Molecular Biology, 1999. **293**(2): p. 295-312.
134. Valpuesta, J.M., et al., *Structure and function of a protein folding machine: the eukaryotic cytosolic chaperonin CCT.* FEBS Lett, 2002. **529**(1): p. 11-6.
135. Bukau, B. and A.L. Horwich, *The Hsp70 and Hsp60 chaperone machines.* Cell, 1998. **92**(3): p. 351-66.

136. Llorca, O., et al., *Eukaryotic chaperonin CCT stabilizes actin and tubulin folding intermediates in open quasi-native conformations.* Embo Journal, 2000. **19**(22): p. 5971-5979.
137. Feldman, D.E., et al., *Tumorigenic mutations in VHL disrupt folding in vivo by interfering with chaperonin binding.* Molecular Cell, 2003. **12**(5): p. 1213-24.
138. Perkins, D.N., et al., *Probability-based protein identification by searching sequence databases using mass spectrometry data.* Electrophoresis, 1999. **20**(18): p. 3551-3567.
139. Thulin, C.D., et al., *The immunolocalization and divergent roles of phosducin and phosducin-like protein in the retina.* Mol Vis, 1999. **5**: p. 40.
140. Scheres, S.H.W., et al., *Maximum-likelihood multi-reference refinement for electron microscopy images.* Journal of Molecular Biology, 2005. **348**(1): p. 139-149.
141. Ludtke, S.J., P.R. Baldwin, and W. Chiu, *EMAN: Semiautomated software for high-resolution single-particle reconstructions.* Journal of Structural Biology, 1999. **128**(1): p. 82-97.
142. Frank, J., et al., *SPIDER and WEB: processing and visualization of images in 3D electron microscopy and related fields.* Journal of Structural Biology, 1996. **116**(1): p. 190-9.
143. Heymann, J.B., *Bsoft: image and molecular processing in electron microscopy.* Journal of Structural Biology, 2001. **133**(2-3): p. 156-69.
144. Schwede, T., et al., *SWISS-MODEL: an automated protein homology-modeling server.* Nucleic Acids Research, 2003. **31**(13): p. 3381-3385.
145. Stearns, D.J., et al., *The Interaction of a Ca-2+-Dependent Monoclonal-Antibody with the Protein-C Activation Peptide Region - Evidence for Obligatory Ca-2+ Binding to Both Antigen and Antibody.* Journal of Biological Chemistry, 1988. **263**(2): p. 826-832.
146. Wall, M.A., et al., *The structure of the G protein heterotrimer Gi alpha 1 beta 1 gamma 2.* Cell, 1995. **83**(6): p. 1047-58.
147. Spiess, C., et al., *Identification of the TRiC/CCT substrate binding sites uncovers the function of subunit diversity in eukaryotic.* Molecular Cell, 2006. **24**(1): p. 25-37.
148. Gomez-Puertas, P., et al., *The substrate recognition mechanisms in chaperonins.* J Mol Recognit, 2004. **17**(2): p. 85-94.
149. Dekker, C., et al., *The crystal structure of yeast CCT reveals intrinsic asymmetry of eukaryotic cytosolic chaperonins.* EMBO J, 2011. **30**(15): p. 3078-90.
150. Booth, C.R., et al., *Mechanism of lid closure in the eukaryotic chaperonin TRiC/CCT.* Nat Struct Mol Biol, 2008. **15**(7): p. 746-53.
151. Lin, Y.F., et al., *Intracellular beta-tubulin/chaperonin containing TCP1-beta complex serves as a novel chemotherapeutic target against drug-resistant tumors.* Cancer Res, 2009. **69**(17): p. 6879-88.
152. Llorca, O., et al., *Analysis of the interaction between the eukaryotic chaperonin CCT and its substrates actin and tubulin.* Journal of Structural Biology, 2001. **135**(2): p. 205-18.
153. Abe, Y., et al., *p90 ribosomal S6 kinase and p70 ribosomal S6 kinase link phosphorylation of the eukaryotic chaperonin containing TCP-1 to growth factor, insulin, and nutrient signaling.* J Biol Chem, 2009. **284**(22): p. 14939-48.
154. Anjum, R. and J. Blenis, *The RSK family of kinases: emerging roles in cellular signalling.* Nat Rev Mol Cell Biol, 2008. **9**(10): p. 747-58.
155. Gao, Y., et al., *Two cofactors and cytoplasmic chaperonin are required for the folding of alpha- and beta-tubulin.* Molecular and Cellular Biology, 1993. **13**(4): p. 2478-85.

156. Feldman, D.E., et al., *Formation of the VHL-elongin BC tumor suppressor complex is mediated by the chaperonin TRiC.* Molecular Cell, 1999. **4**(6): p. 1051-1061.
157. Fenton, W.A., et al., *Residues in chaperonin GroEL required for polypeptide binding and release.* Nature, 1994. **371**(6498): p. 614-9.
158. Coyle, J.E., et al., *Structural and mechanistic consequences of polypeptide binding by GroEL.* Folding & Design, 1997. **2**(6): p. R93-R104.
159. Hayer-Hartl, M.K., et al., *Conformational specificity of the chaperonin GroEL for the compact folding intermediates of alpha-lactalbumin.* EMBO J, 1994. **13**(13): p. 3192-202.
160. Reissmann, S., et al., *Essential function of the built-in lid in the allosteric regulation of eukaryotic and archaeal chaperonins.* Nat Struct Mol Biol, 2007. **14**(5): p. 432-40.
161. Posokhova, E., et al., *Disruption of the chaperonin containing TCP-1 function affects protein networks essential for rod outer segment morphogenesis and survival.* Mol Cell Proteomics, 2011. **10**(1): p. M110 000570.
162. Kitamura, E., et al., *Disruption of the gene encoding the beta1-subunit of transducin in the Rd4/+ mouse.* Invest Ophthalmol Vis Sci, 2006. **47**(4): p. 1293-301.
163. Akagi, K., et al., *Cre-mediated somatic site-specific recombination in mice.* Nucleic Acids Res, 1997. **25**(9): p. 1766-73.
164. Wu, S., et al., *A protocol for constructing gene targeting vectors: generating knockout mice for the cadherin family and beyond.* Nature Protocols, 2008. **3**(6): p. 1056-76.
165. Chomczynski, P., *One-hour downward alkaline capillary transfer for blotting of DNA and RNA.* Anal Biochem, 1992. **201**(1): p. 134-9.
166. Li, S., et al., *Rhodopsin-iCre transgenic mouse line for Cre-mediated rod-specific gene targeting.* Genesis, 2005. **41**(2): p. 73-80.
167. Zhang, H., et al., *Deletion of PrBP/delta impedes transport of GRK1 and PDE6 catalytic subunits to photoreceptor outer segments.* Proc Natl Acad Sci U S A, 2007. **104**(21): p. 8857-62.
168. Baehr, W., et al., *The function of guanylate cyclase 1 and guanylate cyclase 2 in rod and cone photoreceptors.* J Biol Chem, 2007. **282**(12): p. 8837-47.
169. Bhosale, P., et al., *Identification and characterization of a Pi isoform of glutathione S-transferase (GSTP1) as a zeaxanthin-binding protein in the macula of the human eye.* J Biol Chem, 2004. **279**(47): p. 49447-54.
170. Goldberg, A.F.X., et al., *An intramembrane glutamic acid governs peripherin/rds function for photoreceptor disk morphogenesis.* Investigative Ophthalmology & Visual Science, 2007. **48**(7): p. 2975-2986.
171. Calvert, P.D., et al., *Phototransduction in transgenic mice after targeted deletion of the rod transducin alpha -subunit.* Proc Natl Acad Sci U S A, 2000. **97**(25): p. 13913-8.
172. Pugh, E.N. and T.D. Lamb, *Amplification and Kinetics of the Activation Steps in Phototransduction.* Biochimica Et Biophysica Acta, 1993. **1141**(2-3): p. 111-149.
173. Lyubarsky, A.L., et al., *UV- and midwave-sensitive cone-driven retinal responses of the mouse: a possible phenotype for coexpression of cone photopigments.* J Neurosci, 1999. **19**(1): p. 442-55.
174. Lobanova, E.S., et al., *Transducin gamma-subunit sets expression levels of alpha- and beta-subunits and is crucial for rod viability.* J Neurosci, 2008. **28**(13): p. 3510-20.
175. Peachey, N.S., et al., *Properties of the mouse cone-mediated electroretinogram during light adaptation.* Neurosci Lett, 1993. **162**(1-2): p. 9-11.

176. Kolesnikov, A.V., et al., *G-Protein beta gamma-Complex Is Crucial for Efficient Signal Amplification in Vision.* Journal of Neuroscience, 2011. **31**(22): p. 8067-8077.
177. Lee, R.H., et al., *A third form of the G protein beta subunit. 1. Immunochemical identification and localization to cone photoreceptors.* J Biol Chem, 1992. **267**(34): p. 24776-81.
178. Ritchey, E.R., et al., *The pattern of expression of guanine nucleotide-binding protein beta3 in the retina is conserved across vertebrate species.* Neuroscience, 2010. **169**(3): p. 1376-91.
179. Kasahara, S., P. Wang, and D.L. Nuss, *Identification of bdm-1, a gene involved in G protein beta-subunit function and alpha-subunit accumulation.* Proc Natl Acad Sci U S A, 2000. **97**(1): p. 412-7.
180. Song, H. and M. Sokolov, *Analysis of protein expression and compartmentalization in retinal neurons using serial tangential sectioning of the retina.* J Proteome Res, 2009. **8**(1): p. 346-51.
181. Sokolov, M., et al., *Phosducin facilitates light-driven transducin translocation in rod photoreceptors. Evidence from the phosducin knockout mouse.* J Biol Chem, 2004. **279**(18): p. 19149-56.
182. Krispel, C.M., et al., *Phosducin regulates the expression of transducin betagamma subunits in rod photoreceptors and does not contribute to phototransduction adaptation.* J Gen Physiol, 2007. **130**(3): p. 303-12.
183. Murph, M. and G.B. Mills, *Targeting the lipids LPA and S1P and their signalling pathways to inhibit tumour progression.* Expert Rev Mol Med, 2007. **9**(28): p. 1-18.